SPATIAL ASPECTS OF SOME TUMOR–IMMUNE AND ECOLOGICAL MODELS

Ph. D. THESIS

by

TEEKAM SINGH

DEPARTMENT OF MATHEMATICS
INDIAN INSTITUTE OF TECHNOLOGY ROORKEE
ROORKEE - 247 667 (INDIA)
DECEMBER, 2018

SPATIAL ASPECTS OF SOME TUMOR–IMMUNE AND ECOLOGICAL MODELS

A THESIS

Submitted in partial fulfilment of the requirements for the award of the degree

of

DOCTOR OF PHILOSOPHY

in

MATHEMATICS

by

TEEKAM SINGH

DEPARTMENT OF MATHEMATICS
INDIAN INSTITUTE OF TECHNOLOGY ROORKEE
ROORKEE - 247 667 (INDIA)
DECEMBER, 2018

DEDICATED TO
MY BELOVED DAUGHTER
AADRITI SINGH

Abstract

This thesis investigates the role of spatial pattern formation in tumor–immune and predator–prey systems. In the first half of the thesis, we have proposed spatiotemporal mathematical models using a system of non-linear partial differential equations (reaction-diffusion equations), to study the qualitative and quantitative analysis of tumor–immune interaction, and predator–prey interaction, considering the role of diffusion and other system parameters. The tumor–immune interaction consists of two separate problems, namely, (i) interaction of solid tumor and effector cells (ii) interaction of malignant gliomas and four immune components with the administration of immunotherapeutic agent T11 target structure (T11TS). Using the combination of analytical and numerical techniques, we investigate spatiotemporal dynamics due to the effect of effector cells and T11 target structure on the growth and spread of solid tumor and malignant gliomas respectively. However, Turing zone is absent in both the problems.

The second half of the thesis consists of diffusive predator–prey system (i) with hunting cooperation in predators and (ii) exhibiting herd behavior for prey with linear and quadratic mortality. Using extensive numerical simulations, we obtain complex patterns, namely, spotted pattern, stripe pattern and mixed pattern in the Turing domain by varying (a) hunting cooperation parameter and (b) linear and quadratic mortality's rates respectively. We also have a non-Turing pattern that exhibits spatiotemporal chaos. Thus, the study of the predator–prey system focusses in many pattern dynamics and help in better understanding of their interaction in real environment.

Acknowledgements

I express my heartiest thanks to the God Almighty and His blessings to write and complete this thesis. It gives me immense pleasure to express my deep sense of gratitude and sincere thanks to my supervisor Dr. Sandip Banerjee, Associate Professor, Department of Mathematics, Indian Institute of Technology Roorkee, for his valuable guidance, constructive comments and encouragement throughout the whole thesis work. I offer my deep sense of reverence and profound indebtedness to him for his sincere concern towards my research work with truly scientific intuition and ideas. His unique way of tackling problems from strong fundamentals and clear ideas about the subject helped me in smooth progress of this research work.

I am indebted to the Department of Mathematics, Indian Institute of Technology Roorkee, to all its faculty and staff for their academic support and encouragement. I owe my sincere gratitude to Dr. N. Sukavanam, Head of the Department, Dr. V. K. Katiyar and Dr. R. C. Mittal former Heads of the Department, who provided me with requisite facilities to carry out my doctoral research. I am thankful to my student research committee (SRC) members, Dr. Dharmendra Singh, Dr. V. K. Katiyar, Dr. Sunita Gakkhar, who spared their valuable time to review my draft thesis and provided me with constructive and valuable suggestion, which helped in improving the quality of the thesis. I gratefully acknowledge the financial support by Ministry of Human Resource Development (MHRD), Government of India (Grant No. OH-31-23-200-428).

Collective and individual acknowledgements are also owed to my colleagues at IIT Roorkee. The inspiration support and cooperation that I have received from them are beyond the scope of my acknowledgement. Many thanks goes, in particular, to Dr. Ram Keval, Dr. Subhas Khajanchi, Dr. Sumana Ghosh, Dr. Ramu Dubey,

Amit Kumar, Deepak Dangwal, Shubham Gupta, Vishnu Singh, Shail Dinkar, Dr. Anju Goel for their cooperation and support, and making my stay at IIT Roorkee a memorable one.

I make an effort to record my affectionate thanks to my parents Mr. Kurey Singh and Mrs. Daya Wati for having faith in me, their unconditional support and love during all my studies. Their encouragement has always given me the strength to move ahead in my life. Without their care and support, this thesis would not have been possible. I wish my heartfelt thanks to my wife Anamika Singh for being my best friend and always providing me positive environment and strength in my life.

At last, but by no means the least, I express my deepest love to my dear daughter: Aadriti Singh, whom I may have neglected way too much during my research work.

Roorkee (Teekam Singh)

December , 2018

Table of Contents

List of Figures

List of Tables

Chapter 1

Introduction

The impact of space may be disregarded to a certain extent, particularly when the population of a given species stay fixed in space at any moment of time. Albeit this assumption is not completely realistic. Individuals of an ecological species do not fixed at all times in space, and their dispersion in space changes incessantly by the self-movement of individuals [98; 105; 120; 122; 125].

All of us are living in a spatial real world, and spatial patterns are found everywhere in nature, and these spatial patterns transform the non-spatial (temporal) dynamical qualitative properties of densities of the population at a spectrum of spatial scale. Spatial pattern formation is a dissipative procedure giving growth to spatiotemporal behavior ruled by internal characteristics or external restrictions into a model. The spatial pattern formation factor of ecological as well as tumor–immune interplays have been recognized as an vital component, of how ecological communities and tumors are composed and is one of the pivotal subject of the natural sciences [110; 114; 117; 143].

The idea of diffusion may be considered as the natural propensity for a cluster of particles at the beginning, concentrated close to a location in space to spread out in time, slowly occupying an ever sizable area close to the initial point. Here, the word "particles" mention not only to physical portion of the matter, but to biological populations or to any other recognizable elements as well. Moreover, the word "space" does not mention only to general Euclidean n-space but can also be an hypothetical living space (such as ecological space) [57; 98; 122; 125].

Diffusion is a natural phenomenon where physical material move from an area of high concentration to an area of low concentration, that is, diffusion is a natural process by which the particle cluster as an entire dispersions according to the non-uniform movement of every particle. Diffusion can be defined to be basically an invariant process by which particle clusters, population, etc., diffuse inside a given space according to individual random movement [125].

Reaction-diffusion systems can be used to represent mathematical models, which describe how the individuals of one or more species distributed in space changes under the effect of two procedures, first is local interaction, in which the species interact with each other, and second is the diffusion, which causes the species to spread out over a surface in space. Mathematically, reaction-diffusion systems take the form of semi-linear parabolic partial differential equations [98; 110; 125].

Using mathematical modeling as a viable tool, complex biological processes are studied. Mathematical modeling can be extremely helpful in analyzing factors that may contribute to the complexity intrinsic in insufficiently understood tumor–immune as well as predator–prey interactions. Likewise, the primary objective of the mathematical modeling of tumor–immune and predator–prey models are, briefly, the analysis of the interplay inside and between biological species and their artificial surrounding, and the examination of the temporal transformation of clusters of individuals of different biological species. It is however true that space and time are indivisible *sibling co-ordinates* and only when population densities (tumor–immune system or predator–prey system) are contemplated in both space and time, actual dynamics can be understood [9; 17; 52; 68; 98; 104; 108; 131; 194; 197].

Majority of models in mathematical ecology or tumor–immune interaction deal with non-spatial variant. The rate of change of the number of individuals u in a population may be manifested as the derivative with respect to time t, du/dt. The model equations of a biological community of interacting individuals and their environment are then founded by equating this derivative to another relation expressing the effect of species interaction on population. Same is the situation with tumor–immune interacting models. This type of straightforward analysis is not practicable when spatial models are considered. Directly connected to species interplay is the

net population via an arbitrary infinitesimal piece of space rather than the spatial rate of change of the population itself, and thus a reasonable manifestation is unreachable without knowledge of the mechanism of motion of the individuals.

1.1 Biological Preliminaries

1.1.1 What is Cancer?

Cancer is a disease which is caused by the abnormal function of our own cells [61; 156]. The growth, proliferation (or differentiation) and death of normal cells are closely controlled and regulated by variety of genetic and biochemical processes. When these processes are interrupted due to some factors, abnormal growth of cells occurs. Cancer starts as an abnormal cell which grows with time into a mass of cells, some of which can spread to the other locations in the body (metastasize), where they grow and upset normal body functions. The causes of cancer may be the result of inherited mutation or environmental factors such as tobacco products, ultraviolet radiation, X-rays, chemicals, etc [156]. These environmental factors can change or alter the genetic makeup of a cell, which may cause the abnormal functioning of the cell. In cancerous cells, the normal control system that prevent abnormal cell growth and differentiation and the invasion of other tissues and organs are disabled.

1.1.2 What are Gliomas?

Gliomas are one of the most generic kind of brain tumors that starts in the gluey supportive tissue of the brain or spine. Gliomas can be gently growing (low category) or rapidly growing (high category) [4; 27; 68]. There are three kinds of gliomas that can generates by gluey supportive cells: astrocytoma, oligodendroglioma and ependymoma, and a tumor that shows the amalgamation of these kinds is called mixed glioma.

(I) Astrocytomas are brain tumors that arise from astrocyte cells, and astrocyte cells are particular type of gluey supportive cells (star-structure brain tissue) in the brain.

(II) Oligodendrogliomas are the rare kind of tumor that occurs in the brain.

Oligodendrogliomas begins from oligodendrocyte cells of the brain.

(III) Ependymomas are special kind of tumors that originates from the ependymal, a tissue of the central nervous system.

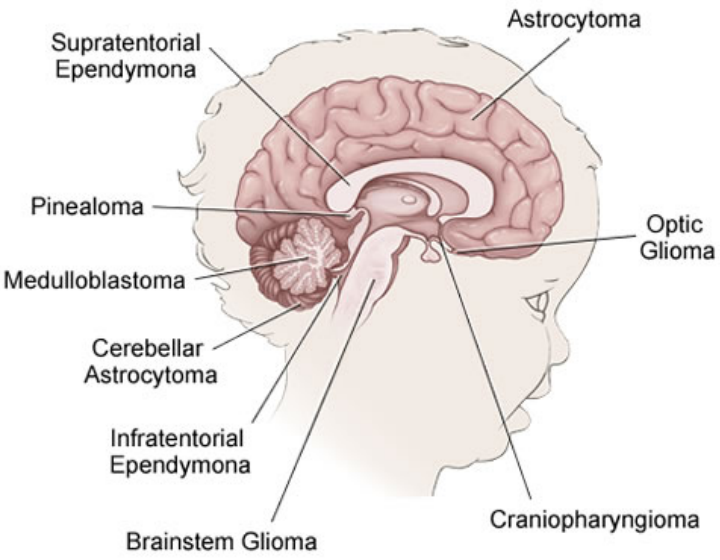

Figure 1.1: Various forms of gliomas in the brain (https://www.acco.org/brain-cancers/).

1.1.3 The Immune System

The immune system is host's natural defence mechanism comprising of many biological structures and processes within an organism that protect our body by fighting against pathogenic organisms and any other kind of diseases. Innate and adaptive immune systems are two major components of the defence mechanisms of the human body against external invaders, including cancer [4; 63].

The innate immune system is the first and foremost protector of our body from external invaders and other pathogens. The system incorporate cells and mechanisms that protect our body from infection by other foreign organisms and pathogens in a non-specific manner and it reacts rapidly against foreign antigen and cancerous cells. Most of the micro-organisms encountered by a healthy individual are rapidly cleared within a few days by the innate immune system. Macrophages, cytotoxic T-lymphocytes, natural killer cells, cytokines, dendritic and mast cells are

the principal components of innate immune system. The adaptive immune system is stimulated and influenced by innate immune system of our body to produce a stronger protection against any external pathogens.

The adaptive immune system is extremely specific to a particular pathogens and cancerous cells, they can easily recognize one micro-organisms from the others and non-self. The adaptive immunity, also called acquired immunity, uses particular antigens to strategically mount an immune response. Unlike the innate immunity, the adaptive immunity depends on small number of cells to carry out its tasks, namely, B cells and T cells. Both B cells and T cells are lymphocytes that are derived from specific types of stem cells, called multipotent hematopoietic stem cells, in the bone marrow. After they are made in the bone marrow, they need to mature and become activated. Each type of cell follows different paths to their final, mature forms. Unlike antibodies, which can bind to antigens directly, T cell receptors can only recognize antigens that are bound to certain receptor molecules, called major histocompatibility complex class 1 (MHC-I) and class 2 (MHC-II). These MHC molecules are membrane-bound surface receptors on antigen-presenting cells, like dendritic cells and macrophages. CD4+ and CD8+ play a role in T cell recognition and activation by binding to either MHC-I or MHC-II.

1.1.3.1 Effector Cells

In antitumor immunity, effector cells are actively involved in the destruction of tumor cells. Key effector cells include natural killer (NK) cells, cytotoxic T cells, and memory T cells. Natural killer cells are the primary cells of innate immunity. The first responders of the immune system, NK cells interact with activating and inhibitory signals from other cells. NK cells rapidly identify and attack tumor cells. Cytotoxic T cells are the primary effector cells of adaptive immunity. Triggered by specific threats, T cells are activated by antigen-presenting cells (APCs). Activated T cells recognize and directly kill cells that produce the target antigen. Memory T cells are derived from activated T cells. Providing sustained immune protection, memory T cells are long-lived and antigen-experienced, and they quickly respond to antigen recurrence. Memory T cells can differentiate into activated T cells, and can provide long-term immunity [90; 91].

1.1.3.2 Macrophages

Macrophages are the sizable leukocytes (white blood cells) that are the necessary part of the immune system. The term *macrophage* exactly means *big eater*. A macrophage has the capacity to search and consume viruses, bacteria, parasites, including cancerous cells. The origin of the macrophage is the white blood cells, called monocytes, which are framed by undifferentiated cells of multicellular organisms in our bone marrow. Monocytes can also travel via the bloodstream and when monocytes leave the blood, they convert into macrophages [1; 43].

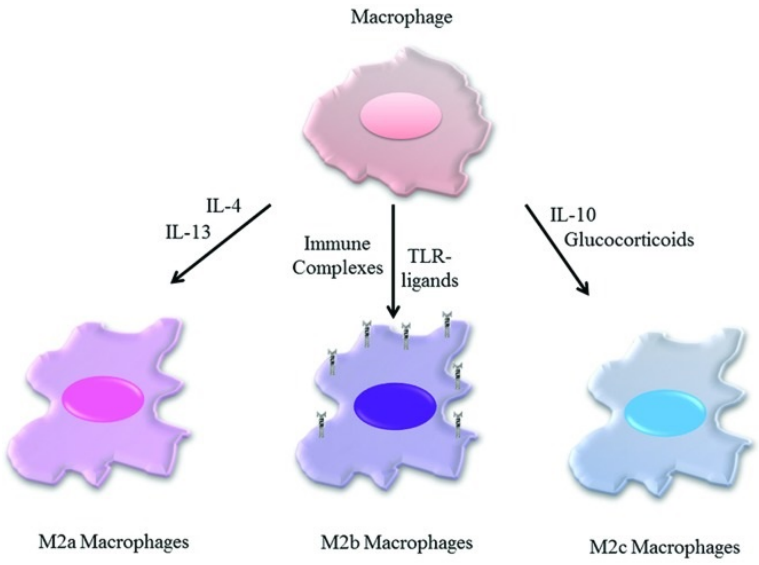

Figure 1.2: Macrophage (https://www.spandidos-publications.com/ijo/).

1.1.3.3 Cytotoxic T-lymphocyte

Cytotoxic T-lymphocytes are one type of white blood cells, which is also known as CD8+ T-Cells. It kills those cells which are infected, particularly with viruses, including cancer, or the cells that are damaged in various ways. Maximum number of the cytotoxic T cells express T cell receptors (TCRs), which can identify a particular antigen. An antigen is a molecule which can stimulate an immune response, and is generally produced by cancer cells or viruses. Antigens inside a cell are bound to class-I molecules and carried to the cell surface by the class-I MHC molecule, where

T-Cell recognizes them. While the TCR is specific for that antigen, it binds to the complex of the class-I MHC molecule and T cell destroys the cell. In order for the TCR for binding to the class-I MHC molecule, the former require to be accompanied by a glycoprotein called CD8, which binds to the maximum portion of the class-I MHC molecules. Hence, the T cells are called CD8+ T cells [29; 60].

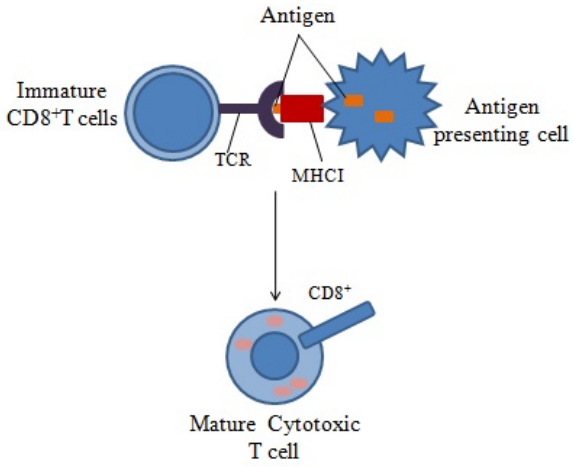

Figure 1.3: Antigen presentation stimulates immature T cells to become cytotoxic CD8+ cells (https://goo.gl/images/XyvxGg).

1.1.3.4 Transforming Growth Factor Beta (TGF-β)

TGF-β is a multi-functional cell protein that belongs to the large family of the transforming growth factor. There are four distinct isoforms of TGF-β, viz., TGF-β_1, TGF-β_2, TGF-β_3 and TGF-β_4. The growth inhibitors TGF-β, inhibit the development of most cell kinds. They can affect cell proliferation and differentiation via indirect procedures involving regulation of expression of cytokines, extracellular matrix molecules and their respective receptors. They are dominant immunosuppressive representatives. They also propel the creation of connective tissue, thereby stimulating lesion medication [50; 186].

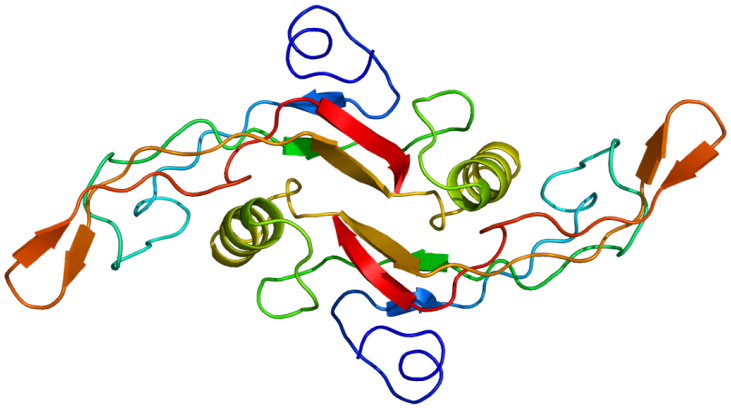

Figure 1.4: Transforming growth factor beta (TGF-β) (https://goo.gl/images/).

1.1.3.5 Interferon Gamma (IFN-γ)

IFN-γ is a cytokine, and the source of IFN-γ is cytotoxic T-lymphocytes. IFN-γ is essential for immunity against pathogenic organisms as well as tumor control. IFN-γ is a crucial activator of macrophages and inducer of type II Major-Histocompatibility-Complex (MHC) molecules, and MHC is a group of the sequence of DNA or RNA that codes for long string of amino acid residues, found on the cells surface that support the immune system recognize exotic physical matters. Nevertheless, deviant IFN-γ expression has been connected with a number of auto-immune and auto-incendiary diseases [155].

1.1.4 Predator–Prey System

Predator–prey system represents the functional dependence of one species on another, where the first species depends on the second species for food. Predation is a mode of life in which food is primarily obtained by killing and consuming organisms. The prey is part of the predator's habitat and if the predators do not get any prey for food, then they become extinct. The functional dependence in general depends on many factors, namely, the various species densities, the efficiency with which the predator can search out and kill the prey, and the handling time [10; 57; 187].

Figure 1.5: Interferon gamma (IFN-γ) (https://goo.gl/images/LQfNno).

1.1.4.1 Herd Behavior

The term 'herd' is used to describe a group of animals of the same species. The herd may be a natural formation, as in the case of wild animals, or may be formed by human intervention, as in the case of domestic animals like cattle. Herds offer individual animal companionship, better foraging opportunities and more chances for mating and reproduction. A herd also offers more protection against predators than a solitary animal would otherwise have on its own. The individual animals in the herd copy or imitate the behavior of the other animals in the herd, particularly that of their closest neighbors. As a result, all the herd members behave in a related fashion and this allows the entire herd to respond to an external circumstance in a similar way, for example, when it moves in a certain direction to get away from an attacking predator. Each individual animal tries to behave exactly as its neighbors in order to protect itself, and tries to minimize the danger to itself by moving along with the others and trying to get deeper into the herd.

The herd behavior of the preys is related to group defence, in which the preys at the boundary of the group hurt most, from the attacks of the predators. The number of preys remaining on the border of the group is proportional to the length of the perimeter of the ground region occupied by the group [25], which in turn is directly proportional to the square root of the area of that grounded region. Hence,

it is reasonable and logical to use square root term for the prey population to portray the model with herd behavior.

1.1.4.2 Hunting Cooperation

Hunting is one of the highly fascinating tactical natural instincts in the animal kingdom. A successful hunt requires a great deal of cooperation and coordination within the group. Hunting cooperation in animal kingdom are very frequent, for example, group hunting enables lionesses to have greater success in capturing preys and it involves both divisions of work and role specialization. It has been connected to the social system of animal species and the evolution of society and thus provides a unique approach to study cooperative behavior [5; 24; 37; 48; 67; 116; 150; 183; 185; 195].

1.2 Mathematical Preliminaries

Some mathematical methods and ideas have been depicted in this segment, which are used to examine the nonlinear dynamics and pattern formation (spatiotemporal models), introduced in this thesis. The details of the ideas are illustrated for non-spatial (ordinary differential equations) as well as spatial (reaction-diffusion partial differential equations) systems.

1.2.1 Stability Analysis

Let $X(t) \in R^n$ depicts the states of a system at time t. The dynamics of the system is ruled by a system of first order nonlinear ordinary differential equations:

$$\dot{X}(t) = G(X(t), \theta), \quad X(0) = X_0, \tag{1.1}$$

where $X = [x_1, x_2, ..., x_n]^T$ stands for the n state variables, θ holds the parameter values and G is a nonlinear function of the state variables and parameter values. If $G(X_*) = 0$, then X_* ia a equilibrium solution of the system. Consider X_0 to be its neighboring point. The equilibrium solution X_* is stable if for all $\epsilon > 0$, there is a $\delta > 0$ such that

$$\| X(t) - X_* \| < \epsilon, \qquad \text{whenever } \| X_* - X_0 \| < \delta.$$

That is, X_* is stable if the equilibrium solutions go ahead to X_* at a said time, stay close to X_* for each future time. X_* is asymptotically stable if neighboring solutions not only stay close, but also approach to X_* as t goes to infinity, for each future time, that is, X_* is stable and

$$\lim_{t\to\infty} X(t) = X_*,$$

then the solution X_* is asymptotically stable.

$$\text{Asymptotic Stability} \Rightarrow \text{Stability}.$$

Stability of an equilibrium solution is a local property. An equilibrium solution X_* which is not stable is called unstable.

1.2.1.1 Local Stability Analysis

The system of interacting populations

$$\frac{dX_i(t)}{dt} = G_i(X_1, X_2, ..., X_n), \tag{1.2}$$

with initial conditions

$$X_i(0) = X_{i0} \geq 0, \qquad i = 1, 2, ..., n. \tag{1.3}$$

Let us suppose that the function G_i is such that the solution of above system is unique.

Let $X(t)$ be any other solution in the vicinity of equilibrium solution X_*, then

$$X = X_* + \eta, \tag{1.4}$$

where $\eta = (\eta_1, \eta_2, ..., \eta_n)$ is a perturbation from the equilibrium solution. Then, the perturbation vector can be written as

$$\frac{d\eta}{dt} = \left.\frac{\partial G}{\partial X}\right|_{X=X_*} \eta \equiv A\eta, \tag{1.5}$$

where $A = (a_{ij})_{n\times n}$ is the variational matrix at the equilibrium solution X_*. Let $\eta(0)$ be the initial perturbation from the equilibrium solution X_*, then the formal matrix solution to (1.5) can be given by

$$\eta(t) = e^{At}\eta(0). \tag{1.6}$$

The system is stable about the equilibrium solution X_* if the perturbation $\eta(t)$ goes to zero as t tends to ∞. This is feasible only if the real parts of the characteristic values of the variational matrix A, namely, $\mathrm{Re}\{\lambda_i\}$, are negative for each i. If $\mathrm{Re}\{\lambda_i\} > 0$ for at least one value of i, then the equilibrium solution is unstable. Since $\eta(t)$ is the solution of linearized system (1.5), which is a close to actual nonlinear system, the stability is referred to local/linear stability only.

Therefore, the characteristic values of the variational matrix decide whether the equilibrium solution is linearly stable or unstable. The characteristic equation for the variational matrix can be written as

$$\det(A - \lambda I) = a_0\lambda^n + a_1\lambda^{n-1} + ... + a_n = 0, \qquad a_0 \neq 0. \tag{1.7}$$

The coefficients $a_i, i = 1, 2, ..., n$ of characteristic equation are all real. The system (1.2) is locally stable about the equilibrium point if all of the eigenvalues have negative real parts. On the other hand, the system is unstable if at least one of the eigenvalues has positive real part. In other words, all the eigenvalues of Jacobian matrix must lie in the left half of the complex plane. Accordingly, the necessary condition (not sufficient) for all eigenvalues to have negative real part is

$$\text{Trace } (A) < 0.$$

In the special case, if Trace $(A) = 0$, then either at least one eigenvalue must lie in the right half plane, or all eigenvalues must be purely imaginary (the pathological case of neutral stability). Another necessary, but not sufficient, condition is

$$(-1)^n \det |A| > 0.$$

Routh-Hurwitz Criterion gives necessary and sufficient conditions to make certain that the real part of all characteristic roots are negative that is belongs to left half complex plane. These conditions, collectively $a_n > 0$, are [121].

$$H_1 = a_1 > 0, \; H_2 = \begin{vmatrix} a_1 & a_3 \\ 1 & a_2 \end{vmatrix} > 0, \; H_3 = \begin{vmatrix} a_1 & a_3 & a_5 \\ 1 & a_2 & a_4 \\ 0 & a_1 & a_3 \end{vmatrix} > 0,$$

$$H_k = \begin{vmatrix} a_1 & a_3 & . & . & . & . \\ 1 & a_2 & a_4 & . & . & . \\ 0 & a_1 & a_3 & . & . & . \\ 0 & 1 & a_2 & . & . & . \\ . & . & . & . & . & . \\ 0 & 0 & . & . & . & a_k \end{vmatrix} > 0, \qquad k = 1, 2, 3, ..., n \tag{1.8}$$

If the values of parameters are such that the above restrictions are simultaneously satisfied, then the given system will be locally asymptotically stable at X_*.

1.2.2 Functional Responses

Functional response is the intake rate of a consumer as a function of food density. The nonlinear functional response was on the basis of a extensive reason regarding the distribution of time of a predator between two activity: *prey searching* and *prey handling*. Functional response is framed in terms of behavior of a particular predator, they are generally included at the level of population in systems that incorporate breeding and demise. The term density is more suitable than functional response since this describes the invasion conduct of the consumer for the natural resources. Functional response is associated with the numerical response, which is the rate of reproduction of a consumer as a function of food density. Following Crawford Stanley Holling (1959), functional response are usually classed into four types, type-I, II, III and IV [75; 76].

Let $f(x)$ is the response of a predator with respect to the specific prey and it is said to be a Holling type functional response if the following conditions hold

(i) $f(0) = 0$, *i.e.* all pass through the origin,

(ii) $f^{'}(x) \geq 0$, all are increasing.

Type-I: $f(x) = ax$, where $a > 0$. This linear functional response assume that the attack rate of the particular consumer accelerates linearly with the density of prey but then quickly and unexpectedly reaches a constant value when consumer is satisfied.

Type-II: $f(x) = \frac{ax}{1+bx}$, where $a > 0$, $b > 0$. This functional response depicts the attack rate accelerates at a decelerating rate with the density of prey until it becomes constant at saturation.

Type-III: $f(x) = \frac{ax^2}{b^2+x^2}$, where $a > 0$, $b > 0$. Type-III functional response in which the attack rate increases initially and then decreases towards satiety. Type-III functional response is naturalistic opponents, which easily move from one food species to another and which concentrate their feeding in areas where definite resource are plentiful.

Type-IV: $f(x) = \frac{ax}{\frac{x^2}{b}+x+c}$, where $a > 0$, $b > 0$, $c > 0$. If $b \to \infty$, then type-IV functional response approaches to type-II. In type-IV functional response, the attack rate initially accelerates gradually, reaches its peak and then decelerates to zero. Such a circumstance may appear because of limitation in food availability for multiple species but when providers of food are depleted, then nevertheless multiple species the available food becomes very low.

1.2.3 Bifurcations

The theory of bifurcation is the mathematical study of sudden changes in the qualitative behavior of the solutions of a nonlinear dynamical system. Bifurcation analysis shows the long term dynamics of the interacting population depending on the system parameters. In particular, equilibrium point(s) can be created, destroyed or their stability can change due to change of parameter values. The parameter values for which the bifurcation occurs are called bifurcating points. In this thesis, we particularly focused on local bifurcations, which occur when a small change in the parameter value of a given dynamical system causes a sudden change in the qualitative behavior of the system in the neighborhood of a critical point of the system. Scientifically, they are important since they provide models of transitions and stabilities as the control parameter is varied. Some different type of local bifurcations are as follows:

- **Hopf bifurcation**: Hopf bifurcation is that type of bifurcation at which a stable equilibrium point loses its stability at a threshold value and gives birth to a limit cycle with the variation of the bifurcation parameter. The system experiences Hopf bifurcation when a purely complex conjugate crosses the boundary of stability. The Hopf bifurcation destroys the temporal symmetry of a system and gives rise to oscillations, which are uniform in space and periodic in time. Two types of Hopf bifurcation are observed, one is supercritical and other is subcritical. Supercritical Hopf bifurcation is a phenomenon in which the unstable limit cycle becomes stable at the bifurcation point. Subcritical Hopf bifurcation is a phenomenon in which the stable limit cycle become unstable at the bifurcation point.

- **Turing bifurcation**: Turing bifurcation is the primary bifurcation that give rise to spatiotemporal patterns, and crucial for almost all reaction-diffusion type mathematical systems for pattern formation in embryology, ecology, epidemiology and to some other areas of biology, physics and chemistry [8; 105; 120; 122; 179]. The primary concept of the Turing bifurcation is that a uniform steady-state solution can be stable to uniform spatiotemporal perturbations, but unstable to definite spatiotemporally changing perturbations, leading to the formation of patterns, that is, a spatial pattern. The straightforward model to contemplate mathematically is fundamentally treated by Turing in 1952, viz, two reaction-diffusion type partial differential equations, the interacting chemicals having distinct coefficients of diffusion. For appropriate reaction kinetics, as the proportion of diffusivity increases (or decreases) from unity, e.g., there is a critical value at which the homogenous equilibrium solution becomes unstable to a particular spatiotemporal mode. Such kind of bifurcation is called the Turing bifurcation.

1.3 Diffusive instability

Spatial patterns are formed via the diffusive instability of the uniform equilibrium solution to small spatiotemporal perturbations. If the uniform equilibrium solution is stable, then small spatiotemporal perturbations from the equilibrium state will

attract towards the equilibrium state. In 1952, Alan Mathison Turing, pointed out how a reaction-diffusion system, showing such instabilities, can form diffusive patterns [179].

Alan Turing, in 1952, demonstrated that the reaction-diffusion system may form the spatial pattern, if the following two conditions holds

- the coexistence steady-state is linearly stable in the non-spatial (without diffusion) system, and
- after adding the diffusion term in system, the coexistence steady-state is linearly unstable.

Proper mathematical analysis demonstrates that, in the beginning of instability, the model initially becomes unstable with regard to a spatiotemporally non-homogenous perturbation with a definite wave-number. Such type of instability is called a **Diffusive-Instability** (Turing instability).

The mathematical foundation of diffusive instability is considered with two state variables, X_1 and X_2, which are subject to one dimensional space, namely,

$$\begin{aligned} \frac{\partial X_1}{\partial t} &= G_1\big(X_1, X_2\big) + d_1 \frac{\partial^2 X_1}{\partial x^2}, \\ \frac{\partial X_2}{\partial t} &= G_2\big(X_1, X_2\big) + d_2 \frac{\partial^2 X_2}{\partial x^2}, \end{aligned} \tag{1.9}$$

where x is space coordinate and t is time. d_1 and d_2 are diffusion coefficients of X_1 and X_2 respectively. $G_1\big(X_1, X_2\big)$ and $G_2\big(X_1, X_2\big)$ are the arbitrary interaction terms of X_1 and X_2 respectively.

To understand the effect of diffusion in pattern formation we assume that in absence of diffusion, that is, when solutions are well mixed, the system has some positive spatially homogeneous steady state, (X_1^*, X_2^*). Mathematically, this means that

$$\begin{aligned} \frac{\partial X_1^*}{\partial t} &= 0 = \frac{\partial X_2^*}{\partial t}, \\ \frac{\partial^2 X_1^*}{\partial x^2} &= 0 = \frac{\partial^2 X_2^*}{\partial x^2}, \end{aligned} \tag{1.10}$$

$$\Rightarrow \quad G_1\big(X_1^*, X_2^*\big) = 0 = G_2\big(X_1^*, X_2^*\big). \tag{1.11}$$

Additionally, we assume that $(\mathrm{X}_1^*,\ \mathrm{X}_2^*)$ is stable with respect to spatially uniform perturbations, that is, system is stable without diffusion.

To examine the effects of small nonhomogeneous perturbation on the stability of the system with respect to homogeneous steady state, we write

$$\begin{aligned} X_1\big(t,x\big) &= X_1^* + X_1^{'}(t,x), \\ X_2\big(t,x\big) &= X_2^* + X_2^{'}(t,x). \end{aligned} \tag{1.12}$$

It is assumed that the perturbations are sufficiently small, that is, we analyze the local stability of the system. Substituting (1.12) into (1.9), using (1.10), and linearizing the equations, we obtain

$$\begin{aligned} \frac{\partial X_1^{'}}{\partial t} &= a_{11}X_1^{'} + a_{12}X_2^{'} + d_1\frac{\partial^2 X_1^{'}}{\partial x^2}, \\ \frac{\partial X_2^{'}}{\partial t} &= a_{21}X_1^{'} + a_{22}X_2^{'} + d_2\frac{\partial^2 X_2^{'}}{\partial x^2}, \end{aligned} \tag{1.13}$$

where

$$\begin{aligned} a_{11} &= \left.\frac{\partial G_1}{\partial X_1}\right|_{\left(X_1^*,\ X_2^*\right)}, \quad a_{12} = \left.\frac{\partial G_1}{\partial X_2}\right|_{\left(X_1^*,\ X_2^*\right)}, \\ a_{21} &= \left.\frac{\partial G_2}{\partial X_1}\right|_{\left(X_1^*,\ X_2^*\right)}, \quad a_{22} = \left.\frac{\partial G_2}{\partial X_2}\right|_{\left(X_1^*,\ X_2^*\right)}, \end{aligned} \tag{1.14}$$

and $X_1^{'}$ and $X_2^{'}$ are perturbations from X_1^* and X_2^*. Equations (1.13) can be written in the compact matrix form:

$$X_t^{'} = AX^{'} + DX_{xx}^{'}, \tag{1.15}$$

where

$$\begin{aligned} X^{'} &= \begin{pmatrix} X_1^{'}(t,x) \\ X_2^{'}(t,x) \end{pmatrix} = \begin{pmatrix} X_1(t,x) - X_1^* \\ X_2(t,x) - X_2^* \end{pmatrix}, \\ A &= \begin{pmatrix} a_{11} & a_{12} \\ a_{21} & a_{22} \end{pmatrix}, \\ D &= \begin{pmatrix} d_1 & 0 \\ 0 & d_2 \end{pmatrix}. \end{aligned}$$

For linear stability analysis, it is sufficient to assume solution of (1.13) in the form

$$\begin{aligned} X_1^{'} &= \exp(\mu t + ikx), \\ X_2^{'} &= \exp(\mu t + ikx), \end{aligned} \tag{1.16}$$

where k and μ are the wavenumber and frequency, respectively. Corresponding characteristic equation is

$$\begin{vmatrix} a_{11} - d_1k^2 - \mu & a_{12} \\ a_{21} & a_{22} - d_2k^2 - \mu \end{vmatrix} = 0. \tag{1.17}$$

Solving for μ, we obtain

$$\mu = \frac{1}{2}\Bigg(a_{11} + a_{22} - k^2(d_1 + d_2) \pm \sqrt{\Big(a_{11} + a_{22} - k^2(d_1 + d_2)\Big)^2 - 4\Big((a_{11} - d_1k^2)(a_{22} - d_2k^2) - a_{12}a_{21}\Big)}\Bigg).$$

The condition $k = 0$ corresponds to the neglect of diffusion and, by definition, perturbations of zero wavenumber are stable when diffusive instability sets in. It is thus required that

$$\begin{aligned} a_{11} + a_{22} &< 0, \\ a_{11}a_{22} - a_{12}a_{21} &> 0. \end{aligned} \tag{1.18}$$

Diffusive instability sets in when at least one of the following conditions is violated subject to the conditions (1.18):

$$\begin{aligned} a_{11} + a_{22} - (d_1 + d_2)k^2 &< 0, \\ (a_{11} - d_1k^2)(a_{22} - d_2k^2) - a_{12}a_{21} &> 0. \end{aligned} \tag{1.19}$$

However, the first condition $a_{11}+a_{22}-(d_1+d_2)k^2 < 0$ is not violated as $a_{11}+a_{22} < 0$, due to stability of spatially homogenous system. Hence, only violation of the second condition $(a_{11} - d_1k^2)(a_{22} - d_2k^2) - a_{12}a_{21} > 0$ gives rise to diffusive instability. Reversal of the second inequality of (1.19) yields

$$Q\big(k^2\big) = d_1d_2k^4 - \big(d_1a_{22} + d_2a_{11}\big)k^2 + a_{11}a_{22} - a_{12}a_{21} < 0. \tag{1.20}$$

The minimum of $Q\big(k^2\big)$ occurs at $k^2 = k_m^2$, where

$$k_m^2 = \frac{d_1 a_{22} + d_2 a_{11}}{2 d_1 d_2} > 0. \tag{1.21}$$

Thus, a sufficient condition for instability is that $Q\big(k_m^2\big)$ must be negative, implying,

$$\big(a_{11}a_{22} - a_{12}a_{21}\big) - \frac{\big(d_1 a_{22} + d_2 a_{11}\big)^2}{4 d_1 d_2} < 0. \tag{1.22}$$

Combination of (1.18), (1.21), and (1.22) leads to the following final criterion for diffusive instability:

$$d_1 a_{22} + d_2 a_{11} > 2\big(a_{11}a_{22} - a_{12}a_{21}\big)^{\frac{1}{2}}\big(d_1 d_2\big)^{\frac{1}{2}} > 0. \tag{1.23}$$

The critical conditions for the occurrence of the instability are obtained when the first inequality of (1.23) is an equality.

1.4 Higher order instability

The stipulation for diffusion-driven instability and spatiotemporal pattern formation in reaction-diffusion system is obtained with the help of local stability analysis of dynamical model close to equilibrium state. As a consequence, the prediction for spatial patterns away from linear system can not be formed with linear structure. Also, the role of nonlinearity associated with reaction-diffusion system can not be captured by linear analysis of the system. The procedure for higher order instability in reaction-diffusion system is based on taking into account spatial perturbations terms of higher order [56; 58; 152].

1.5 Spatiotemporal chaos

The concept of chaos originally came into existence in the context of non-spatial dynamics of a spatially homogenous system. The consideration of space in the model system makes the dynamics more complex and creates the possibility of getting chaos even in those cases where it is almost impossible otherwise. This phenomenon is termed as spatiotemporal chaos, to distinguish it from the purely non-spatial chaos of a homogenous system. When the local kinetics of the system is oscillatory, for a

extensive class of initial states, the evolution of the system leads to the formation of a non stationary asymmetrical structures corresponding to spatiotemporal chaos. First, the spatiotemporal chaos appears inside a subdivision of the whole domain of the system. This subdivision of whole space then steadily get bigger with time and, eventually, the spatiotemporal chaos occupies the entire domain, replacing the steady pattern [9; 10; 39; 116; 133; 142].

1.6 Literature Review

The primary work of Alan Mathison Turing (1952) in the field of spatial pattern formation was motivated by the nonlinear complexity of self-organizing models [179]. The impact of diffusion on pattern's emergence in reaction-diffusion models has been discussed extensively by Alan Turing. Turing introduced the diffusive instability, in which an initially stable steady state of a dynamical system can become unstable if we contemplate diffusion in the dynamical system. If the parameter value of diffusion coefficients reaches a critical value, the model will show Turing bifurcation. The research work of Alan Turing in the area of spatial pattern formation, a subarea of mathematical biology. Turing's patterns in biology has obtained notability, when in 1972, Segel et al. gave a biologically equitable formulation of a diffusive model and examined its properties with the help of numerical simulations [157]. Spatial patterns formation in nature are ubiquitous, with illustrations like zebra stripe patterns on animals skin, Turing patterns in a coherent quantum field, language dispersal and competition in the community, or diffusive patterns in predator–prey models [8; 122; 136; 157]. The spatial patterns formation factor of ecological, and tumor–immune interplays has been recognized as an vital component in how ecological communities are composed [19; 93; 110; 115; 122; 124; 130; 144]. Pioneering research work of Turing [179], the systematic investigation on spatial patterns modeled by reaction-diffusion partial differential equations models, which gives a general mathematical structure for depicting spatial pattern in models from various field of study including but not restricted to chemistry [126; 182; 190], physics [8; 16; 38; 78; 192], biology [19; 83; 96; 100; 110; 133; 134; 194], and so on, notably

during the last several decades. Applications of Turing's phenomenon in mathematical biology differ from modeling of the spatial dynamics of tumor–immune system [108; 128] to the spatiotemporal complexity of predator–prey systems [141; 144; 157].

1.6.1 Tumor–immune systems

Tumor–immune system dynamics has a long history in mathematical biology. The theoretical study of tumor–immune dynamics has been investigated by many researchers [11; 12; 13; 27; 28; 33; 35; 46; 47; 59; 61; 62; 63; 68; 72; 73; 81; 82; 88; 90; 91; 95; 104; 106; 108; 119; 122; 123; 128; 131; 132; 135; 137; 145; 147; 148; 154; 160; 165; 167; 169; 176; 177; 178; 194]. We first look through some existing mathematical models, where the authors have studied the interaction between tumor/cancer cells and the host immune system through the mathematical modeling using the simplest models to the more complicated models.

Tumors are well known for their potential for invasive proliferation as well as their diffusive aggression of the normal appearing parenchyma peripheral to the bulk lesion. The growth and progression of a solid tumor is a complex phenomenon, incumbent on the interaction of several internal and external components, that is, interactions between the tumor and the immune system components [61]. Several tumors are solid and disperse factually by pressure effects induced by the increasing number of tumor cells. Some tumor cells have the potential to migrate beyond the domain boundary of the tumor growth, thus creating a diffusive tumor.

Over the last several decades, tumor evolution and the dynamics of the immune system components have been a considerable focus for both experimentalists and mathematical modelers. Mathematical modeling in this area stems from the early chemical diffusion and differential equation models of Burton and Greenspan [27; 68] and has grown into an extensive field of literature with studies presented using ordinary and partial differential equations [27; 28; 35; 63; 68; 72; 73; 90; 91; 108; 128; 131; 145; 147; 148; 165; 167; 194], cellular automata [47; 59; 135] and many statistically based studies [113; 139; 154; 176].

Burton [27] developed a diffusive model which investigated both the distribution of oxygen in a spheroidal tumor where the blood supply is completely confined to the surface and the resulting relative radius of the central zone to the total radius, which

was then used to describe how the growth curve could fit a Gompertzian expression. In [28], authors proposed a mathematical model to explain the growth of an avascular tumor in response to an externally nutrient. The evolution of the tumor depends on the equilibrium between expansive strengths caused by cell spreading and cell-cell adhesion strengths which exist to maintain the tumor's compactness. Greenspan [68], proposed a simple mathematical model of tumor growth by diffusion, which is constructed in order to examine and evaluate different hypotheses concerning the evolution of a solid carcinoma. A primary objective of Greenspan's study is to infer the chemical source of growth inhibition from the most easily obtained data.

Kuznetsov and Knott [90] proposed a deterministic model where they describe the mechanisms underlying tumor growth, suppression and regrowth and fit to data on B-cell lymphoma. They indicated that either a modest change in the effectiveness of killer suppression or the existence of a variant non-immunogenic clone of the tumor cells can explain the regrowth of a tumor after initial suppression. Kuznetsov et al. [91] proposed a mathematical model considering the interaction between cytotoxic T-lymphocytes (termed as effector cells) and its response to the growth of immunogenic tumor. They studied the immune-stimulating of tumor growth, *sneaking through* of the tumor and formation of a tumor dormant state. From the numerical simulation, using realistic parameter values, it has been predicted that for a large set of system parameters that, the course of the growth of tumor and its clinical manifestation have a recurrent profile with 3–4 months cycle. Banerjee et al.[12] also presented a mathematical model for the interactions between the glioma and the components of immune system, which objects in designing efficacious glioma therapy. The system encompasses deliberations of the interactive dynamics of brain tumor, macrophages, CD8+T-cells, TGF_{β}, IFN_{γ} and the T11 target structures. They discussed sensitivity analysis, and identify which variables are more sensitive then the others and the parameters are computed from the published *in-vivo* data. Numerical simulations were used for model validation and confirmation.

In [128], Owen and Sherratt presented a brief survey of the main properties and interactions of such tumor associated macrophages, leading to the construction of a mathematical model for the spatial interactions of tumor cells, macrophages and

normal tissue cells, focusing on the ability of macrophages to kill tumor cells. Analysis of the homogeneous steady states shows that, normal tissue is unstable to the introduction of mutant cells despite such an immune response, but that the composition of the resulting tumor can be significantly altered. Pettet et al. in [145], proposed a mathematical model to explain the observed internalization of microspheres and H-thymidine labeled cells in steady state multicellular spheroids. The model uses the conventional ideas of nutrient diffusion and consumption by the cells. The model accounts for the spatial and temporal variations in the cell categories together with mitosis, conversion between categories and cell death. Numerical solutions demonstrate that the model predicts the behavior similar to existing models but has some novel effects.

Banerjee and Sarkar [154] proposed a predator–prey like tumor–immune interaction deterministic model by considering tumor cell as prey and cell mediated immune system (cytotoxic T-lymphocytes) as predator. By allowing random fluctuations around the positive interior equilibrium point, they extended their model to a stochastic model and investigated its stability analytically as well as numerically. Tran et al. [176] proposed a stochastic model which describes subpopulation emerging in heterogeneous tumors. They have used the Fokker-Planck or forward Kolmogrov equation in their model. They observed from the numerical simulation that the stochastic model describes the same basic dynamics as its counter part via a convective component, but that for each simulation, a distribution of tumor size mixes can also be derived from diffusion component in the model. These distributions yield estimates for subpopulation extinction probabilities. Swanson et al. [165] proposed a mathematical model of gliomas based on spreading and diffusion rates to include the impacts of mobility of cell in white matter as compared to grey matter. Numerical simulations of Swanson et al. model shows good understanding with clinically observed solid tumor geometries and propose ways of tumor invasion not noticeable on computed tomography or magnetic resonance imaging images. In [194], authors assume that the diffusion is ubiquitous within cells, and it is competent of propelling spontaneous spatial pattern in reaction-diffusion systems on a spatially homogeneous domain. In this study, authors investigate the dynamics of a diffusive cancer system controlled by microRNA and obtain the conditions that the

system undergoes a Hopf-bifurcation and a Turing-bifurcation, and also obtain the explicit condition on how the dynamics of the diffusive cancer network evolve.

1.6.2 Predator–prey systems

Mechanisms and scenarios characterizing the spatial population distribution of ecological species in spatial habitat are a focus of special interest in population dynamics. The spatial population distribution is affected by the proliferation capacity of the species and interactions between individuals [184]. Spatial pattern formation of predator–prey systems have started based upon the elementary work of Alan Turing on morphogenesis [179]. The spatial predator–prey systems are studied to comprehend the role of random mobility of the prey and predator, inside their residence. A fully comprehensive elucidation of the spatial impact on ecological species interplays can be observed in the book, written by Okubo et.al. [125].

Spatial mathematical model is an appropriate tool for investigating fundamental mechanism of complex spatiotemporal population dynamics. An appropriate mathematical structure to explain the spatial aspect of population dynamics is specified by reaction–diffusion equations. Reaction–diffusion models were initial applied to describe the ecological pattern formation by Segel and Jackson in 1972 [157], based on the primary work of Alan Turing [179]. Over the last several decades, lot of articles have been published on the spatial dynamics of predator–prey models based on reaction–diffusion equations and different types of patterns have been depicted for these models [8; 9; 10; 14; 18; 19; 34; 52; 53; 55; 70; 74; 99; 104; 105; 109; 114; 117; 120; 122; 125; 141; 142; 144; 152; 157; 159; 170; 180; 181; 183; 185; 187; 191; 193; 197].

Segel and Jackson [157] proposed a predator–prey mathematical model with diffusion, and exhibit that in the existence of diffusion, it is feasible that small change in the parameter values will bring about a interruption of the homogenous stationary state and the evolution of spatial nonhomogeneous densities distributions at a definite wavelength. In [10], the authors contemplate spatial distribution of the densities of preys and predators, in a ratio-dependent model. They also exhibits that the model can evolve the diffusive patterns inside the Turing space. Banerjee et al. [9], consider a improved spatial model of the non-spatial Holling–Tanner model, by

introducing the diffusive terms. In this study, the authors analyzed in detail with both Turing and non-Turing outlooks. Guan et al.[70] presented the spatiotemporal dynamics of improved LeslieGower predator–prey system. The authors also performed numerical simulations and observed that the system demonstrates complex spatial patterns, namely, spots patterns, stripes patterns and mixed patterns. The spatiotemporal dynamics of a predator–prey model is delineated by reaction–diffusion equations with logistic growth of the prey, and Holling type-II functional response of the predator, by Petrovskii et al. in [142]. They also exhibits that initially the spatial pattern begins inside a small domain of the system, and this small domain steadily evolves with time and, eventually, these spatial pattern occupy the entire domain. Yuan et al. [193] proposed a predator–prey model with square-root functional response and second order death term in predator population. They obtained the conditions for spatial patterns by using linear stability analysis. Using extensive numerical simulations, they found complex pattern replication, namely, spotted pattern, stripe pattern and mixed pattern in the Turing domain, by varying the death rate of predators.

Dubey et al. in [52] proposed a mathematical model for a predator–prey interplay with self and cross-diffusion term. This model is analyzed with positive initial condition and zero-flux boundary conditions. Conditions for local stability, global stability and instability are acquired. The impact of the wavelength which can drive a model to instability is explored. The impact of time-dependent diffusion coefficients on the stability of the model is also investigated. Spatial heterogeneity in few predator–prey systems has been noticed even though their surroundings habitat appears homogeneous [114]. To describe this spatial heterogeneity phenomenon, authors proposed a predator–prey interplay model with diffusive impacts. This model can reasonably be applied to certain earthly plant-herbivore models. In [117], Morozov et al. shows that, in this model, species spread through propagation of population wave fronts, there exists an factually distinct invasion system which we call a patchy (small isolated area) invasion. Authors show that the dynamics of this model corresponds to spatial chaos and compute the primary Lyapunov exponent. Eventually, the authors discuss the involvements of this phenomenon for invasive species management and control. Wang et al. in [187], explore the emergence of

predator–prey system with Michaelis Menten type functional response and reaction-diffusion. The outcomes of numerical simulations show that the density distribution dynamics of population transform is the emergence of stripe like or patched or existence of both. This study exhibits that the spatial system has not only more complex patterns in the space, but also chaos and spiral waves.

1.7 Organization of the Thesis

The aim of this thesis is to study mathematical models of interaction of tumor–immune system, and predator–prey interaction system, when space is taken into account. The main focus is on the analysis of the spatiotemporal dynamics of tumor cells and immune cells, and complex pattern formation, namely, spotted pattern, stripe pattern and mixed pattern in the predator–prey system by changing different parameter of the system. The numerical simulations are carried out to explore the heterogeneity and complexity in nonlinear mathematical models. This thesis consists of six chapters and are organized as follows:

Chapter 1 : A brief introduction of tumor–immune system, and predator–prey system, are given here. The necessary concepts of interaction of tumor–immune system, and predator–prey system are highlighted. Mathematical preliminaries which are required to analyze our models also stated here. Moreover, a brief literature review is given to illuminate the idea presented in the thesis.

Chapter 2 : A mathematical model, consisting of a system of two coupled reaction–diffusion equations describing the interaction between solid tumor and immune system (termed as effector cells), is proposed here. The main focus is on the analysis of the spatiotemporal dynamics of tumor cells and immune cells. The resulting system is analyzed and numerical simulations are presented. Different types of spatial patterns with respect to different initial conditions, and times are observed. Their analysis and mechanism of spatiotemporal pattern formation in immunogenic tumor are studied. Spatiotemporal perturbation around non-spatial steady state beyond the linear regime are obtained based on the analysis of higher order perturbation terms.

Chapter 3 : Gliomas are well known for their potential for aggressive proliferation as well as their diffusive invasion. A mathematical model, using reaction-diffusion equations, is proposed to study dynamics of glioma cells, macrophages, cytotoxic T-lymphocytes, immuno-suppressive factor TGF-β and immuno-stimulatory cytokine interferon-γ in spatiotemporal domain with the administration of immunotherapeutic agent T11 target structure (T11TS). First, we revisit the linear stability analysis of the model in the temporal domain, followed by rigorous investigation of the model in the spatiotemporal domain. Higher order stability is also discussed in the spatiotemporal domain. Using the combination of analytical and numerical techniques, we investigate the effect of T11 target structure on the growth and spread of malignant gliomas. It is observed that the immunotherapeutic agent T11 target structure along with the immune components, is able to control the aggressive spread of the malignant gliomas.

Chapter 4 : In this chapter, we have investigated a spatial predator–prey model with hunting cooperation in predators. Using linear stability analysis, we obtain the condition for diffusive instability and identify the corresponding domain in the space of controlling parameters. Using extensive numerical simulations, we obtain complex patterns, namely, spotted pattern, stripe pattern and mixed pattern in the Turing domain, by varying the hunting cooperation in predators and carrying capacity of prey parameters. The results focus on the effect of hunting cooperation in pattern dynamics of a diffusive predator–prey model and help us in better understanding of the dynamics of the predator–prey interaction in real environment.

Chapter 5 : In this chapter, we have investigated a diffusive predator–prey model exhibiting herd behavior for preys with linear and quadratic mortality term for predators. Using linear stability analysis, we obtain the conditions for diffusive instability and identify the corresponding Turing as well as non-Turing zone in the space of control parameters. Using extensive numerical simulations, we obtain spatiotemporal patterns for both non-Turing (model with linear mortality) and Turing (model with quadratic mortality) cases by varying mortality rates, the search efficacy of predators for preys and the rate of conversion of prey biomass to predator biomass. The non-Turing pattern exhibits spatiotemporal chaos whereas the Turing patterns focuses in many pattern dynamics and help us in the better understanding

of the dynamics of the predator–prey interaction in real environment.

Chapter 6 : Finally, results from overall investigations are summarized in this chapter along with a brief discussion on the scope for future research work.

Chapter 2

Spatiotemporal dynamics of immunogenic tumors

2.1 Introduction

In recent years, there are evidences indicating that the immune system can recognize and eliminate malignant tumors. The immune response to a tumor is usually cell mediated with cytotoxic T lymphocytes and natural killer cells, playing a dominant role. A number of mathematical models of the interactions between the immune system and a growing tumor have been developed and studied [4; 42; 43; 44; 69; 101; 113; 139; 149; 151; 173; 174]. The kinetics of cell mediated cytotoxicity *in vitro* have also been described by mathematical models [29; 94; 103; 112; 138; 139; 172; 173; 174]. With such models, numerical estimates of biologically significant parameters have been obtained, a number of phenomena interpreted, and predictions made. Many researches have begun to explore the mathematical modeling of different aspects of the spatial features associated with the immune response to solid tumor, where partial differential equations have been used considerably for the spatial aspects of tumor-immune system interactions [108; 127; 186; 188]. Numerical simulation and bifurcation analysis of these models have demonstrated diverse patterns of spatiotemporal dynamics of the immune and tumor cells within tumor tissue, even in dormant tumors, which are being controlled by cytotoxic T-lymphocytes.

A mathematical model describing the growth of a solid tumor in the presence of an immune system response is presented in [108], where the authors have studied the analysis of the spatiotemporal dynamics of tumor cells, immune cells and chemokineses in an immunogenic tumor. In [127], Owen et al. investigated the role of chemotaxis and chemokineses production, and the efficacy of macrophages as vehicle for drug delivery to hypoxic tumor sites. The model is based upon a growing avascular tumor spheroid, in which the volume is filled by tumor cells, macrophages and extracellular material, tumor cell proliferation and death is regulated by nutrient diffusion. In [188], Webb et al. developed a mathematical model to compare the responses of avascular tumor spheroids to two modes of action: either the macrophages deliver an enzyme that activates an externally applied pro-drug (bystander model), or they deliver cytotoxic factors directly (local model). The models Webb et al. developed comprise partial differential equations for a multi-phase mixture of tumor cells, macrophages and extracellular fluid, coupled to a moving boundary representing the spheroid surface. In [186], Wang et al. investigated the growth and motility of oncogene-expressing human mammary epithelial cells under exposure to TGF-β.

In this chapter, a mathematical model depicting the spatial dynamics of a solid tumor under the vigilance of the immune response (termed as effector cells), is presented. The spatial model is an extension of the model in [91]. The dynamics of the interplay between tumor cells and immune cells, in a solid tumor, at some stage prior to angiogenesis are discussed.

2.2 The mathematical model

A mathematical model of tumor and generic effector cells interaction through the system of nonlinear ordinary differential equations has already been studied in temporal domain by Kuznetsov et al. [91]. Motivated from their work and to make the model more realistic, we extend their model in a spatiotemporal domain to study its spatial dynamics. Let $E(X, Y, t)$ and $T(X, Y, t)$ be the densities of generic effector cells and tumor cells, respectively, at any time t and at spatial location (X, Y) within the square bounded domain Γ having boundary $\partial\Gamma$. The governing equations

are

$$\frac{\partial E\left(X,Y,t\right)}{\partial t} = s + \frac{pET}{g+T} - mET - dE + D_1\left(\frac{\partial^2 E}{\partial X^2} + \frac{\partial^2 E}{\partial Y^2}\right),$$
$$\frac{\partial T\left(X,Y,t\right)}{\partial t} = aT\left(1-bT\right) - nET + D_2\left(\frac{\partial^2 T}{\partial X^2} + \frac{\partial^2 T}{\partial Y^2}\right), \tag{2.1}$$

subjected to known non-negative initial distribution of populations,

$$E(X,Y,0) = E_0(X,Y) \geq 0, \quad T(X,Y,0) = T_0(X,Y) \geq 0,$$
$$(X,Y) \in \Gamma = [0,L] \times [0,L], \tag{2.2}$$

and zero-flux boundary conditions

$$\frac{\partial E}{\partial \nu} = \frac{\partial T}{\partial \nu} = 0, \quad (X,Y) \in \partial\Gamma. \tag{2.3}$$

Note: It is a well established fact that tumors secrete a diffusible chemical compound known as tumor angiogenesis factor (TAF) into the surrounding tissue. This stimulates nearby blood vessels to migrate towards and finally penetrate the tumor. When a tumor is removed, the tumor angiogenesis factor (TAF) diffuses away naturally over a certain period of time. To stop that, zero flux boundary conditions are considered, which means neither tumor or immune components leave the domain.

In the model, the tumor grow logistically in absence of any immune system with intrinsic growth rate a, that is, the maximal growth rate of the tumor cell population is a. $\frac{1}{b}$ is the utmost carrying competency of the biotic atmosphere of the tumor cell population and n is the rate at which effector cell eradicates tumor cells and the parameter m, is the rate of eradication of effector cell population by tumor cells. s is the constant rate of flow of effector cell population and d is the natural decay of the effector cells. The term $\frac{pET}{g+T}$ depicts the rate at which effector cell population accumulates in the realm of tumor cell population (localization due to the presence of the tumor), that is, immunogenicity. Here, the domain is assumed to be uniform, that is, the system parameters do not depend on space or time. The parameters D_1, a, b, n, D_2, s, p, g, m, d are all positive constants. D_1 and D_2 are diffusion coefficient of the effector and tumor cells, respectively. The governing system can be written in terms of dimensionless variables as follows:

$$\begin{aligned}\frac{\partial u(x,y,\tau)}{\partial \tau} &= \sigma + \frac{\rho uv}{\eta+v} - \mu uv - \delta u + \left(\frac{\partial^2 u}{\partial x^2} + \frac{\partial^2 u}{\partial y^2}\right),\\ \frac{\partial v(x,y,\tau)}{\partial \tau} &= \alpha v(1-\beta v) - uv + \kappa\left(\frac{\partial^2 v}{\partial x^2} + \frac{\partial^2 v}{\partial y^2}\right),\end{aligned} \tag{2.4}$$

$$\text{where,} \quad u = \frac{E}{E_0}, \quad v = \frac{T}{T_0}, \quad \sigma = \frac{s}{nE_0T_0}, \quad \rho = \frac{p}{nT_0}, \quad \beta = bT_0,$$
$$\eta = \frac{g}{T_0}, \quad \mu = \frac{m}{n} = \frac{k_3}{k_2}, \quad \delta = \frac{d}{nT_0}, \quad \alpha = \frac{a}{nT_0}, \quad \kappa = \frac{D_2}{D_1},$$
$$X = \sqrt{\frac{D_1}{nT_0}}\, x, \quad Y = \sqrt{\frac{D_1}{nT_0}}\, y, \quad t = \frac{\tau}{nT_0},$$

subjected to the initial conditions

$$u(x, y, 0) = u_0(x, y) \geq 0, \quad v(x, y, 0) = v_0(x, y) \geq 0, \quad (x, y) \in \Gamma, \tag{2.5}$$

and boundary conditions

$$\frac{\partial u}{\partial \nu} = \frac{\partial v}{\partial \nu} = 0, \quad (x, y) \in \partial\Gamma. \tag{2.6}$$

u, v are dimensionless effector and tumor cell densities, τ, x, y are dimensionless time and space variables and $\kappa\,(= D_2/D_1)$ is the ratio of diffusion coefficients.

2.3 Analysis of non-spatial system

Kuznetsov et al. [91] have done the detailed analysis of the non-spatial system. Here, we highlight few results that we need for the analysis of spatiotemporal system.

(i) The system has two equilibria, namely,

(a) $\mathrm{E}_1\left(\frac{\sigma}{\delta}, 0\right)$, (tumor free state).

(b) Interior equilibrium $\mathrm{E}_2(u^*, v^*)$, where $u^* = \alpha(1 - \beta v^*)$ and v^* be the root of the following cubic equation

$$C_3v^3 + C_2v^2 + C_1v + C_0 = 0,$$

with coefficients

$$\begin{aligned} C_0 &= \eta\left(\frac{\sigma}{\alpha} - \delta\right), \\ C_1 &= \frac{\sigma}{\alpha} + \rho - \mu\eta - \delta + \delta\eta\beta, \\ C_2 &= -\mu + (\mu\eta + \delta - \rho)\,\beta, \\ C_3 &= \mu\beta. \end{aligned}$$

The feasibility of the roots of above cubic equation can be checked using Descartes' rule of sign. Clearly, $C_3 > 0$. Possible variations in signs of cubic polynomial are as follows:

$+ \quad + \quad + \quad + \quad \rightarrow$ 0 positive roots
$+ \quad + \quad + \quad - \quad \rightarrow$ 1 positive roots
$+ \quad + \quad - \quad + \quad \rightarrow$ 2 positive roots
$+ \quad - \quad + \quad + \quad \rightarrow$ 2 positive roots
$+ \quad - \quad - \quad + \quad \rightarrow$ 2 positive roots
$+ \quad + \quad - \quad - \quad \rightarrow$ 1 positive roots
$+ \quad - \quad + \quad - \quad \rightarrow$ 3 positive roots
$+ \quad - \quad - \quad - \quad \rightarrow$ 1 positive roots

So, it is mathematically justified about the feasible existence of the interior equilibrium points. With the parameter values, given in Table (2.1), we get 3 positive roots, which is one of the possibility, verified by Descartes' rule of sign.

(ii) The general Jacobian matrix corresponding to the system [91] is given by

$$\mathbf{J}^* = \begin{pmatrix} a_{11} & a_{12} \\ a_{21} & a_{22} \end{pmatrix},$$

where

$a_{11} = \frac{\rho v}{\eta+v} - \mu v - \delta, \quad a_{12} = \frac{\rho u}{(\eta+v)} - \frac{\rho u v}{(\eta+v)^2} - \mu u, \quad a_{21} = -v, \quad a_{22} = \alpha - u - 2\alpha\beta v.$

(iii) The eigenvalues of the Jacobian matrix J^*, corresponding to the equilibrium point $\mathrm{E}_1\left(\frac{\sigma}{\delta}, 0\right)$ are $-\delta$, $(\alpha\delta - \sigma)/\delta$. It is clear from the eigenvalues that the equilibrium point $\mathrm{E}_1\left(\frac{\sigma}{\delta}, 0\right)$ is asymptotically stable if $\alpha\delta < \sigma$ and unstable if $\alpha\delta > \sigma$.

(iv) The characteristics equation about the equilibrium point (u^*, v^*) is

$$\lambda^2 - \left(\alpha - \delta - u^* - 2\alpha\beta v^* - \mu v^* + \frac{\rho v^*}{\eta + v^*}\right)\lambda + \frac{u^*\left[-\rho v^{*2} + \delta(\eta + v^*)^2\right]}{(\eta + v^*)^2} + \frac{\alpha(\eta + v^*)(-1 + 2\beta v^*)\{\delta(\eta + v^*) + v^*\left[-\rho + \mu(\eta + v^*)\right]\}}{(\eta + v^*)^2} = 0.$$

The system is stable if

$$\alpha - \delta - u^* - 2\alpha\beta v^* - \mu v^* + \frac{\rho v^*}{\eta + v^*} < 0$$

and

$$\frac{u^*\left[-\rho v^{*2} + \delta(\eta+v^*)^2\right] + \alpha(\eta+v^*)(-1+2\beta v^*)\{\delta(\eta+v^*) + v^*[-\rho+\mu(\eta+v^*)]\}}{(\eta+v^*)^2} > 0.$$

(v) The system parameters have the values, shown in Table (2.1).

(vi) With these set of parameters, the system

(a) is unstable about the tumor free equilibrium $(\frac{\sigma}{\delta},\ 0)$=(0.3155, 0).

(b) is stable about $(u^*, v^*) = (1.6092,\ 8.1897)$ and $(u^*, v^*) = (0.1729,\ 447.1)$ equilibrium points. The third value $(u^*, v^*) = (0.7598,\ 267.8)$ is unstable.

Parameters	Values	Parameters	Values	Source
s	$1.3 \times 10^4\ cells\ day^{-1}$	σ	0.1181	[91]
p	$0.1245\ day^{-1}$	ρ	1.131	[91]
g	$2.019 \times 10^7\ cells$	η	20.19	[91]
m	$3.422 \times 10^{-10}\ day^{-1}\ cells^{-1}$	μ	0.00311	[91]
d	$0.0412\ day^{-1}$	δ	0.3743	[91]
a	$0.18\ day^{-1}$	α	1.636	[91]
b	$2.0 \times 10^{-9} cells^{-1}$	β	0.002	[91]
n	$1.101 \times 10^{-7}\ day^{-1}\ cells^{-1}$	-	1.000	[91]
D_1	$1.0\ units$	κ	2.5	-
D_2	$2.5\ units$	-	-	-

Table 2.1: Parameter values used for numerical simulation.

2.4 Analysis of spatiotemporal system

Incorporating the diffusion terms into the growth equations for the effector and tumor cell population, we now investigate the spread of both effector and tumor cells in two dimensional domain. Taking the spatial perturbations about the interior equilibrium point, we get,

$$\begin{aligned} u(x,y,\tau) &= u^* + \epsilon \exp((k_x x + k_y(y))i + \lambda_k t), \\ v(x,y,\tau) &= v^* + \eta \exp((k_x x + k_y(y))i + \lambda_k t), \end{aligned} \tag{2.7}$$

where ϵ and η are chosen to be small and $k = \sqrt{\left(k_x^2 + k_y^2\right)}$ is the wave number.

Substituting (2.7) in (2.4), and linearizing the model equations around interior steady-state $\mathrm{E}_2\,(u^*, v^*)$, we obtain

$$\underline{\mathbf{w_t}} = \mathbf{J}^* + \mathbf{D}\ \nabla^2 \underline{\mathbf{w}}, \tag{2.8}$$

where $\underline{\mathrm{w}_t} = \begin{bmatrix} u_t \\ v_t \end{bmatrix}$, $\underline{\mathrm{w}} = \begin{bmatrix} u \\ v \end{bmatrix}$ and $\mathrm{J}^* = \begin{bmatrix} f_u & f_v \\ g_u & g_v \end{bmatrix}_{(u^*, v^*)}$.
Now, using linear stability analysis, the system of PDEs (2.8) leads to the following form of the spatial system

$$\lambda \underline{\mathbf{w}} = \mathbf{J}^*\ \mathbf{w} - \mathbf{D}\ k^2\ \underline{\mathbf{w}}, \tag{2.9}$$

where $\mathbf{w}(\mathbf{x}, \mathbf{y}, \mathbf{t}) \equiv [u(x, y, t), v(x, y, t)]^T$, k is the wave number, $\mathbf{J}^*$ is Jacobian matrix of the spatially homogeneous model system (2.4) and $\mathbf{D}$ is the diffusion coefficients matrix:

$$\mathbf{D}\ =\ \begin{pmatrix} 1 & 0 \\ 0 & \kappa \end{pmatrix}.$$

The eigenvalues (λ's) of the system (2.9) are obtained from the following characteristics equation

$$\left|\left(\mathbf{J}^* - \mathbf{D}k^2\right) - \lambda \mathbf{I}\right| = 0.$$

Substituting the value of $\mathbf{J}^*$ and $\mathbf{D}$ in the above equation, we obtain

$$\begin{vmatrix} a_{11} - k^2 - \lambda & a_{12} \\ a_{21} & a_{22} - \kappa k^2 - \lambda \end{vmatrix} = 0.$$

System will be stable if $a_1(k^2) > 0$ and $a_2(k^2) > 0$. The spatial homogenous steady-state will become unstable due to spatial perturbation when at least one root of characteristic equation $\lambda^2 + a_1(k^2)\ \lambda + a_2(k^2) = 0$ is positive. This requires at least one of the following two inequalities to be violated:

$$\begin{aligned} &\text{(i)} \qquad a_1(k^2) = (1+\kappa)k^2 - a_{11} - a_{22} > 0, \\ &\text{(ii)} \qquad a_2(k^2) = \kappa k^4 - (a_{11}\kappa + a_{22})k^2 + a_{11}a_{22} - a_{12}a_{21} > 0. \end{aligned} \tag{2.10}$$

As κ and k^2 are both positive and $a_{11} + a_{22} < 0$ (stability of the temporal steady state), $a_1(k^2) > 0$ always holds. Therefore, condition for diffusive instability about

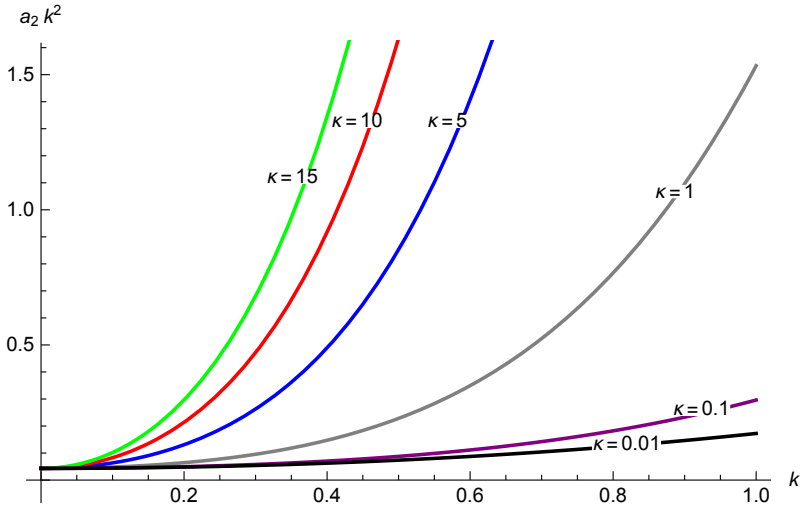

Figure 2.1: Plot of $a_2(k^2)$ against k for parameter values given in Table (2.1) and different values of κ.

(u^*, v^*) is $a_2(k^2) < 0$,

$$\Rightarrow \quad (\alpha - u^* - 2\alpha\beta v^*) + \kappa\left(\frac{\rho v^*}{\eta + v^*} - \mu v^* - \delta\right)$$
$$> 2\sqrt{(\alpha - u^* - 2\alpha\beta v^*)\left(\frac{\rho v^*}{\eta + v^*} - \mu v^* - \delta\right) + v^*\left(\frac{\rho u^*}{\eta + v^*} - \frac{\rho u^* v^*}{(\eta + v^*)^2} - \mu u^*\right)}\ \kappa^{1/2},$$

and about tumor free steady state $(u^*, 0)$ is

$$\alpha - u^* - \kappa\delta > 2\sqrt{u^*\delta - \alpha\delta}\ \kappa^{1/2}. \tag{2.11}$$

The eigenvalues of the dispersion curve (characteristics polynomial) of non-trivial equilibrium points $\mathrm{E}_2(u^*, v^*)$, cannot be determined analytically. Hence, we numerically look into the quantitative analysis using the parameter values given in [91]. We plotted the dispersion curve, which clearly shows that after spatial perturbation, the spatiotemporal dynamics remain stable, that is, $\mathrm{Re}(\lambda) < 0$ (see Figure. (2.1)). Tumor free steady state is also unstable after adding spatial perturbation from 2.11. Hence, the Turing instability condition does not hold here. So, there is no possibility of occurring the Turing pattern.

2.5 Higher order stability analysis

In this section, we use higher order spatiotemporal perturbation term to check the stability of the system [152], for this we have chosen a general two dimensional reaction diffusion system with previous specific choice of parameter values. The reaction diffusion partial differential equation system are described as follows:

$$\begin{cases} f \equiv u_t = \sigma + \frac{\rho uv}{\eta+v} - \mu uv - \delta u + u_{xx} + u_{yy}, \\ g \equiv v_t = \alpha v\,(1-\beta v) - uv + \kappa\,(v_{xx} + v_{yy})\,, \end{cases} \tag{2.12}$$

with zero-flux boundary conditions and initial condition of cells population within two dimensional bounded spatial domain. The interior steady state points $\mathrm{E}_2(u^*, v^*)$ for the temporal system corresponding to the system is a spatially homogenous steady states point for the system. We assume that the equilibrium point $\mathrm{E}_2(u^*, v^*)$ are locally stable for the non-spatial system. The spatial perturbations $p(x, y, t)$ and $q(x, y, t)$ on the equilibrium point u^* and v^*, which is defined by $u = u^* + p(x, y, t)$, $v = v^* + q(x, y, t)$ and expanding the non-spatial part by Taylor series expansion up to third order about equilibrium point, we get following expressions:

$$\begin{aligned} p_t = f_u\ p + f_v\ q + \frac{f_{uu}}{2}p^2 + \frac{f_{vv}}{2}q^2 + f_{uv}pq + \frac{f_{uuu}}{6}p^3 + \frac{f_{vvv}}{6}q^3 + \frac{f_{uuv}}{2}p^2q + \frac{f_{uvv}}{2}pq^2 \\ + p_{xx} + p_{yy}, \\ q_t = g_u\ p + g_v\ q + \frac{g_{uu}}{2}p^2 + \frac{g_{vv}}{2}q^2 + g_{uv}pq + \frac{g_{uuu}}{6}p^3 + \frac{g_{vvv}}{6}q^3 + \frac{g_{uuv}}{2}p^2q + \frac{g_{uvv}}{2}pq^2 \\ + \kappa\,(q_{xx} + q_{yy})\,, \end{aligned} \tag{2.13}$$

Expressing the spatiotemporal perturbations $p(x, y, t)$ and $q(x, y, t)$ as

$$\begin{aligned} p(x, y, t) &= p(t)\ \cos(k_x x)\ \cos(k_y y), \\ q(x, y, t) &= q(t)\ \cos(k_x x)\ \cos(k_y y), \end{aligned}$$

with zero-flux boundary condition, system (2.13) reduces to

$$\begin{aligned} p_t = f_u\ p + f_v\ q + \frac{f_{uu}}{2}p^2 + \frac{f_{vv}}{2}q^2 + f_{uv}pq + \frac{f_{uuu}}{6}p^3 + \frac{f_{vvv}}{6}q^3 + \frac{f_{uuv}}{2}p^2q + \frac{f_{uvv}}{2}pq^2 \\ - k^2 p, \\ q_t = g_u\ p + g_v\ q + \frac{g_{uu}}{2}p^2 + \frac{g_{vv}}{2}q^2 + g_{uv}pq + \frac{g_{uuu}}{6}p^3 + \frac{g_{vvv}}{6}q^3 + \frac{g_{uuv}}{2}p^2q + \frac{g_{uvv}}{2}pq^2 \\ - \kappa k^2 q, \end{aligned} \tag{2.14}$$

where $k^2 = k_x^2 + k_y^2$. It is clear from (2.14) that the growth or decay of first order perturbation terms depends on the second order perturbation terms. Further, we need the dynamical system for second-order perturbation terms involved in (2.14). Multiplying the first equation by $2p$ and second equation by $2q$ respectively in (2.14) and neglecting third order perturbation term, we have the dynamical equation of second order perturbations as

$$\begin{aligned}
\left(p^2\right)_t &= 2f_u p^2 + 2f_v pq + f_{uu} p^3 + f_{vv} pq^2 + 2f_{uv} p^2 q - 2k^2 p^2, \\
\left(q^2\right)_t &= 2g_u pq + 2g_v q^2 + g_{vv} q^3 + g_{uu} p^2 q + 2g_{uv} pq^2 - 2\kappa k^2 q^2, \\
(pq)_t &= g_u p^2 + f_v q^2 + (f_u + g_v)\, pq + \frac{g_{uu}}{2} p^3 + \frac{f_{vv}}{2} q^3 + \left(\frac{f_{uu}}{2} + g_{uv}\right) p^2 q \\
&\qquad + \left(\frac{g_{vv}}{2} + f_{uv}\right) pq^2 - k^2 (1+\kappa)\, pq.
\end{aligned} \tag{2.15}$$

The dynamical equations for third order perturbation terms can be obtained from (2.14) (neglecting fourth and fifth order terms) as follows:

$$\begin{aligned}
\left(p^3\right)_t &= 3f_u p^3 + 3f_v p^2 q - 3k^2 p^3, \\
\left(q^3\right)_t &= 3g_v q^3 + 3g_u pq^2 - 3\kappa k^2 q^3, \\
\left(p^2 q\right)_t &= g_u p^3 + \left(2f_u + g_v - 2k^2 - \kappa k^2\right) p^2 q + 2f_v pq^2, \\
\left(pq^2\right)_t &= f_v q^3 + 2g_u p^2 q + \left(f_u + 2g_v - k^2 - 2\kappa k^2\right) pq^2.
\end{aligned} \tag{2.16}$$

The truncation of fourth and higher order terms in Taylor series expansion and neglecting of fourth and higher order perturbation terms during derivation of dynamical equations (2.14) to (2.16) leads to a closed system of equations for $p,\ q,\ p^2,\ q^2,\ pq,\ p^3,\ q^3,\ p^2q,\ pq^2$, otherwise, one cannot avoid infinite hierarchy of dynamical equations for perturbation terms. Truncation of higher order terms does not affect the understanding of the role of leading order non-linearity. Applicability and significance of the analysis can be justified with the perturbation terms up to the order four, for the system (2.12) with the suitable choice of parameter values.

The dynamical equations (2.14–2.16) can be written into a compact matrix form as follows:

$$\frac{dL}{dt} = AL, \tag{2.17}$$

where $L = [p,\ q,\ p^2,\ q^2,\ pq,\ p^3,\ q^3,\ p^2q,\ pq^2]^T$ and

$$\mathbf{A} = \begin{pmatrix} a_{11} & f_v & \frac{f_{uu}}{2} & \frac{f_{vv}}{2} & f_{uv} & \frac{f_{uuu}}{6} & \frac{f_{vvv}}{6} & \frac{f_{uuv}}{2} & \frac{f_{uvv}}{2} \\ g_u & a_{22} & \frac{g_{uu}}{2} & \frac{g_{vv}}{2} & g_{uv} & \frac{g_{uuu}}{6} & \frac{g_{vvv}}{6} & \frac{g_{uuv}}{2} & \frac{g_{uvv}}{2} \\ 0 & 0 & a_{33} & 0 & 2f_v & f_{uu} & 0 & 2f_{uv} & f_{vv} \\ 0 & 0 & 0 & a_{44} & 2g_u & 0 & g_{vv} & g_{uu} & 2g_{uv} \\ 0 & 0 & g_u & f_v & a_{55} & \frac{g_{uu}}{2} & \frac{f_{vv}}{2} & \frac{f_{uu}}{2} + g_{uv} & \frac{g_{vv}}{2} + f_{uv} \\ 0 & 0 & 0 & 0 & 0 & a_{66} & 0 & 3f_v & 0 \\ 0 & 0 & 0 & 0 & 0 & 0 & a_{77} & 0 & 3g_u \\ 0 & 0 & 0 & 0 & 0 & g_u & 0 & a_{88} & 2f_v \\ 0 & 0 & 0 & 0 & 0 & 0 & f_v & 2g_u & a_{99} \end{pmatrix},$$

with $a_{11} = f_u - k^2$, $a_{22} = g_v - \kappa k^2$, $a_{33} = 2f_u - 2k^2$, $a_{44} = 2g_v - 2\kappa k^2$, $a_{55} = f_u + g_v - (1+\kappa)\,k^2$, $a_{66} = 3f_u - 3k^2$, $a_{77} = 3g_v - 3\kappa k^2$, $a_{88} = 2f_u + g_v - (2+\kappa)\,k^2$, $a_{99} = f_u + 2g_v - (1+2\kappa)\,k^2$.

We take the solution of system (2.17) in the form $L(t) \sim e^{\lambda t}$, where λ's $\equiv \lambda(k)$ are the eigenvalues of A and λ's are the solution of the following equation

$$|A - \lambda I| = 0, \tag{2.18}$$

where I is the 9×9 unit matrix. Numerically, using the parameter values given in Table 2.1, all the eigenvalues of the matrix A are -0.318348, -1.46982, -0.636696, -2.93964, -1.78817, -0.955044,-4.40946,-2.10652,-3.25799. Therefore, the system is stable about (u^*, v^*). However, tumor free steady state point is unstable since the eigenvalues of A are -0.01, 1.310478, -0.02, 2.620956, 1.300478, -0.03, 3.931434, 1.290478, 2.610956 about $(u^*, 0)$.

2.6 Numerical simulation

The spatiotemporal model (2.4) is solved numerically in two dimensional space with the help of finite difference method for spatial derivatives. Euler method is utilized for the reaction part and standard five point finite difference method is utilized for the diffusion part. The numerical integration of the reaction-diffusion partial differential equations (2.4) is employed by using splitting method. The value of time step and space step have been chosen sufficiently small for avoiding the numerical

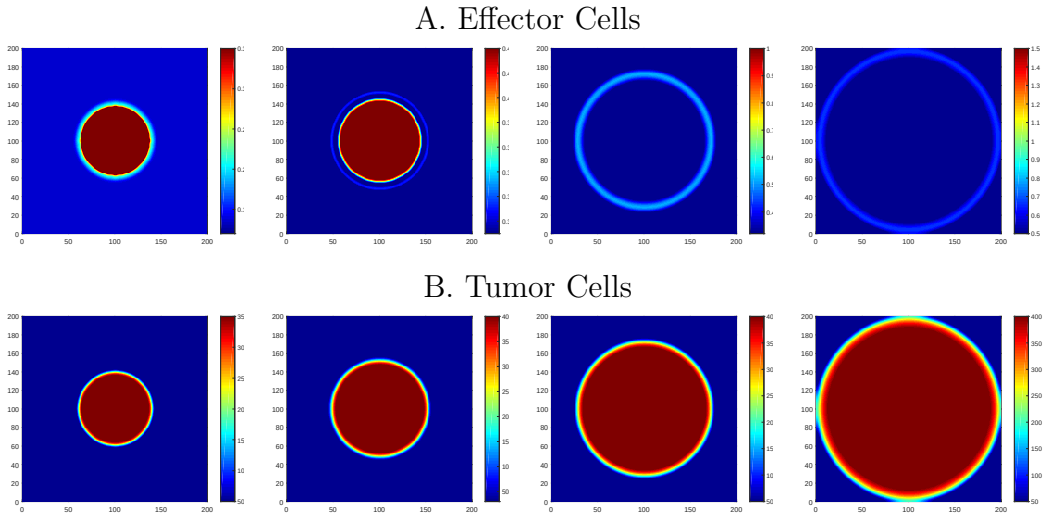

Figure 2.2: Spatial distribution of densities of the effector cell (Panel A) and tumor cell (Panel B) at times corresponding to 91, 182, 273 and 364 days respectively, when $\alpha\delta > \sigma$. The parameter values are given in Table 2.1.

artifacts. We performed all the numerical simulations over the zero-flux boundary condition with 200×200 domain size and time-step $\Delta t = 0.002$. The initial density distribution of immune cells and tumor cells are chosen in such a way that they are located at the center of the domain.

The model is numerically simulated, which shows the spatial distribution within the tissue of effector and tumor cell densities.

Case 1. $\alpha\delta > \sigma$

Figure (2.2)A and (2.2)B show the spatial distribution within the tissue of effector and tumor cell densities at time $\tau = 91$, 182, 273 and 364 respectively. Initially, the effectors cells are dense (panel A) but with time fails to control the growth of tumor cells. Panel B shows that the density of tumor, which was in the dormant stage, started to grow with time. This can be interpreted as tumor sneaking through, which refers to a phenomena in which low dense of tumor cells can escape immune surveillance and grow into large tumors.

Case 2. $\alpha\delta < \sigma$.

In this case, the tumor free equilibrium is stable and the interior equilibrium is unstable. Figure (2.3)A and (2.3)B show the spatial distribution of the effector and

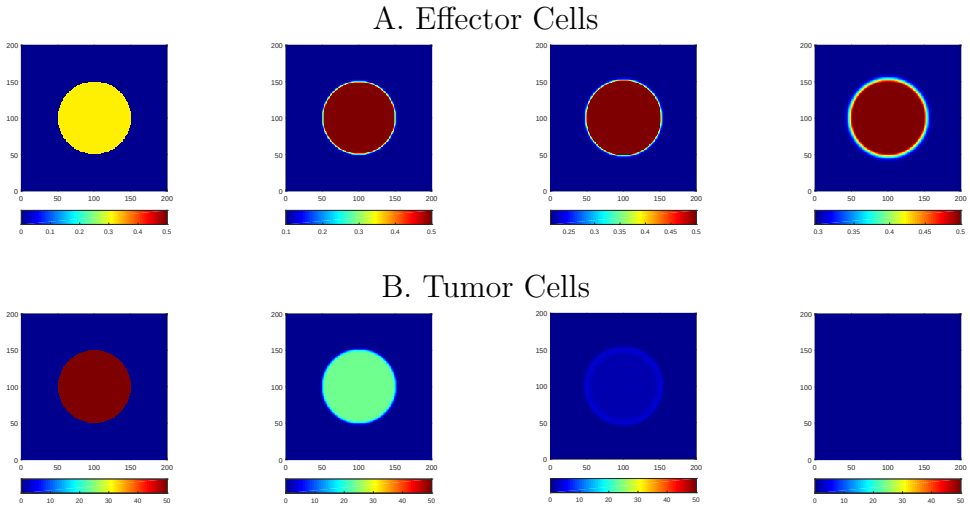

Figure 2.3: Spatial distribution of densities of the effector cell (Panel A) and tumor cell (Panel B) at times corresponding to 91, 182, 273 and 364 days respectively, when $\alpha\delta < \sigma$. In this case, $\alpha = 0.2$, $\delta = 0.3743$, $\sigma = 0.1181$, $\kappa = 2.5$.

tumor cell densities within the tissue at times $\tau = 91$, 182, 273 and 364 respectively. The first panel (A) shows that the effector cells are less dense initially but quickly recovers with time. On the other hand, the tumor cells are highly dense at initial time but soon the effector cells eradicate them within an year.

Figure (2.4) shows the effect of carrying capacity on tumor dormancy. With $\beta = 0.002$ (carrying capacity $\frac{1}{\beta} = 500$), the tumor is in dormant stage (panel A). For $\beta = 0.0002$ (carrying capacity $\frac{1}{\beta} = 5000$) (panel B) and $\beta = 0.00002$ (carrying capacity $\frac{1}{\beta} = 50000$) (panel C), the tumor relapses from the dormant stage and started to grow. This shows that tumor cells can modify their micro-environment such that it can sustain a large population, that is, they construct a niche, which increases the carrying capacity of the population. Increased carrying capacity is achieved through a number of mechanisms of which some are internal to the cell and others, that are brought about by changing the micro-environment of the cell.

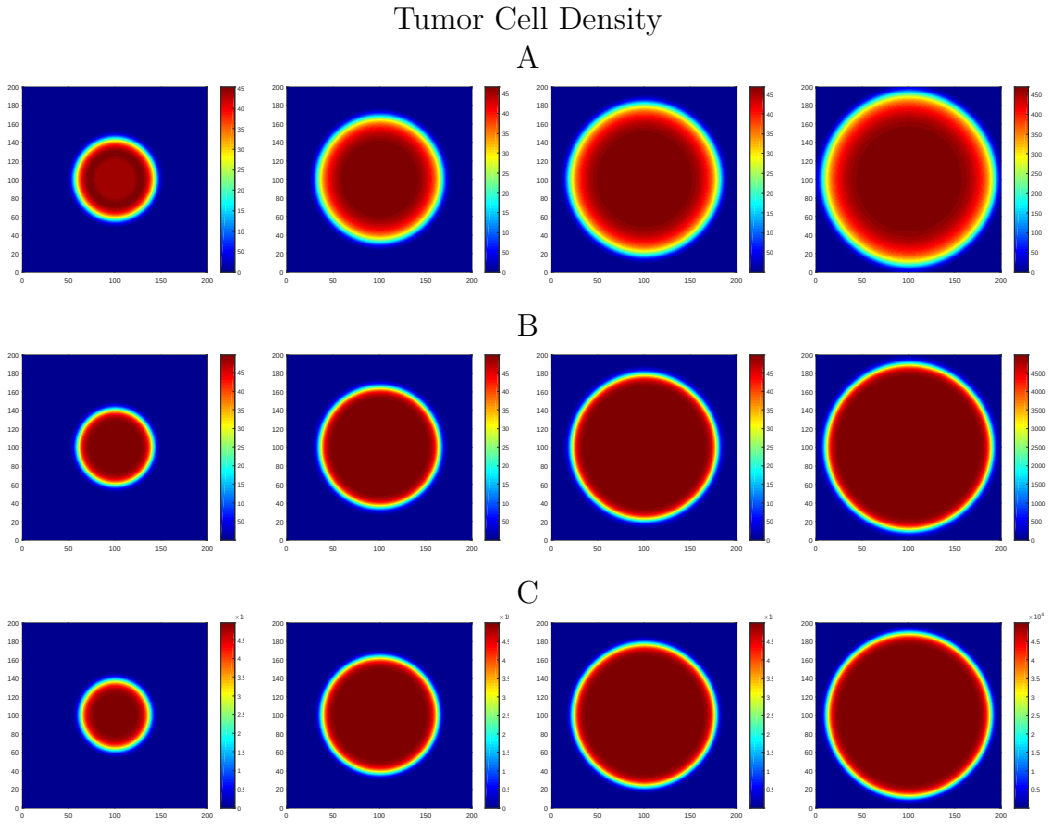

Figure 2.4: Spatial distribution of densities of the tumor cell population from the dormant stage at times $\tau = 91$, 182, 273 and 364 days respectively, with increasing carrying capacity: Panel A: $\beta = 0.002$ (carrying capacity $\frac{1}{\beta} = 500$); Panel B: $\beta = 0.0002$ (carrying capacity $\frac{1}{\beta} = 5000$) and Panel C: $\beta = 0.00002$ (carrying capacity $\frac{1}{\beta} = 50000$). The parameter values are obtained from Table 2.1.

2.7 Conclusion

In this chapter, we have focused our attention on a spatiotemporal mathematical model describing the growth of a solid tumor in presence of an immune responses, which is termed as effector cells. The proposed model is a modification of the non-spatial model by Kuznetsov et al. [91], by extending it to a spatiotemporal one. Local stability analysis of the spatiotemporal model reveals that the tumor free equilibrium exists and is stable, when the intrinsic growth rate of the tumor is less then the ratio of constant input of the effector cells and its decay rate ($\alpha < \frac{\sigma}{\delta}$). The interior equilibrium does not exist in this case. However, when $\alpha > \frac{\sigma}{\delta}$, three interior

equilibria (u^*, v^*) exist, of which two of them are stable. The immune system fails to control the tumor growth in this case. The system is also subjected to higher order spatiotemporal perturbation terms for stability check, but the results remains same as obtained from linear stability analysis.

One interesting phenomenon of evolution of carrying capacity and expansion of tumor cell population is observed. This observation allows us to relate the tumor's volumetric growth rate to the host organs's functionality conveying composite infrastructure. When the carrying capacity of the primary host organ is about to be exceeded, metastasis will be triggered. While the biological processes involved in cancer expansion may lead to some upward adjustment of the carrying capacity, presumably these parenchymal and stromal compensation mechanisms are limited and tumor cells will eventually spread to distant sites.

Chapter 3

Spatiotemporal dynamics of malignant gliomas and immune system considering the role of immunotherapeutic agent T11 target structure

3.1 Introduction

Gliomas are highly diffusive heterogenous group of intracranial neoplasms accounting nearby 50% of primary brain tumors called by malignancy of gliomas. Gliomas are difficult to treat due to its sequestered location beyond the blood-brain-barrier. Gliomas vary from low-to high grade, namely glioblastomas, which constitute the most malignant form of brain cancer, having an extremely poor prognosis. Glioblastoma has a survival rate from 6 month to 12 months [6; 84; 85]. Treatments like chemotherapy, surgery, radiation therapy have limited success due to the gliomas's heterogeneity, genomic instability and the location of blood-brain-barrier. In particular, glioma is a rapidly evolving type of brain tumor, well known for its aggressive and diffusive behavior [168]. This diffusive invasion has lead several research efforts through mathematical modeling to explore the glioma's proliferation

with the aid of reaction-diffusion equations, aiming to predict its spatial evolution [27; 30; 33; 47; 72; 108; 119; 122; 128; 131; 161; 164; 165; 166].

In our present study, we explore the spatiotemporal dynamics of the mathematical model developed by Banerjee et. al. [12; 79; 80]. In their model, interaction between malignant gliomas and immune components, namely, macrophages, cytotoxic T-lymphocytes, TGF-β and IFN-γ, has been investigated using reaction-diffusion equations, considering the constant infusion of exogenous immunotherapeutic drug T11 target structure (T11TS). The aim of our work is to identify the Turing as well as non-Turing zone due to added diffusion terms to the system and to numerically simulate the system that will demonstrate the extent of invasion of the gliomas, controlled by the immunotherapeutic drug T11 target structure. The analysis and ramification present in this chapter will be a building block towards a comprehensive study of the rudimentary mechanism in the spatiotemporal dynamics of gliomas.

Many literatures have explained the spatiotemporal dynamics of malignant glioma growth in presence of immune system interaction with the help of reaction-diffusion equations [23; 27; 31; 32; 33; 47; 72; 86; 87; 108; 119; 122; 128; 131; 146; 161; 164; 165; 166; 175]. Sherratt et al. [128] proposed a mathematical model through reaction-diffusion equations by considering the spatiotemporal interactive dynamics of mutant cells, macrophages and the normal tissue cells and by spatiotemporal dynamics, the authors investigated the existence of traveling-wave solutions of normal tissues and growing tumor. Swanson et al. in [166], explored a mathematical model for chemotherapy of malignant gliomas, which assumes the brain structure to be inhomogeneous that makes diffusion process space dependent. Swanson et al. [167] proposed a mathematical model of gliomas growth and aggressiveness with treatment and without treatment strategy, using partial differential equations. Several research papers have been published by Murray and Swanson on spatiotemporal modeling of brain tumors [72; 122; 164; 165; 166; 167]. Stein et al. [161] developed a continuum three dimensional reaction-diffusion mathematical model for brain tumor invasion and dispersion to elucidate in vitro experiments. Their spatiotemporal reaction-diffusion model qualitatively reproduces the experimental investigations, and stipulates that the endogenous (wild-type) receptor (U87WT) invasive cells have a stronger directional mobility bias. Stein et al. [161] claimed that a single

gliomas population model studied by Swanson et al. [164; 167] is not sufficient to reproduce these two kinetics since they exhibit different proliferative and dispersive characteristics.

3.2 The mathematical model

A mathematical model of glioma and immune system interaction through the system of nonlinear ordinary differential equations has been studied in non-spatial domain with immunotherapeutic agent T11 target structure [12]. Motivated from the work, we extend this model in spatiotemporal domain to study its spatial dynamics. Let G, M, C_T, T_β and I_γ be the densities of glioma cells, macrophages, CD8+ T cells, cytokine TGF-β and IFN-γ, respectively, at time t and at spatial location (x, y). Malignant glioma grows logistically in absence of immune system with intrinsic growth rate r_1 and maximal glioma cells burden $G_{\max}$ (carrying capacity) and the glioma cells are eradicated by the immune-system components macrophages (M) and activated cytotoxic T-lymphocytes (C_T) at the rates α_1 and α_2 respectively, Michaelis-Menton term is being incorporated to bring out the accessibility of the glioma cells to macrophages and CD8+ T cells, k being the half saturation constant. The immuno-suppressive factor TGF-β secreted by malignant gliomas down-regulates the activity of both the immuno-stimulatory components macrophages and cytotoxic T-lymphocytes [50]. This explains the term $\frac{1}{T_\beta+e_1}$, e_1 being the Michaelis constant. Thus, the glioma's density is

$$\frac{dG}{dt} = \underbrace{r_1 G\left(1-\frac{G}{G_{\max}}\right)}_{growth\ term} - \underbrace{\left(\frac{1}{T_\beta+e_1}\right)(\alpha_1 M+\alpha_2 C_T)\left(\frac{G}{G+k_1}\right)}_{elimination\ term}. \quad (3.1)$$

The macrophages are highly heterogeneous in nature, in terms of its activation and proliferation [1]. We assume that the macrophages grow logistically with intrinsic growth rate r_2 and maximum carrying capacity $M_{\max}$. The macrophages are activated by the immuno-stimulatory cytokine interferon-γ (IFN-γ) at the rate a_1, and it is down-regulated by immuno-suppressive factor transforming growth factor-β (TGF-β), k_4 and e_2 being the saturation constants. The cell-count of macrophage

population decreases due to the interaction with malignant gliomas at the rate α_3 and their interactions follow the Michaelis-Menten saturation dynamics with half-saturation constant k_2. Thus, the equation for macrophage's density is

$$\frac{dM}{dt} = \underbrace{r_2 M\left(1-\frac{M}{M_{\max}}\right)}_{growth\ term} + \underbrace{a_1\left(\frac{I_\gamma}{k_4+I_\gamma}\right)}_{proliferation}\underbrace{\left(\frac{1}{T_\beta+e_2}\right)}_{down-regulation} - \underbrace{\alpha_3\left(\frac{G}{k_2+G}\right)M}_{inactivation\ term}. \tag{3.2}$$

The recruitment of cytotoxic T-lymphocytes occurs due to direct presence of malignant gliomas, a_2 being the antigenicity of gliomas which triggers an immune response. The recruitment of cytotoxic T-lymphocytes is inhibited by immunosuppressive cytokine TGF-β, where k_5 is termed as inhibitory parameter. The clearance of cytotoxic T-lymphocytes by glioma population occur through the Michaelis-Menten saturation dynamics at the rate α_4, k_3 being the half saturation constant. Thus, the equation for cytotoxic T-lymphocyte's density is

$$\frac{dC_T}{dt} = \underbrace{a_2 G}_{recruitment\ term}\underbrace{\left(\frac{1}{k_5+T_\beta}\right)}_{inhibition\ term} - \underbrace{\mu_1 C_T}_{natural\ death} - \underbrace{\alpha_4\left(\frac{G}{k_3+G}\right)C_T}_{inactivation\ term}. \tag{3.3}$$

Glioma induced cytokine TGF-β, prostaglandin E_2 and IL-10 suppress the activity of immune system and stimulate the production of malignant glioma cells. When the gliomas are small in size, it secretes small amount of TGF-β to obtain ample nutrients from the neighboring tissues. But, when the gliomas are sufficiently large resulting in lack of nutrients, oxygen and space, it begins to secrete TGF-β to stimulate angiogenesis by down-regulating the production of immuno-stimulatory components [50; 129]. TGF-β has a constant source rate s_1 in the central nervous system (CNS). The production of TGF-β is proportional to the glioma size, with rate b_1. TGF-β decays at the rate μ_2. Thus, the equation for the TGF-β's density is

$$\frac{dT_\beta}{dt} = \underbrace{s_1 + b_1 G}_{growth\ term} - \underbrace{\mu_2 T_\beta}_{death\ term}. \tag{3.4}$$

The source of IFN-γ is cytotoxic T-lymphocytes, at a linear production rate b_2 per unit of cytotoxic T-lymphocytes density. The density of IFN-γ decays linearly

at the rate μ_3. Thus, the equation for IFN-γ's density is

$$\frac{dI_\gamma}{dt} = \underbrace{b_2 C_T}_{generation\ term} - \underbrace{\mu_3 I_\gamma}_{decay\ term}. \tag{3.5}$$

The external factor administration of immunotherapeutic agent T11 target structure, activates different anti-tumor immune system components including CD8+ T cells and macrophages and we assume that this T11 target structure will have an effect on the cell count of macrophages and CD+8 T cells [118]. In mathematical terms, we represent the administration of T11 target structure by a constant input T_s.

The mathematical model governing the spatiotemporal dynamics of the glioma cell and immune system interaction with T11 target structure can be described by the following system of reaction-diffusion equations:

$$\begin{aligned}
\frac{\partial G(x,y,t)}{\partial t} &= r_1 G\left(1-\frac{G}{G_{\max}}\right) - \frac{(\alpha_1 M + \alpha_2 C_T)G}{(e_1+T_\beta)(G+k_1)} + D_1\nabla^2 G,\\
\frac{\partial M(x,y,t)}{\partial t} &= r_2 M\left(1-\frac{M}{M_{\max}}\right) + a_1\left(\frac{I_\gamma}{k_4+I_\gamma}\right)\left(\frac{1}{T_\beta+e_2}\right) - \alpha_3\frac{GM}{k_2+G} + \\
&\qquad T_s + D_2\nabla^2 M,\\
\frac{\partial C_T(x,y,t)}{\partial t} &= a_2 G\frac{1}{k_5+T_\beta} - \mu_1 C_T - \alpha_4\frac{G}{k_3+G}C_T + T_s + D_3\nabla^2 C_T,\\
\frac{\partial T_\beta(x,y,t)}{\partial t} &= s_1 + b_1 G - \mu_2 T_\beta + D_4\nabla^2 T_\beta,\\
\frac{\partial I_\gamma(x,y,t)}{\partial t} &= b_2 C_T - \mu_3 I_\gamma + D_5\nabla^2 I_\gamma.
\end{aligned} \tag{3.6}$$

Here, ∇^2 is the Laplacian operator in cartesian coordinates. D_1, D_2, D_3, D_4 and D_5 are diffusion coefficients for glioma, macrophages, cytotoxic T-lymphocytes, TGF-β and IFN-γ respectively. All system parameters are positive. The zero-flux boundary conditions and positive initial distribution of glioma and immune system are described by

(i) for 1-dimension case $\left(\nabla^2 \equiv \frac{\partial^2}{\partial x^2}\right)$, initial conditions

$$\begin{aligned}
G(x,0)>0,\ M(x,0)>0,\ C_T(x,0)>0,\ T_\beta(x,0)>0,\ I_\gamma(x,0)>0,\\
\text{for } x\in\Omega_1 = [0,\ L].
\end{aligned} \tag{3.7}$$

(ii) for 2-dimension case $\left(\nabla^2 \equiv \frac{\partial^2}{\partial x^2} + \frac{\partial^2}{\partial y^2}\right)$, initial conditions

$$\begin{aligned} &G(x,y,0) = G_0(x,y) > 0,\ M(x,y,0) = M_0(x,y) > 0, \\ &C_T(x,y,0) = C_{T0}(x,y) > 0,\ T_\beta(x,y,0) = T_{\beta 0}(x,y) > 0, \\ &I_\gamma(x,y,0) = I_{\gamma 0}(x,y) > 0,\ \text{for } (x,y) \in \Omega_2 \ = \ [0,\ L] \times [0,\ L], \end{aligned} \tag{3.8}$$

and zero flux (Neumann) boundary conditions

$$\frac{\partial G}{\partial n} = \frac{\partial M}{\partial n} = \frac{\partial C_T}{\partial n} = \frac{\partial T_\beta}{\partial n} = \frac{\partial I_\gamma}{\partial n} = 0,\ \text{on } (x,y) \in \partial\Omega_2,\ t\ >\ 0. \tag{3.9}$$

Here, L denotes the size of the system in the direction of $(x,\ y)$, n is the outward unit normal on the boundary Ω_2.

3.3 Analysis of non-spatial system

Banerjee et al. [12; 79; 80] have done the detailed analysis of the non-spatial system of the proposed model. Here, we highlight few results that we need for the analysis of spatiotemporal system.

3.3.1 Analysis of non-spatial system without T11 target structure ($\mathbf{T}_s = 0$)

(i) System (3.6) has three biologically relevant equilibrium states, namely,

(a) boundary homogenous steady-state, $\mathrm{E}_1\left(0, 0, 0, \frac{s_1}{\mu_2}, 0\right)$,

(b) glioma free homogenous steady-state, $\mathrm{E}_2\left(0, M_{max}, 0, \frac{s_1}{\mu_2}, 0\right)$,

(c) interior homogenous steady-state, $\mathrm{E}^*\left(G^*, M^*, C_T^*, T_\beta^*, I_\gamma^*\right)$.

The interior equilibrium E^* is rather difficult to assess explicitly. By using the set of parameter values given in Table 3.1, the unique positive interior fixed point E^* is approximately given by $\mathrm{G}^* = 875419$, $\mathrm{M}^* = 943092$, $\mathrm{C}_T^* = 303.397$, $\mathrm{T}_\beta^* = 9134.33$, $\mathrm{I}_\gamma^* = 0.303397$.

(ii) The general Jacobian matrix corresponding to the system is given by

$$\mathbf{J}^* = \begin{pmatrix} a_{11} & a_{12} & a_{13} & a_{14} & a_{15} \\ a_{21} & a_{22} & a_{23} & a_{24} & a_{25} \\ a_{31} & a_{32} & a_{33} & a_{34} & a_{35} \\ a_{41} & a_{42} & a_{43} & a_{44} & a_{45} \\ a_{51} & a_{52} & a_{53} & a_{54} & a_{55} \end{pmatrix}, \text{ where}$$

$a_{11} = r_1\left(1 - \frac{2G}{G_{\max}}\right) - \frac{k_1(\alpha_1 M + \alpha_2 C_T)}{(T_\beta + e_1)(G+k_1)^2}$, $a_{12} = -\frac{\alpha_1 G}{(T_\beta+e_1)(G+k_1)}$, $a_{13} = -\frac{\alpha_2 G}{(T_\beta+e_1)(G+k_1)}$, $a_{14} = \frac{G(\alpha_1 M+\alpha_2 C_T)}{(T_\beta+e_1)^2(G+k_1)}$, $a_{15} = 0$, $a_{21} = -\frac{\alpha_3 k_2 M}{(G+k_2)^2}$, $a_{22} = r_2(1 - \frac{2M}{M_{\max}}) - \frac{\alpha_3 G}{G+k_2}$, $a_{23} = 0$, $a_{24} = -\frac{a_1 I_\gamma}{(k_4+I_\gamma)(T_\beta+e_2)^2}$, $a_{25} = \frac{a_1 k_4}{(k_4+I_\gamma)^2(T_\beta+e_2)}$, $a_{31} = \frac{a_2}{k_5+T_\beta} - \frac{\alpha_4 k_3 C_T}{(G+k_3)^2}$, $a_{32} = 0$, $a_{33} = -\mu_1 - \frac{\alpha_4 G}{G+k_3}$, $a_{34} = -\frac{a_2 G}{(k_5+T_\beta)^2}$, $a_{35} = 0$, $a_{41} = b_1$, $a_{42} = 0$, $a_{43} = 0$, $a_{44} = -\mu_2$, $a_{45} = 0$, $a_{51} = 0$, $a_{52} = 0$, $a_{53} = b_2$, $a_{54} = 0$, $a_{55} = -\mu_3$.

(iii) The eigenvalues of the Jacobian matrix J^*, corresponding to the homogenous steady-state $E_1\left(0, 0, 0, \frac{s_1}{\mu_2}, 0\right)$ are r_1, r_2, $-\mu_1$, $-\mu_2$, $-\mu_3$. It is clear from the eigenvalues that the homogenous steady-state E_1 is hyperbolic saddle point with two dimensional unstable manifold and three dimensional stable manifold.

(iv) The eigenvalues of the Jacobian matrix J^*, corresponding to the homogenous steady-state $E_2\left(0, M_{\max}, 0, \frac{s_1}{\mu_2}, 0\right)$ are $r_1 - \frac{\alpha_1 M_{\max}\mu_2}{k_1(s_1+e_1\mu_2)}$, $-r_2$, $-\mu_1$, $-\mu_2$ and $-\mu_3$. If $r_1 < \frac{\alpha_1 M_{\max}\mu_2}{k_1(s_1+e_1\mu_2)}$, E_2 is locally asymptotically stable and if $r_1 > \frac{\alpha_1 M_{\max}\mu_2}{k_1(s_1+e_1\mu_2)}$, E_2 is a saddle point. If $r_1 = \frac{\alpha_1 M_{\max}\mu_2}{k_1(s_1+e_1\mu_2)}$, no definite conclusion is obtained about the local stability of E_2. From clinical point of view, E_2 has an impact as it gives an idea under what circumstances glioma free state can be obtained.

(v) The characteristics equation of the Jacobian matrix J^* corresponding to the homogenous steady-state E^* is

$$\lambda^5 + \rho_1\lambda^4 + \rho_2\lambda^3 + \rho_3\lambda^2 + \rho_4\lambda + \rho_5 = 0$$

where, $\rho_1 = -a_{11} - a_{22} - a_{33} - a_{44} - a_{55}$, $\rho_2 = -a_{12}a_{21} + a_{11}a_{22} - a_{13}a_{31} + a_{11}a_{33} + a_{22}a_{33} - a_{14}a_{41} + a_{11}a_{44} + a_{22}a_{44} + a_{33}a_{44} + a_{11}a_{55} + a_{22}a_{55} + a_{33}a_{55} + a_{44}a_{55}$, $\rho_3 = a_{13}a_{22}a_{31} + a_{12}a_{21}a_{33} - a_{11}a_{22}a_{33} + a_{14}a_{22}a_{41} - a_{12}a_{24}a_{41} + a_{14}a_{33}a_{41} - a_{13}a_{34}a_{41} + a_{12}a_{21}a_{44} - a_{11}a_{22}a_{44} + a_{13}a_{31}a_{44} - a_{11}a_{33}a_{44} - a_{22}a_{33}a_{44} + a_{12}a_{21}a_{55} -$

$a_{11}a_{22}a_{55}+a_{13}a_{31}a_{55}-a_{11}a_{33}a_{55}-a_{22}a_{33}a_{55}+a_{14}a_{41}a_{55}-a_{11}a_{44}a_{55}-a_{22}a_{44}a_{55}-a_{33}a_{44}a_{55}$, $\rho_4 = -a_{14}a_{22}a_{33}a_{41}+a_{12}a_{24}a_{33}a_{41}+a_{13}a_{22}a_{34}a_{41}-a_{13}a_{22}a_{31}a_{44}-a_{12}a_{21}a_{33}a_{44}+a_{11}a_{22}a_{33}a_{44}-a_{12}a_{25}a_{31}a_{53}-a_{13}a_{22}a_{31}a_{55}-a_{12}a_{21}a_{33}a_{55}+a_{11}a_{22}a_{33}a_{55}-a_{14}a_{22}a_{41}a_{55}+a_{12}a_{24}a_{41}a_{55}-a_{14}a_{33}a_{41}a_{55}+a_{13}a_{34}a_{41}a_{55}-a_{12}a_{21}a_{44}a_{55}+a_{11}a_{22}a_{44}a_{55}-a_{13}a_{31}a_{44}a_{55}+a_{11}a_{33}a_{44}a_{55}+a_{22}a_{33}a_{44}a_{55}$, $\rho_5 = -a_{12}a_{25}a_{34}a_{41}a_{53}+a_{12}a_{25}a_{31}a_{44}a_{53}+a_{14}a_{22}a_{33}a_{41}a_{55}-a_{12}a_{24}a_{33}a_{41}a_{55}-a_{13}a_{22}a_{34}a_{41}a_{55}+a_{13}a_{22}a_{31}a_{44}a_{55}+a_{12}a_{21}a_{33}a_{44}a_{55}-a_{11}a_{22}a_{33}a_{44}a_{55}$.

(vi) The constant coefficients ρ_1, ρ_2, ρ_3, ρ_4 and ρ_5 can be easily calculated from the Jacobian matrix J^*. According to Routh-Hurwitz criteria [92], it follows that the interior homogenous steady-state E^* is locally stable if the following conditions holds:

$$\begin{aligned} \rho_i &> 0, \quad i = 1,2,3,4,5, \\ \rho_1\rho_2\rho_3 &> \rho_3^2 + \rho_1^2\rho_4, \\ (\rho_1\rho_4 - \rho_5)(\rho_1\rho_2\rho_3 - \rho_3^2 - \rho_1^2\rho_4) &> \rho_5(\rho_1\rho_2 - \rho_3)^2 + \rho_1\rho_5^2. \end{aligned}$$

(vii) Using the parameter values in Table 3.1, the characteristic equation is given by

$$\lambda^5 + 7.48329\lambda^4 + 3.92509\lambda^3 + 0.634109\lambda^2 + 0.0344307\lambda + 0.000281034 = 0,$$

which satisfies the Routh-Hurwitz criteria. The eigenvalues are $\lambda_1 = -6.93$, $\lambda_2 = -0.311879$, $\lambda_3 = -0.129576$, $\lambda_4 = -0.101997$ and $\lambda_5 = -0.00983845$, which implies that, the non-spatial system is locally asymptotically stable. From the biological point of view, the interior homogenous steady-state E^* is important as it gives us an idea under what conditions glioma population can persist.

3.3.2 Analysis of non-spatial system with T11 target structure ($\mathbf{T}_s \neq 0$)

(i) The model (3.6) has two biologically relevant equilibrium states, namely,
(a) glioma free homogenous steady-state, $E_{T1}\left(0, \tilde{M}, \frac{T_s}{\mu_1}, \frac{s_1}{\mu_2}, \frac{b_2 T_s}{\mu_1\mu_3}\right)$, where

$$\tilde{M} = \frac{1}{2}\left(M_{max} + \sqrt{{M_{max}}^2 + 4\frac{M_{max}T_s}{r_2}\left(1 + \frac{a_1 b_2 \mu_2}{(s_1+e_2\mu_2)(b_2T_s+k_4\mu_1\mu_3)}\right)}\right)$$

(b) interior equilibrium state, $\hat{\mathrm{E}} = \left(\hat{G}, \hat{M}, \hat{C_T}, \hat{T_\beta}, \hat{I_\gamma}\right)$.

Employing the parameter values given in Table 3.1, we obtain two interior equilibrium points, viz, high density glioma steady state $\hat{\mathrm{E}}_1 = (860096, 2273300, 77$ $30000, 9135.63, 7730)$ and less dense glioma steady state $\hat{\mathrm{E}}_2 = (25077.8, 2291410$ $, 52040000, 9134.94, 52040)$.

(ii) The eigenvalues around $\hat{\mathrm{E}}_1$ are -6.93, -0.129387, -0.102, -0.0542781, -0.0095, all negative and real, that is, $\hat{\mathrm{E}}_1$ is locally asymptotically stable. However, eigenvalues around $\hat{\mathrm{E}}_2$ are -6.93, -0.102, -0.0455234, -0.0217779, 0.00730967, all real but not all negative, pointing that the system is unstable.

(iii) The glioma free equilibrium state $\mathrm{E}_{T1}\left(0, \tilde{M}, \frac{T_s}{\mu_1}, \frac{s_1}{\mu_2}, \frac{b_2T_s}{\mu_1\mu_3}\right)$ of the model (3.6) is locally asymptotically stable if $r_1 < \frac{\mu_2}{k_1(s_1+e_1\mu_2)}\left(\frac{\alpha_1}{2}\tilde{M} + \frac{\alpha_2 T_s}{\mu_1}\right)$.

3.4 Analysis of the spatiotemporal model

3.4.1 Analysis of spatial model without T11 target structure ($\mathbf{T}_s = 0$)

We now concentrate on the spatial dynamics produced by model (3.6). We incorporate diffusion terms into the growth equations for the glioma, macrophage, cytotoxic T-lymphocyte, immuno-suppressive factor TGF-β and immuno-stimulatory cytokine interferon-γ cell population, to investigate the spread of glioma, macrophage and cytotoxic T-lymphocyte in one and two-dimensional domain. Taking the spatiotemporal perturbations about the interior homogenous steady-state E^*=(G^*, M^*,

Parameters	Values	Source
r_1	$0.01\ h^{-1}$	[12]
G_{max}	$8.8265 \times 10^5\ cell$	[12]
e_1	$10^4\ pg$	[140]
α_1	$1.5\ pg\ h^{-1}$	[12]
α_2	$0.12\ pg\ h^{-1}$	[12]
k_1	$2.7 \times 10^4\ cell$	[118]
r_2	$0.3307\ h^{-1}$	[12]
M_{max}	$10^6\ cell$	[71]
a_1	$0.1163\ cell\ h^{-1}$	[12]
k_4	$1.05 \times 10^4\ pg$	[163]
e_2	$10^4\ pg$	[140]
α_3	$0.0194\ h^{-1}$	[12]
k_2	$2.7 \times 10^4\ cell$	[118]
a_2	$0 - 0.5\ h\ pg^{-1}$	[153]
k_5	$2 \times 10^3\ pg$	[12]
μ_1	$0.0074\ h^{-1}$	[12]
α_4	$0.1694\ h^{-1}$	[12]
k_3	$3.34452 \times 10^5\ cell$	[12]
s_1	$6.3305 \times 10^4\ ph\ h^{-1}$	[12]
b_1	$5.70 \times 10^{-6}\ pg\ cell^{-1}\ h^{-1}$	[12]
μ_2	$6.93\ h^{-1}$	[12]
b_2	$1.02 \times 10^{-4}\ pg\ cell^{-1}\ h^{-1}$	[12]
μ_3	$0.102\ h^{-1}$	[12]

Table 3.1: Parameter values used for numerical simulation.

C_T^*, T_β^*, I_γ^*) as

$$\begin{aligned} G(x,y,t) &= G^* + \epsilon \exp(\lambda_k t + (k_x x + k_y y)i), \\ M(x,y,t) &= M^* + \eta \exp(\lambda_k t + (k_x x + k_y y)i), \\ C_T(x,y,t) &= C_T^* + \rho \exp(\lambda_k t + (k_x x + k_y y)i), \\ T_\beta(x,y,t) &= T_\beta^* + \xi \exp(\lambda_k t + (k_x x + k_y y)i), \\ I_\gamma(x,y,t) &= I_\gamma^* + \sigma \exp(\lambda_k t + (k_x x + k_y y)i), \end{aligned} \tag{3.10}$$

where ϵ, η, ρ, ξ, σ are chosen to be real small numbers, $k = \sqrt{k_x^2 + k_y^2}$ is the wave number. We substitute (3.10) into the model (3.6). It is possible to linearize (3.6) about the homogenous steady state E^*, we obtain

$$\mathbf{W_t} = \mathbf{J}^*\mathbf{W} + \mathbf{D}\ \nabla^2\mathbf{W}, \tag{3.11}$$

$$\text{where, } \mathrm{W}_t = \begin{bmatrix} G_t \\ M_t \\ C_{Tt} \\ T_{\beta_t} \\ I_{\gamma_t} \end{bmatrix}, \quad \mathrm{W} = \begin{bmatrix} G \\ M \\ C_T \\ T_\beta \\ I_\gamma \end{bmatrix}, \quad \mathrm{J}^* = \begin{bmatrix} a_{11} & a_{12} & a_{13} & a_{14} & a_{15} \\ a_{21} & a_{22} & a_{23} & a_{24} & a_{25} \\ a_{31} & a_{32} & a_{33} & a_{34} & a_{35} \\ a_{41} & a_{42} & a_{43} & a_{44} & a_{45} \\ a_{51} & a_{52} & a_{53} & a_{54} & a_{55} \end{bmatrix}_{(G^*, M^*, C_T^*, T_\beta^*, I_\gamma^*)}.$$

Now, using linear stability analysis, the system of PDEs (3.11) leads to the following form of the spatial system

$$\lambda \mathbf{W} = \mathbf{J}^* \mathbf{W} - \mathbf{D}\ k^2\ \mathbf{W}, \tag{3.12}$$

where k is the wave number, $\mathbf{J}^*$ is Jacobian matrix of the spatially homogeneous system (3.6) and $\mathbf{D}$ is the diffusion coefficients matrix

$$\mathbf{D} = \begin{pmatrix} D_1 & 0 & 0 & 0 & 0 \\ 0 & D_2 & 0 & 0 & 0 \\ 0 & 0 & D_3 & 0 & 0 \\ 0 & 0 & 0 & D_4 & 0 \\ 0 & 0 & 0 & 0 & D_5 \end{pmatrix}.$$

The eigenvalues $(\lambda_i,\ i = 1, 2, 3, 4, 5)$ of the system (3.12) are obtain by the solution of the following characteristics equation

$$\left| \left(\mathbf{J}^* - \mathbf{D}k^2 \right) - \lambda \mathbf{I} \right| = 0.$$

In explicit form, we have,

$$\begin{vmatrix} a_{11} - D_1 k^2 - \lambda & a_{12} & a_{13} & a_{14} & a_{15} \\ a_{21} & a_{22} - D_2 k^2 - \lambda & a_{23} & a_{24} & a_{25} \\ a_{31} & a_{32} & a_{33} - D_3 k^2 - \lambda & a_{34} & a_{35} \\ a_{41} & a_{42} & a_{43} & a_{44} - D_4 k^2 - \lambda & a_{45} \\ a_{51} & a_{52} & a_{53} & a_{54} & a_{55} - D_5 k^2 - \lambda \end{vmatrix} = 0,$$

$$\Rightarrow \quad \lambda^5 + a_1(k^2)\ \lambda^4 + a_2(k^2)\ \lambda^3 + a_3(k^2)\ \lambda^2 + a_4(k^2)\ \lambda + a_5(k^2) = 0, \tag{3.13}$$

where $a_i(k^2),\ (i = 1, 2, 3, 4, 5)$ are evaluated with parameter values from Table 3.1. The coefficients of characteristic equation (3.13) are as follows

$$\begin{aligned}
a_1(k^2) = &\quad 7.4837 + 3.012k^2,\\
a_2(k^2) = &\quad 3.9281 + 22.3811k^2 + 2.0361k^4,\\
a_3(k^2) = &\quad 0.635297 + 10.7014k^2 + 14.925k^4 + 0.02406k^6,\\
a_4(k^2) = &\quad 0.0345 + 1.4451k^2 + 5.8488k^4 + 0.1561k^6 + 0.00004k^8,\\
a_5(k^2) = &\quad 0.0003 + 0.05948k^2 + 0.4434k^4 + 0.0185k^6 + 0.0001k^8 + 2 \times 10^{-8}k^{10}
\end{aligned}$$

System will be stable if (apply Routh–Hurwitz stability criterion)

$$\begin{aligned}
&(i) \quad a_i\big(k^2\big) > 0, \quad i = 1, 2, 3, 4, 5,\\
&(ii) \quad h_1\big(k^2\big) = a_1\big(k^2\big)a_2\big(k^2\big)a_3\big(k^2\big) - a_3^2\big(k^2\big) + a_1^2\big(k^2\big)a_4\big(k^2\big) > 0, \qquad (3.14)\\
&(iii) \quad h_2\big(k^2\big) = \Big(a_1\big(k^2\big)a_4\big(k^2\big) - a_5\big(k^2\big)\Big)\Big(a_1\big(k^2\big)a_2\big(k^2\big)a_3\big(k^2\big) - a_3^2\big(k^2\big) -\\
&\qquad a_1^2\big(k^2\big)a_4\big(k^2\big)\Big) - a_5\big(k^2\big)\Big(a_1\big(k^2\big)a_2\big(k^2\big) - a_3\big(k^2\big)\Big)^2 + a_1\big(k^2\big)a_5^2\big(k^2\big) > 0.
\end{aligned}$$

The spatial homogenous steady state will become unstable due to spatial perturbation when at least one root of characteristic equation is positive. This requires at least one out of the following inequalities (3.14) to be violated. As all $D_i^{'}s,\ (i = 1, 2, 3, 4, 5)$ and k^2 are positive, $a_i(k^2) > 0, (i = 1, 2, 3, 4, 5)$ always holds. Hence, conditions for diffusive instability about $\mathrm{E}^* = (G^*, M^*, C_T^*, T_\beta^*, I_\gamma^*)$ are either $h_1(k^2) < 0$ or $h_2(k^2) < 0$ (Expression for $h_1(k^2)$ and $h_2(k^2)$ evaluated with parameter values from Table 3.1 are given below).

$$h_1(k^2) = 16.3378 + 332.416k^2 + 1883.76k^4 + 2960.48k^6 + 1020.1k^8 + 91.3793k^{10} + 0.146606k^{12} \qquad (3.15)$$

and

$$h_2(k^2) = 3.984 + 211.2k^2 + 3922.18k^4 + 31130.7k^6 + 112578k^8 + 176486k^{10} + 102645k^{12} + 24400k^{14} + 2169.4k^{16} + 45.0705k^{18} + 0.0752648k^{20} + 0.0000178103k^{22} \qquad (3.16)$$

The glioma free steady state $\mathrm{E}_2\left(0, M_{max}, 0, \frac{s_1}{\mu_2}, 0\right)$ is unstable if

$$h_3(k^2) = 3.5597 \times 10^{24} + 1.0596 \times 10^{26}k^2 + 4.526 \times 10^{25}k^4 + 4.296 \times 10^{24}k^6 + 1.45763 \times 10^{17}k^8 + 1.11144 \times 10^{9}k^{10} + 0.1466k^{12} < 0 \quad (3.17)$$

and

$$h_4(k^2) = 6.0689 \times 10^{36} + 6.0185 \times 10^{40}k^2 + 1.8413 \times 10^{42}k^4 + 1.236 \times 10^{43}k^6 + 5.0951 \times 10^{42}k^8 + 4.842 \times 10^{41}k^{10} + 1.373 \times 10^{38}k^{12} + 9.3 \times 10^{30}k^{14} + 1.935 \times 10^{23}k^{16} + 1.223 \times 10^{15}k^{18} + 2923 \times k^{20} + 0.00001k^{22} < 0. \quad (3.18)$$

The eigenvalues of the dispersion curve (characteristics polynomial) of interior homogenous steady-state $\mathrm{E}^* = (G^*, M^*, C_T^*, T_\beta^*, I_\gamma^*)$, cannot be determined analytically. Hence, we plot the dispersion curve (see Fig. 3.1), which clearly shows that after spatiotemporal perturbation, the spatial dynamics remain stable, that is, $\mathrm{Re}(\lambda) < 0$. Tumor free steady state is unstable after adding spatial perturbation. Hence, the Turing instability condition does not hold here. So, there is no possibility of occurring Turing pattern.

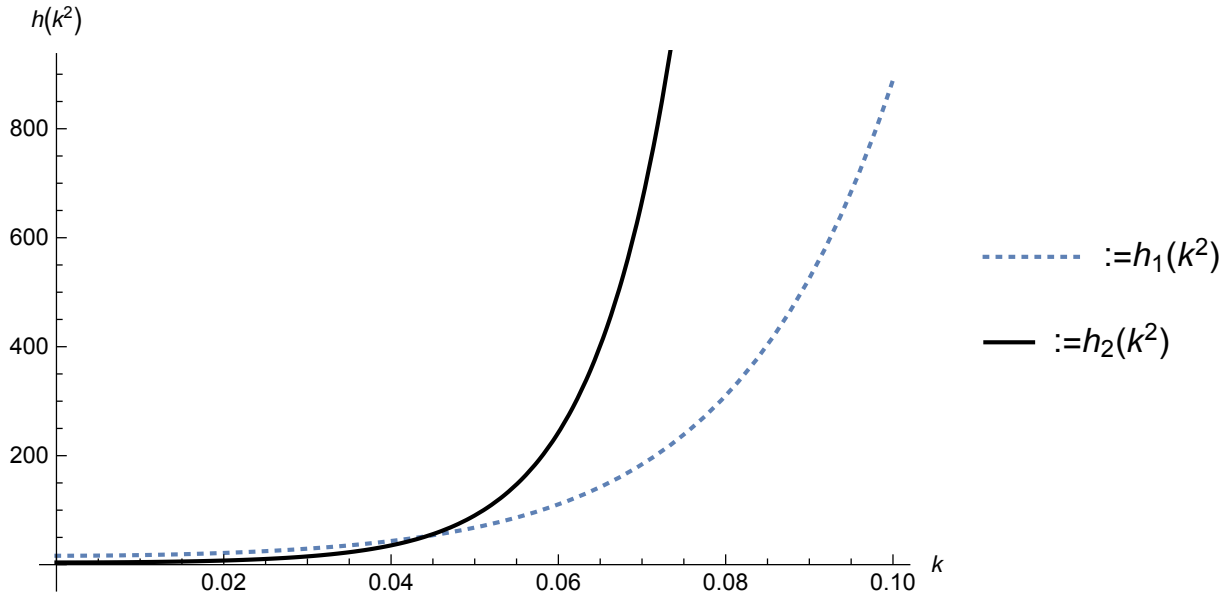

Figure 3.1: *Dispersion curve* $\left(h_1(k^2)\ \&\ h_2(k^2)\right)$ *for the system (3.6) without T11 target structure (T11TS), against the wave number(k). The parameter values are specified in Table 3.1.*

3.4.2 Analysis of spatial model with T11 target structure ($\mathbf{T}_s \neq 0$)

Proceeding in the same manner and taking spatiotemporal perturbations about the interior homogenous steady-state $\hat{\mathrm{E}}_1 = \left(\hat{G}, \hat{M}, \hat{C}_T, \hat{T}_\beta, \hat{I}_\gamma\right)$, we obtain the characteristic equation for the spatial model, with the help of Jacobian matrix around $\hat{\mathrm{E}}_1$, as

$$\lambda^5 + b_1(k^2)\ \lambda^4 + b_2(k^2)\ \lambda^3 + b_3(k^2)\ \lambda^2 + b_4(k^2)\ \lambda + b_5(k^2) = 0, \tag{3.19}$$

where

$$\begin{aligned}
b_1(k^2) = &\quad 8.36254 + 11k^2,\\
b_2(k^2) = &\quad 10.2299 + 32.0318k^2 + 45k^4,\\
b_3(k^2) = &\quad 2.1142 + 29.3039k^2 + 7.111k^4 + 85k^6,\\
b_4(k^2) = &\quad 0.1281 + 3.21873k^2 + 3.742k^4 + 1.01592k^6 + 74k^8,\\
b_5(k^2) = &\quad 0.0011 + 8.2257k^2 + 3.427k^4 + 3.4286k^6 + 4.876k^8 + 24k^10.
\end{aligned}$$

The homogenous steady-state will become unstable due to spatiotemporal perturbation when at least one root of characteristic equation is positive. All diffusion coefficients ($D_i^{'}s, i = 1, 2, 3, 4, 5$) and wave number ($k^2$) are positive therefore $b_i(k^2) > 0, (i = 1, 2, 3, 4, 5)$ always holds. This requires that at least one out of following inequalities is violated, that is,

$$(i)\ \ m_1(k^2) = b_1(k^2)b_2(k^2)b_3(k^2) > \left(b_3(k^2)\right)^2 + \left(b_1(k^2)\right)^2 b_4(k^2), \tag{3.20}$$

and

$$(ii)\ m_2(k^2) = \left(b_1(k^2)b_4(k^2) - b_5(k^2)\right)\Big(b_1(k^2)b_2(k^2)b_3(k^2) - (b_3(k^2))^2 - (b_1(k^2))^2 b_4(k^2)\Big) > b_5(k^2)\left(b_1(k^2)b_2(k^2) - b_3(k^2)\right)^2 + b_1(k^2)\left(b_5(k^2)\right)^2, \tag{3.21}$$

that is,

$$\begin{aligned}
m_1(k^2) &= 2.5896 \times 10^4(3.87836 + 1.50986k^2 + 2.29518k^4 + 9.7175k^6 + 6.1791k^8 + \\
&\qquad 1.323k^{10} + k^{12}) > 0
\end{aligned}$$

and

$$\begin{aligned}
m_2(k^2) &= 1.64171 \times 10^5(2.60294 + 3.3661k^2 + 1.3595k^4 + 1.7524k^6 + 2.7412k^8 + \\
&\qquad 1.484k^{10} + 2.657k^{12} + 3.257k^{14} + 1.4335k^{16} + 2.9091k^{18} + 2.779k^{20} + k^{22}) > 0
\end{aligned}$$

The eigenvalues of the dispersion curve (characteristics polynomial (3.19)) of interior homogenous steady-state $\hat{\mathrm{E}}_1 = \left(\hat{G}, \hat{M}, \hat{C}_T, \hat{T}_\beta, \hat{I}_\gamma\right)$, cannot be determined analytically. We plot the dispersion curve (see Fig. 3.2), which clearly shows that after spatiotemporal perturbation the spatial dynamics remain stable, that is, $\mathrm{Re}(\lambda) < 0$. Therefore, no possibility of occurring Turing bifurcation.

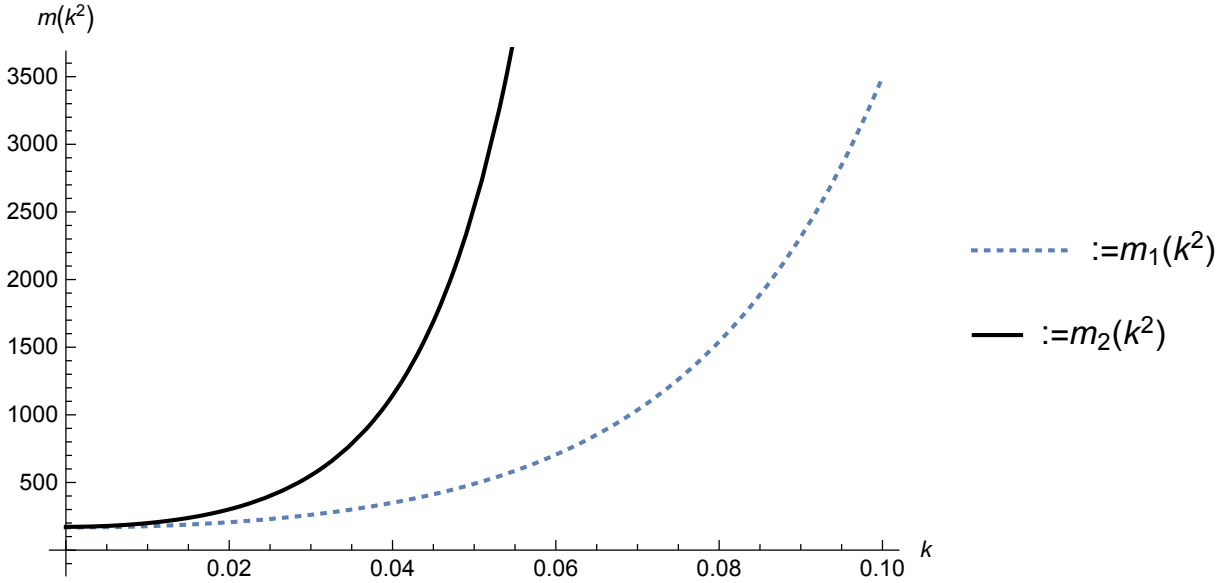

Figure 3.2: *Dispersion curve* $\left(m_1(k^2)\ \&\ m_2(k^2)\right)$ *for the system (3.6) with T11 target structure (T11TS), against the wave number(k). The parameter values are specified in Table 3.1.*

3.5 Higher order stability analysis

3.5.1 Higher order stability analysis without T11 target structure ($\mathbf{T}_s = 0$)

In this section, we use higher order spatiotemporal perturbation term to check the stability of the system [152], for this we have chosen with previous specific choice of parameter values. The interior steady state points $\mathrm{E}^* = (G^*, M^*, C_T^*, T_\beta^*, I_\gamma^*)$ for the non-spatial system corresponding to the system is a spatially homogenous steady states point for the system. We assume that the homogenous steady-state $\mathrm{E}^* = (G^*, M^*, C_T^*, T_\beta^*, I_\gamma^*)$ are locally stable for the non-spatial system. The spatial

perturbations $p(x,y,t)$, $q(x,y,t)$, $r(x,y,t)$, $m(x,y,t)$ and $n(x,y,t)$ on the homogenous steady-state G^*, M^*, ${C_T}^*$, ${T_\beta}^*$ and ${I_\gamma}^*$ is defined by $G = G^* + p(x,y,t)$, $M = M^* + q(x,y,t)$, $C_T = {C_T}^* + r(x,y,t)$, $T_\beta = {T_\beta}^* + m(x,y,t)$, $I_\gamma = {I_\gamma}^* + n(x,y,t)$. Expanding the non-spatial part by Taylor series expansion up to third order about homogenous steady-state, we get following expressions:

$$\begin{aligned}
p_t &= f_G\, p + f_M\, q + f_{C_T}\, r + f_{T_\beta}\, m + f_{I_\gamma}\, n + \frac{f_{GG}}{2}\, p^2 + \frac{f_{MM}}{2}\, q^2 + \frac{f_{C_TC_T}}{2}\, r^2 \\
&\quad + \frac{f_{T_\beta T_\beta}}{2}\, m^2 + \frac{f_{I_\gamma I_\gamma}}{2}\, n^2 + f_{GM}\, pq + f_{MC_T}\, qr + f_{C_TT_\beta}\, rm + f_{T_\beta I_\gamma}\, mn + \\
&\quad f_{I_\gamma G}\, np + D_1\left(p_{xx} + p_{yy}\right), \\
q_t &= g_G\, p + g_M\, q + g_{C_T}\, r + g_{T_\beta}\, m + g_{I_\gamma}\, n + \frac{g_{GG}}{2}\, p^2 + \frac{g_{MM}}{2}\, q^2 + \frac{g_{C_TC_T}}{2}\, r^2 \\
&\quad + \frac{g_{T_\beta T_\beta}}{2}\, m^2 + \frac{g_{I_\gamma I_\gamma}}{2}\, n^2 + g_{GM}\, pq + g_{MC_T}\, qr + g_{C_TT_\beta}\, rm + g_{T_\beta I_\gamma}\, mn + \\
&\quad g_{I_\gamma G}\, np + D_2\left(q_{xx} + q_{yy}\right), \\
r_t &= h_G\, p + h_M\, q + h_{C_T}\, r + h_{T_\beta}\, m + h_{I_\gamma}\, n + \frac{h_{GG}}{2}\, p^2 + \frac{h_{MM}}{2}\, q^2 + \frac{h_{C_TC_T}}{2}\, r^2 \\
&\quad + \frac{h_{T_\beta T_\beta}}{2}\, m^2 + \frac{h_{I_\gamma I_\gamma}}{2}\, n^2 + h_{GM}\, pq + h_{MC_T}\, qr + h_{C_TT_\beta}\, rm + h_{T_\beta I_\gamma}\, mn + \\
&\quad h_{I_\gamma G}\, np + D_3\left(r_{xx} + r_{yy}\right), \\
m_t &= u_G\, p + u_M\, q + u_{C_T}\, r + u_{T_\beta}\, m + u_{I_\gamma}\, n + \frac{u_{GG}}{2}\, p^2 + \frac{u_{MM}}{2}\, q^2 + \frac{u_{C_TC_T}}{2}\, r^2 \\
&\quad + \frac{u_{T_\beta T_\beta}}{2}\, m^2 + \frac{u_{I_\gamma I_\gamma}}{2}\, n^2 + u_{GM}\, pq + u_{MC_T}\, qr + u_{C_TT_\beta}\, rm + u_{T_\beta I_\gamma}\, mn + \\
&\quad u_{I_\gamma G}\, np + D_4\left(m_{xx} + m_{yy}\right), \\
n_t &= v_G\, p + v_M\, q + v_{C_T}\, r + v_{T_\beta}\, m + v_{I_\gamma}\, n + \frac{v_{GG}}{2}\, p^2 + \frac{v_{MM}}{2}\, q^2 + \frac{v_{C_TC_T}}{2}\, r^2 \\
&\quad + \frac{v_{T_\beta T_\beta}}{2}\, m^2 + \frac{v_{I_\gamma I_\gamma}}{2}\, n^2 + v_{GM}\, pq + v_{MC_T}\, qr + v_{C_TT_\beta}\, rm + v_{T_\beta I_\gamma}\, mn + \\
&\quad v_{I_\gamma G}\, np + D_5\left(n_{xx} + n_{yy}\right). \qquad (3.22)
\end{aligned}$$

Now, expressing the spatiotemporal perturbations $p(x,y,t)$, $q(x,y,t)$, $r(x,y,t)$, $m(x,y,t)$ and $n(x,y,t)$ as

$$\begin{aligned}
p(x,y,t) &= p(t)\cos(k_x x)\cos(k_y y), \\
q(x,y,t) &= q(t)\cos(k_x x)\cos(k_y y), \\
r(x,y,t) &= r(t)\cos(k_x x)\cos(k_y y), \\
m(x,y,t) &= m(t)\cos(k_x x)\cos(k_y y), \\
n(x,y,t) &= n(t)\cos(k_x x)\cos(k_y y),
\end{aligned}$$

with zero-flux boundary condition, the system (3.22) reduces to

$$\begin{aligned}
p_t &= f_G\ p + f_M\ q + f_{C_T}\ r + f_{T_\beta}\ m + f_{I_\gamma}\ n + \frac{f_{GG}}{2}\ p^2 + \frac{f_{MM}}{2}\ q^2 + \frac{f_{C_TC_T}}{2}\ r^2 + \\
&\quad \frac{f_{T_\beta T_\beta}}{2}\ m^2 + \frac{f_{I_\gamma I_\gamma}}{2}\ n^2 + f_{GM}\ pq + f_{MC_T}\ qr + f_{C_TT_\beta}\ rm + f_{T_\beta I_\gamma}\ mn + \\
&\quad f_{I_\gamma G}\ np - D_1k^2p, \\
q_t &= g_G\ p + g_M\ q + g_{C_T}\ r + g_{T_\beta}\ m + g_{I_\gamma}\ n + \frac{g_{GG}}{2}\ p^2 + \frac{g_{MM}}{2}\ q^2 + \frac{g_{C_TC_T}}{2}\ r^2 + \\
&\quad \frac{g_{T_\beta T_\beta}}{2}\ m^2 + \frac{g_{I_\gamma I_\gamma}}{2}\ n^2 + g_{GM}\ pq + g_{MC_T}\ qr + g_{C_TT_\beta}\ rm + g_{T_\beta I_\gamma}\ mn + \\
&\quad g_{I_\gamma G}\ np - D_2k^2q, \\
r_t &= h_G\ p + h_M\ q + h_{C_T}\ r + h_{T_\beta}\ m + h_{I_\gamma}\ n + \frac{h_{GG}}{2}\ p^2 + \frac{h_{MM}}{2}\ q^2 + \frac{h_{C_TC_T}}{2}\ r^2 + \\
&\quad \frac{h_{T_\beta T_\beta}}{2}\ m^2 + \frac{h_{I_\gamma I_\gamma}}{2}\ n^2 + h_{GM}\ pq + h_{MC_T}\ qr + h_{C_TT_\beta}\ rm + h_{T_\beta I_\gamma}\ mn + \\
&\quad h_{I_\gamma G}\ np - D_3k^2r, \\
m_t &= u_G\ p + u_M\ q + u_{C_T}\ r + u_{T_\beta}\ m + u_{I_\gamma}\ n + \frac{u_{GG}}{2}\ p^2 + \frac{u_{MM}}{2}\ q^2 + \frac{u_{C_TC_T}}{2}\ r^2 + \\
&\quad \frac{u_{T_\beta T_\beta}}{2}\ m^2 + \frac{u_{I_\gamma I_\gamma}}{2}\ n^2 + u_{GM}\ pq + u_{MC_T}\ qr + u_{C_TT_\beta}\ rm + u_{T_\beta I_\gamma}\ mn + \\
&\quad u_{I_\gamma G}\ np - D_4k^2m, \\
n_t &= v_G\ p + v_M\ q + v_{C_T}\ r + v_{T_\beta}\ m + v_{I_\gamma}\ n + \frac{v_{GG}}{2}\ p^2 + \frac{v_{MM}}{2}\ q^2 + \frac{v_{C_TC_T}}{2}\ r^2 + \\
&\quad \frac{v_{T_\beta T_\beta}}{2}\ m^2 + \frac{v_{I_\gamma I_\gamma}}{2}\ n^2 + v_{GM}\ pq + v_{MC_T}\ qr + v_{C_TT_\beta}\ rm + v_{T_\beta I_\gamma}\ mn+, \\
&\quad v_{I_\gamma G}\ np - D_5k^2n, \qquad (3.23)
\end{aligned}$$

where $k^2 = k_x^2 + k_y^2$. It is clear from system (3.23) that the growth or decay of first order perturbation terms depends on the second order perturbation terms. Further, we need the dynamical system for second-order perturbation terms involved in (3.23). Multiplying the first equation by $2p$, second equation by $2q$, third equation by $2r$, fourth equation by $2m$ and fifth equation by $2n$ respectively in (3.23) and neglecting of third order perturbation term, we have the dynamical equation of

second order perturbations as

$$
\begin{aligned}
\left(p^2\right)_t &= 2f_G p^2 + 2f_M pq + 2f_{C_T} pr + 2f_{T_\beta} pm + 2f_{I_\gamma} pn - 2D_1 k^2 p^2,\\
\left(q^2\right)_t &= 2g_G pq + 2g_M q^2 + 2g_{C_T} qr + 2g_{T_\beta} qm + 2g_{I_\gamma} qn - 2D_2 k^2 q^2,\\
\left(r^2\right)_t &= 2h_G pr + 2h_M rq + 2h_{C_T} r^2 + 2h_{T_\beta} rm + 2h_{I_\gamma} rn - 2D_3 k^2 r^2,\\
\left(m^2\right)_t &= 2u_G pm + 2u_M mq + 2u_{C_T} mr + 2u_{T_\beta} m^2 + 2u_{I_\gamma} mn - 2D_4 k^2 m^2,\\
\left(n^2\right)_t &= 2v_G pn + 2v_M nq + 2v_{C_T} nr + 2v_{T_\beta} nm + 2v_{I_\gamma} n^2 - 2D_5 k^2 n^2,\\
(pq)_t &= f_M q^2 + g_G p^2 + (f_G + g_M) qp + f_{C_T} qr + g_{C_T} pr + f_{T_\beta} qm + g_{T_\beta} mp\\
&\qquad + f_{I_\gamma} qn + g_{I_\gamma} np - k^2 (D_1 + D_2) pq,\\
(qr)_t &= h_M q^2 + g_{C_T} r^2 + (g_M + h_{C_T}) qr + h_G qp + h_{T_\beta} qm + h_{I_\gamma} qn + g_G rp\\
&\qquad + g_{T_\beta} rm + g_{I_\gamma} rn - k^2 (D_2 + D_3) rq,\\
(rm)_t &= u_{C_T} r^2 + h_{I_\gamma} m^2 + (u_{T_\beta} + h_{C_T}) rm + u_{I_\gamma} rn + u_G pr + u_M qr + h_G mp\\
&\qquad + h_M qm + h_{I_\gamma} nm - k^2 (D_3 + D_4) rm,\\
(mn)_t &= v_{T_\beta} m^2 + u_{I_\gamma} n^2 + (v_{I_\gamma} + u_{T_\beta}) mn + v_G pm + v_M qm + v_{C_T} rm + u_G np\\
&\qquad + u_M qn + u_{C_T} nr - k^2 (D_4 + D_5) mn,\\
(np)_t &= f_{I_\gamma} n^2 + v_G p^2 + (v_{I_\gamma} + f_G) pn + f_M qn + f_{C_T} rn + f_{T_\beta} mn + v_M qp\\
&\qquad + v_{C_T} rp + v_T mp - k^2 (D_5 + D_1) np. \qquad (3.24)
\end{aligned}
$$

The truncation of third and higher order terms in Taylor series expansion and neglecting third and higher order perturbation terms during derivation of dynamical equations (3.23 – 3.24) leads to a closed system of equations for $p,\ q,\ r,\ m,\ n,\ p^2,\ q^2,\ r^2,\ m^2,\ n^2,\ pq,\ qr,\ rm,\ mn,\ np$, otherwise, one cannot avoid infinite hierarchy of dynamical equations for perturbation terms. Truncation of higher order terms does not affect the understanding of the role of leading order non-linearity. Applicability and significance of the analysis can be justified with the perturbation terms up to order three for the system (2.12) with the suitable choice of parameter values. The dynamical equations (3.23–3.24) can be written into a compact matrix form as follows:

$$\frac{dX}{dt} = BX, \qquad (3.25)$$

where $X = [p,\ q,\ r,\ m,\ n,\ p^2,\ q^2,\ r^2,\ m^2,\ n^2,\ pq,\ qr,\ rm,\ mn,\ np]^T$ and

$$\mathbf{B} = \begin{pmatrix}
b_{11} & f_M & f_{C_T} & f_{T_\beta} & f_{I_\gamma} & \frac{f_{GG}}{2} & \frac{f_{GG}}{2} & \frac{f_{C_TC_T}}{2} & \frac{f_{T_\beta T_\beta}}{2} & \frac{f_{I_\gamma I_\gamma}}{2} & f_{GM} & f_{MC_T} & f_{C_TT_\beta} & f_{T_\beta I_\gamma} & f_{I\gamma G} \\
g_G & b_{22} & g_{C_T} & g_{T_\beta} & g_{I_\gamma} & \frac{g_{GG}}{2} & \frac{g_{MM}}{2} & \frac{g_{C_TC_T}}{2} & \frac{g_{T_\beta T_\beta}}{2} & \frac{g_{I_\gamma I_\gamma}}{2} & g_{GM} & g_{MC_T} & g_{C_TT_\beta} & g_{T_\beta I_\gamma} & g_{I\gamma G} \\
h_G & h_M & b_{33} & h_{T_\beta} & h_{I_\gamma} & \frac{h_{GG}}{2} & \frac{h_{MM}}{2} & \frac{h_{C_TC_T}}{2} & \frac{h_{T_\beta T_\beta}}{2} & \frac{h_{I_\gamma I_\gamma}}{2} & h_{GM} & h_{MC_T} & h_{C_TT_\beta} & h_{T_\beta I_\gamma} & h_{I\gamma G} \\
u_G & u_M & u_{C_T} & b_{44} & u_{I_\gamma} & \frac{u_{GG}}{2} & \frac{u_{MM}}{2} & \frac{u_{C_TC_T}}{2} & \frac{u_{T_\beta T_\beta}}{2} & \frac{u_{I_\gamma I_\gamma}}{2} & u_{GM} & u_{MC_T} & u_{C_TT_\beta} & u_{T_\beta I_\gamma} & u_{I\gamma G} \\
v_G & v_M & v_{C_T} & v_{T_\beta} & b_{55} & \frac{v_{GG}}{2} & \frac{v_{MM}}{2} & \frac{v_{C_TC_T}}{2} & \frac{v_{T_\beta T_\beta}}{2} & \frac{v_{I_\gamma I_\gamma}}{2} & v_{GM} & v_{MC_T} & v_{C_TT_\beta} & v_{T_\beta I_\gamma} & v_{I\gamma G} \\
0 & 0 & 0 & 0 & 0 & b_{66} & 0 & 0 & 0 & 0 & 2f_M & 0 & 0 & 0 & 2f_{I_\gamma} \\
0 & 0 & 0 & 0 & 0 & 0 & b_{77} & 0 & 0 & 0 & 2g_G & 2g_{C_T} & 0 & 0 & 0 \\
0 & 0 & 0 & 0 & 0 & 0 & 0 & b_{88} & 0 & 0 & 0 & 2h_M & 2h_{T_\beta} & 0 & 0 \\
0 & 0 & 0 & 0 & 0 & 0 & 0 & 0 & b_{99} & 0 & 0 & 0 & 2u_{C_T} & 2u_{I_\gamma} & 0 \\
0 & 0 & 0 & 0 & 0 & 0 & 0 & 0 & 0 & b1010 & 0 & 0 & 0 & 2v_{T_\beta} & 2v_G \\
0 & 0 & 0 & 0 & 0 & g_G & f_M & 0 & 0 & 0 & b_{1111} & f_{C_T} & 0 & 0 & g_{I_\gamma} \\
0 & 0 & 0 & 0 & 0 & 0 & h_M & g_{C_T} & 0 & 0 & h_G & b_{1212} & g_{T_\beta} & 0 & 0 \\
0 & 0 & 0 & 0 & 0 & 0 & 0 & u_{C_T} & h_{I_\gamma} & 0 & 0 & u_M & b_{1313} & h_{I_\gamma} & 0 \\
0 & 0 & 0 & 0 & 0 & 0 & 0 & 0 & v_{T_\beta} & u_{I_\gamma} & 0 & 0 & v_{c_T} & b_{1414} & u_G \\
0 & 0 & 0 & 0 & 0 & v_G & 0 & 0 & 0 & f_{I_\gamma} & v_M & 0 & 0 & f_{T_\beta} & b_{1515}
\end{pmatrix}$$

with

$b_{11} = f_G - D_1k^2$, $b_{22} = g_M - D_2k^2$, $b_{33} = h_{C_T} - D_3k^2$, $b_{44} = u_{T_\beta} - D_4k^2$, $b_{55} = v_{I_\gamma} - D_5k^2$, $b_{66} = 2\left(f_G - D_1k^2\right)$, $b_{77} = 2\left(g_M - D_2k^2\right)$, $b_{88} = 2\left(h_{C_T} - D_3k^2\right)$, $b_{99} = 2\left(u_{T_\beta} - D_4k^2\right)$, $b_{1010} = 2\left(v_{I_\gamma} - D_5k^2\right)$, $b_{1111} = f_G + g_M - k^2\left(D_1 + D_2\right)$, $b_{1212} = g_M + h_{C_T} - k^2\left(D_2 + D_3\right)$, $b_{1313} = h_{C_T} + u_{T_\beta} - k^2\left(D_3 + D_4\right)$, $b_{1414} = u_{T_\beta} + v_{I_\gamma} - k^2\left(D_4 + D_5\right)$, $b_{1515} = f_G + v_{I_\gamma} - k^2\left(D_1 + D_5\right)$.

We take the solution of system (3.25) of the form $X(t) \sim e^{\lambda t}$, where $\lambda' s \equiv \lambda(k)$, are the eigenvalues of B and $\lambda' s$ are the solution of the following equation

$$|B - \lambda I| = 0, \tag{3.26}$$

where I is the 15×15 unit matrix. Numerically, using the parameter values given in Table 3.1, all the eigenvalues of the matrix B are negative, namely, -13.86, -7.06007, -7.032, -6.93, -0.623962, -0.442052, -0.321919, -0.311981, -0.260143, -0.204, -0.130072, $-0.1\ 11939$, -0.102, -0.01, and -0.00993845. Therefore, the system is stable about $\mathrm{E}^* = (G^*, M^*, C_T^*, T_\beta^*, I_\gamma^*)$. However, glioma free steady state point is unstable since the eigenvalues of B are -13.86, -7.032, -6.9375, -6.93, -0.6616, -0.3383, -0.3308, -0.323803, -0.204, -0.102, -0.0950034, -0.015, 0.0139933, -0.0075, and 0.00699664 (one positive) about $\mathrm{E}_2\left(0, M_{max}, 0, \frac{s_1}{\mu_2}, 0\right)$.

3.5.2 Higher order stability analysis with T11 target structure ($\mathbf{T}_s \neq 0$)

Proceeding in the same manner as above subsection and using the parameter values which are given in Table 3.1, all the eigenvalues of the matrix B are negative, that is, -13.86, -7.05947, -7.032, -6.93, -2.38354, -1.32126, -1.20135, -1.19177, -0.258942, -0.204, -0.129487, -0.111597, -0.102, -0.0191933, and -0.00958105. Therefore, the system is stable about $\hat{\mathrm{E}}_1 = \left(\hat{G}, \hat{M}, \hat{C_T}, \hat{T_\beta}, \hat{I_\gamma}\right)$. The system is also stable about glioma free steady state $\mathrm{E}_{T1}\left(0, \tilde{M}, \frac{T_s}{\mu_1}, \frac{s_1}{\mu_2}, \frac{b_2 T_s}{\mu_1 \mu_3}\right)$, since the eigenvalues are -13.86, -7.032, -6.9375, -6.93, -2.39366, -1.22502, -1.20433, -1.19683, -0.204, -0.130193, -0.102, -0.0563853, -0.0281927, -0.015, and -0.0075.

3.6 Numerical simulation

The spatiotemporal model (3.6) is solved numerically in one and two dimensional space with the help of finite difference method for spatial derivatives. Euler method is utilized for the reaction part and standard five point finite difference method is utilized for the diffusion part. The numerical integration of the reaction-diffusion partial differential equations (3.6) is employed by using splitting method. The value of time step and space step have been chosen sufficiently small for avoiding the numerical artifacts, so we have taken time step $\Delta t = 0.002$ and space step $\Delta x = \Delta y = 1$. We perform numerical simulations over the zero-flux boundary condition with domain size in one dimension [0, 1000] and 160×160 units in two-dimensional spaces. The initial density distribution of glioma, macrophage, cytotoxic T-lymphocyte, TGF - β and IFN - γ are chosen in such a way that they are relevant biologically.

The biological motivation of this work is to study the heterogeneous patterns of glioma cells and the immune system components, namely, macrophages and cytotoxic T-lymphocytes.

Figure 3.3 shows the snapshots of the numerical simulations of glioma density distribution over space (1D). A periodic temporal behavior together with a smooth spatial glioma distribution is observed for times t=50, 100, 150, 200, 300 and 400 days respectively (Figures 3.3(a–f)). Figure 3.4 shows similar dynamics when nu-

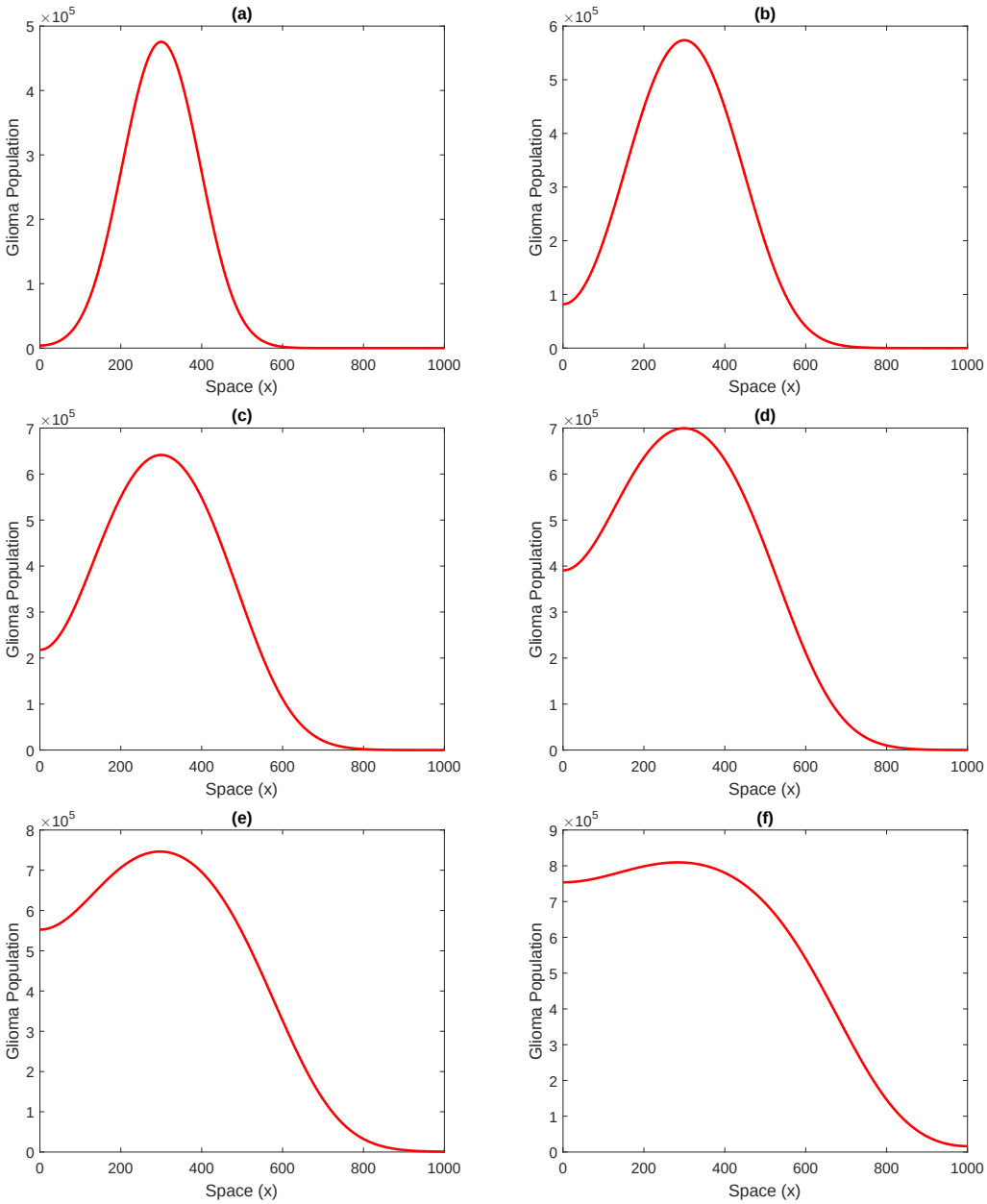

Figure 3.3: *The glioma cells density* $G(t, x)$ *at time* $T = 50, 100, 150, 200, 300$ *and* 400 *days respectively, without T11TS in one dimensional space. Values of* D_1, D_2, D_3, D_4, D_5 *are 4, 1, 2, 1, 3 respectively. Other parameter values are specified in Table 3.1.*

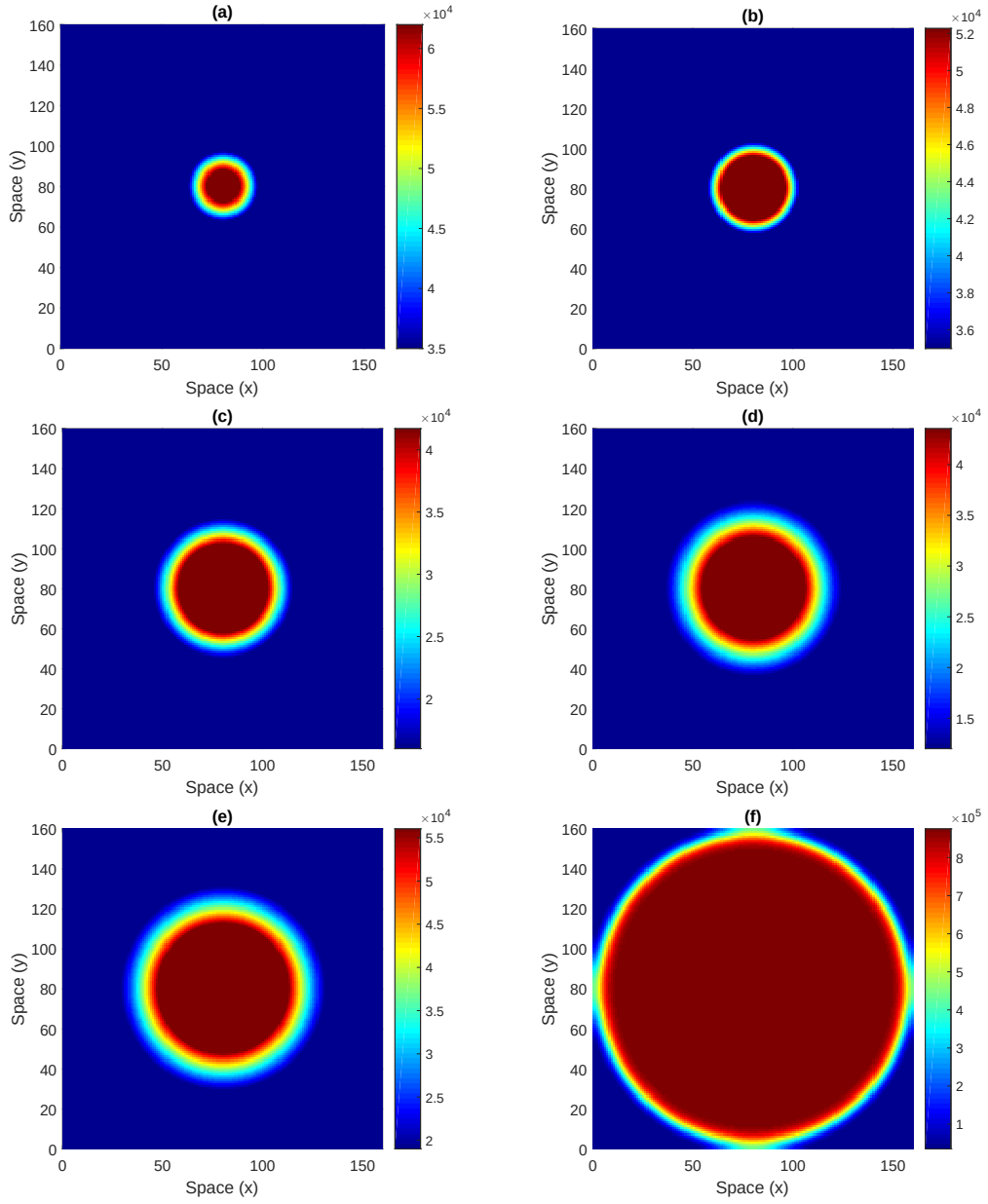

Figure 3.4: *The glioma cells density* $G(t, x, y)$ *at time* $T = 50, 100, 150, 200, 300$ *and* 400 *days respectively, without T11TS in two dimensional space. Values of* D_1, D_2, D_3, D_4, D_5 *are 4, 1, 2, 1, 3 respectively. Other parameter values are specified in Table 3.1.*

merical simulation of glioma densities in two dimensional space is considered for times t=50, 100, 150, 200, 300 and 400 days respectively. In the beginning, the glioma spreads in small mass (Figures 3.4(a, b)) and then turns aggressive to invade the entire domain (Figures 3.4(c–f)). At time T = 400, the initial clumps of glioma cells reaches approximate at the boundary. We observe that the boundary domain represents a zone of solid tissue that the gliomas density are powerless to infiltrate due to zero-flux boundary conditions and hence begin to move in the backward direction. The immune components fail to control the growth of malignant gliomas.

Figure 3.5 shows the snapshots of numerical simulation of density of macrophages in one dimension space. Solitary traveling patches of macrophage density are seen in Figures 3.5(a–f). The spread of the macrophages over space is via propagation of a traveling pulse, which is nonstationary and propagates with constant speed. However, the spread of macrophages are restricted due to high aggressive spread of gliomas. In this case, the invasiveness is absent both in front of the pulse and its wake, which means that invasion of macrophages have failed, implying that macrophages have failed to control the growth and spread of malignant gliomas. Figure 3.6 shows the snapshots of macrophage spread in 2D spaces at t=50, 100, 150, 200, 300 and 400 days respectively.

The snapshots in Figure 3.7 describes the one dimensional numerical simulations of the cytotoxic T-lymphocytes density and in Figure 3.8 depicts the two dimensional numerical simulations of the cytotoxic T-lymphocytes density at t=50, 100, 150, 200, 300 and 400 days respectively. It is clear that the rate of flow of malignant gliomas is faster than the flow of cytotoxic T-lymphocytes. Therefore, the immune response is too weak to control the growth of untreated gliomas.

Figure 3.9 shows the spatiotemporal dynamics of malignant gliomas after the administration of T11 target structure. Figure 3.9(a) is the snapshot of the spread of glioma, just two days after the administration of the immunotherapeutic drug T11 target structure. After t=10 days, the spread of malignant gliomas is curbed by the drug (Figure 3.9(b)). Figures 3.9(c) and 3.9(d) show the snapshots of spatiotemporal spread of the malignant gliomas after the administration of T11 target structure respectively, in the span of six days each. Figure 3.10 shows the snapshots of the spread of malignant gliomas after the second (Figure 3.10(a,b,c)) and third (Figure

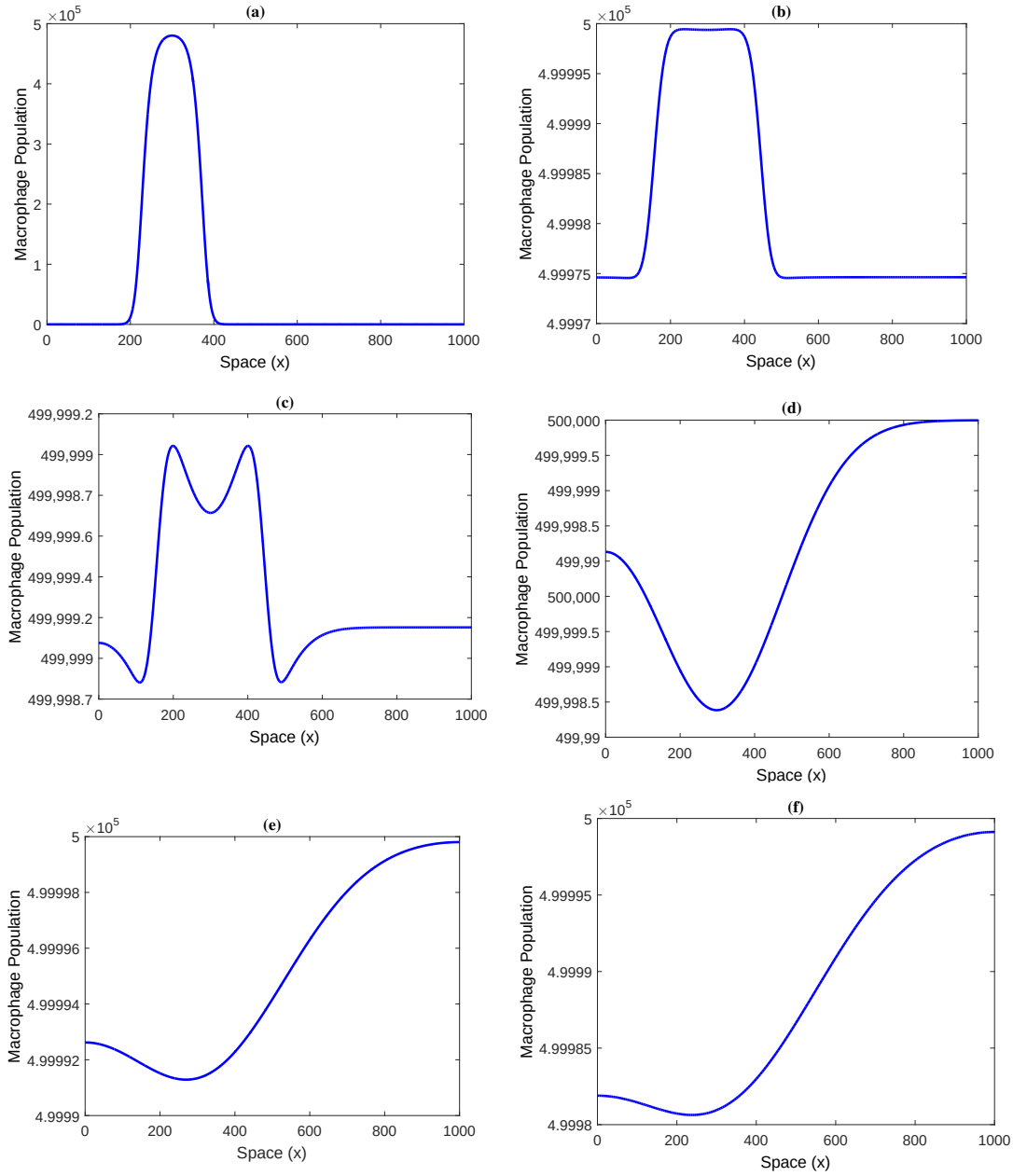

Figure 3.5: *The macrophage cells density* $M(t,x)$ *at time* $T = 50, 100, 150, 200, 300$ *and* 400 *days respectively, without T11TS in one dimensional space. Values of* D_1*,* D_2*,* D_3*,* D_4*,* D_5 *are 4, 1, 2, 1, 3 respectively. Other parameter values are specified in Table 3.1.*

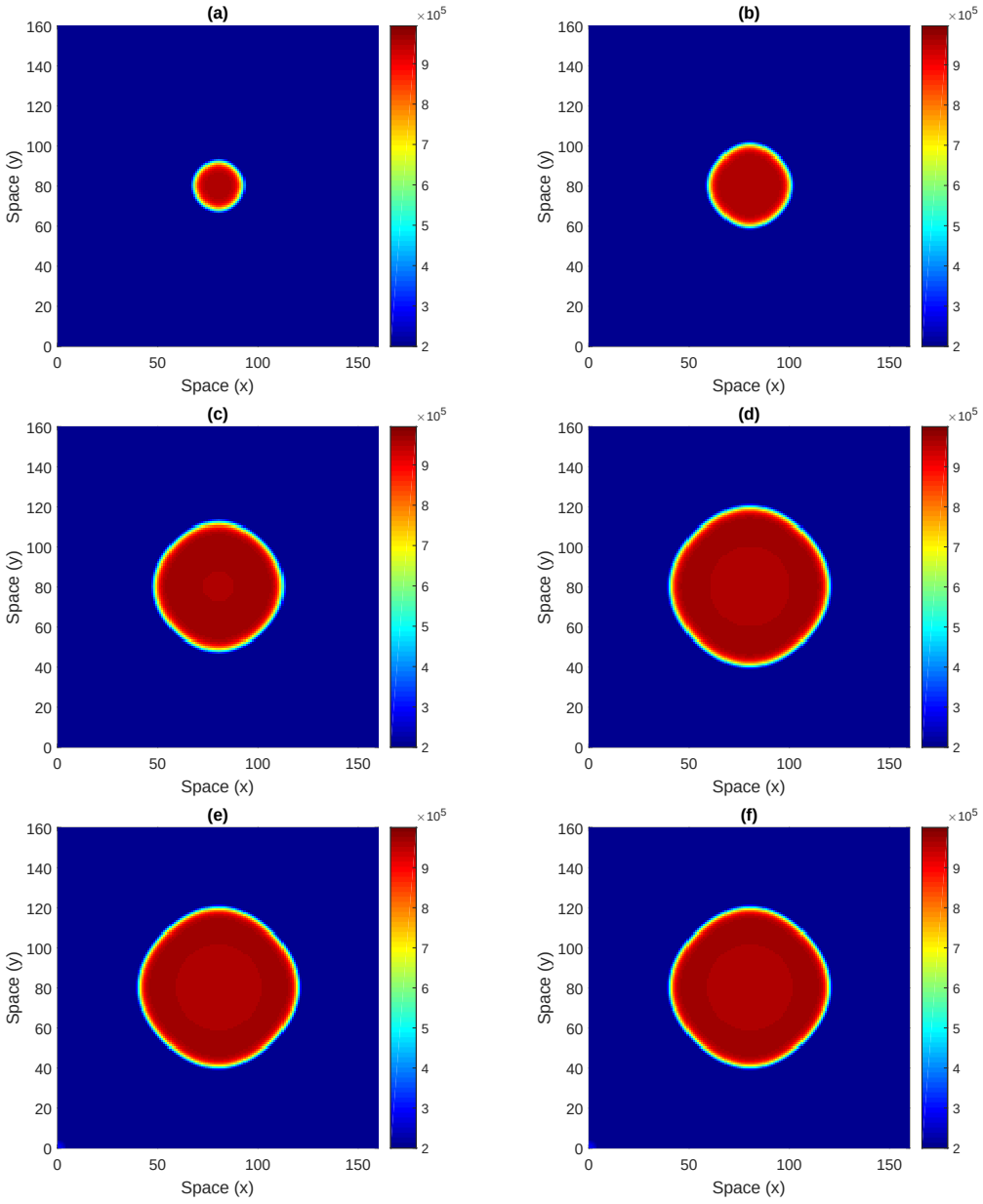

Figure 3.6: *The macrophage cells density* $M(t, x, y)$ *at time* $T = 50$, 100, 150, 200, 300 *and* 400 *days respectively, without T11TS in two dimensional space. Values of* D_1, D_2, D_3, D_4, D_5 *are 4, 1, 2, 1, 3 respectively. Other parameter values are specified in Table 3.1.*

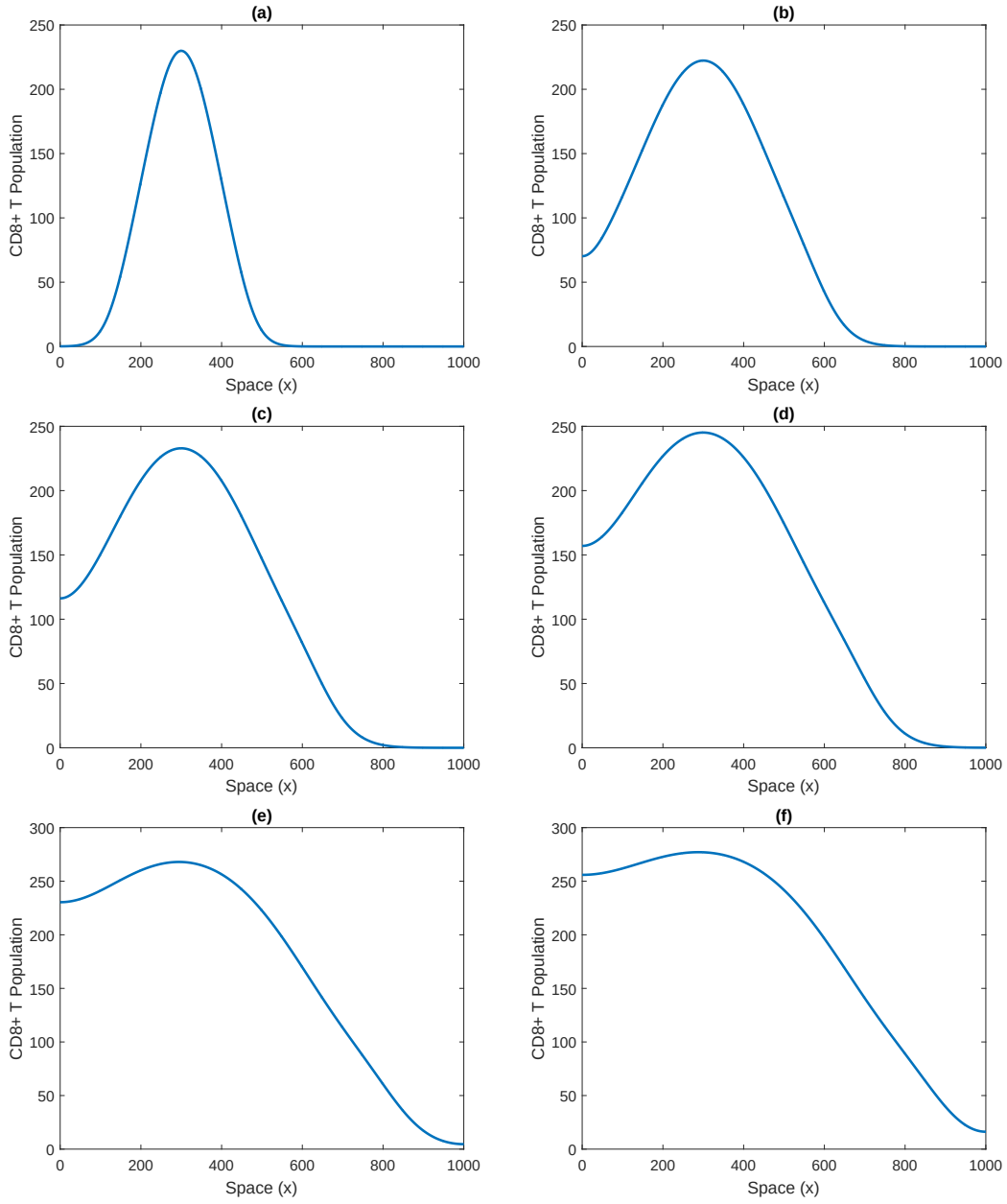

Figure 3.7: *The cytotoxic T-lymphocytes cells density* $C_T(t, x)$ *at time* $T = 50$, 100, 150, 200, 300 *and* 400 *days respectively, without T11TS in one dimensional space. Values of* D_1, D_2, D_3, D_4, D_5 *are 4, 1, 2, 1, 3 respectively. Other parameter values are specified in Table 3.1.*

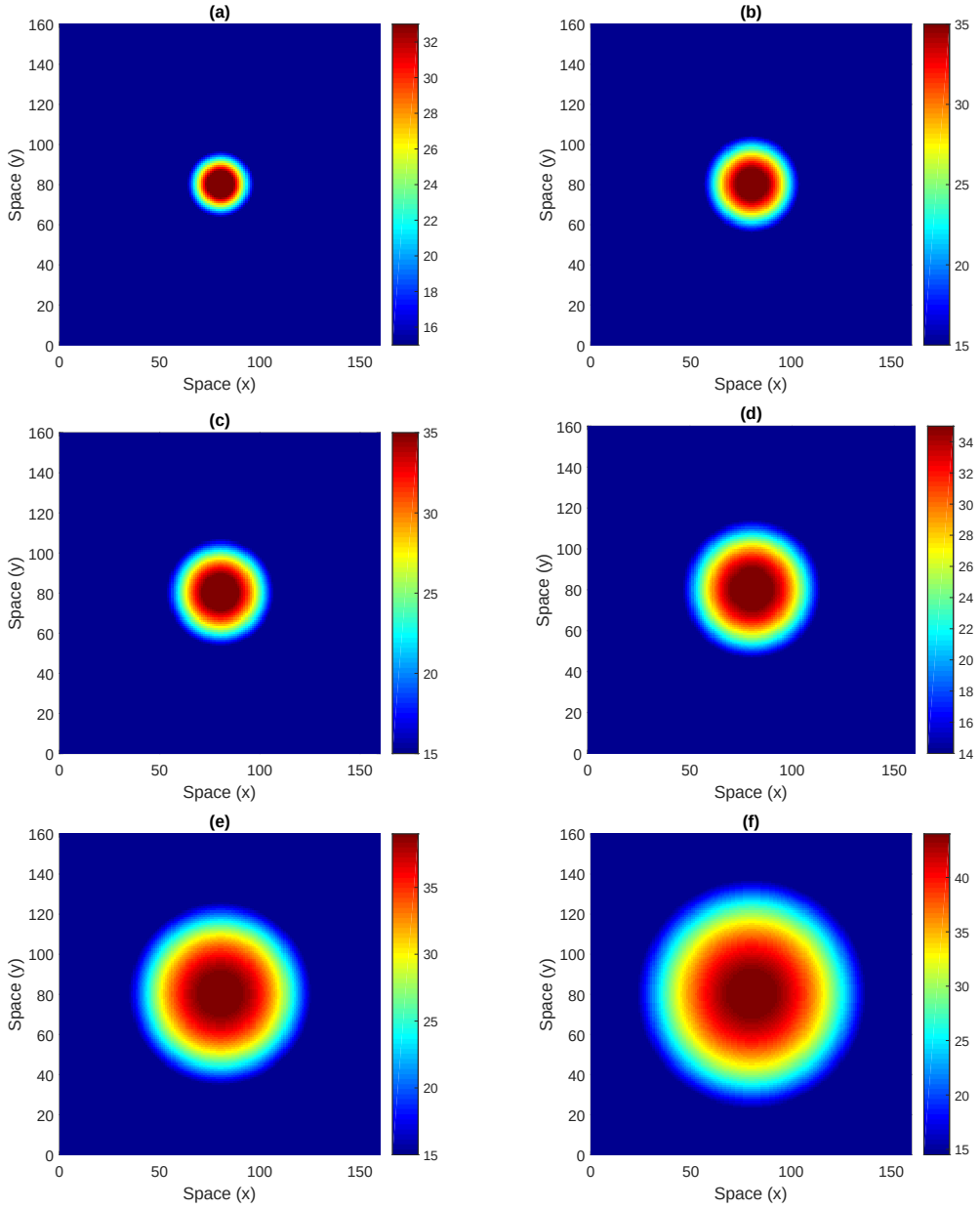

Figure 3.8: *The cytotoxic T-lymphocytes cells density* $C_T(t, x, y)$ *at time* $T = 50, 100, 150, 200, 300$ *and* 400 *days respectively, without T11TS in two dimensional space. Values of* D_1*,* D_2*,* D_3*,* D_4*,* D_5 *are 4, 1, 2, 1, 3 respectively. Other parameter values are specified in Table 3.1.*

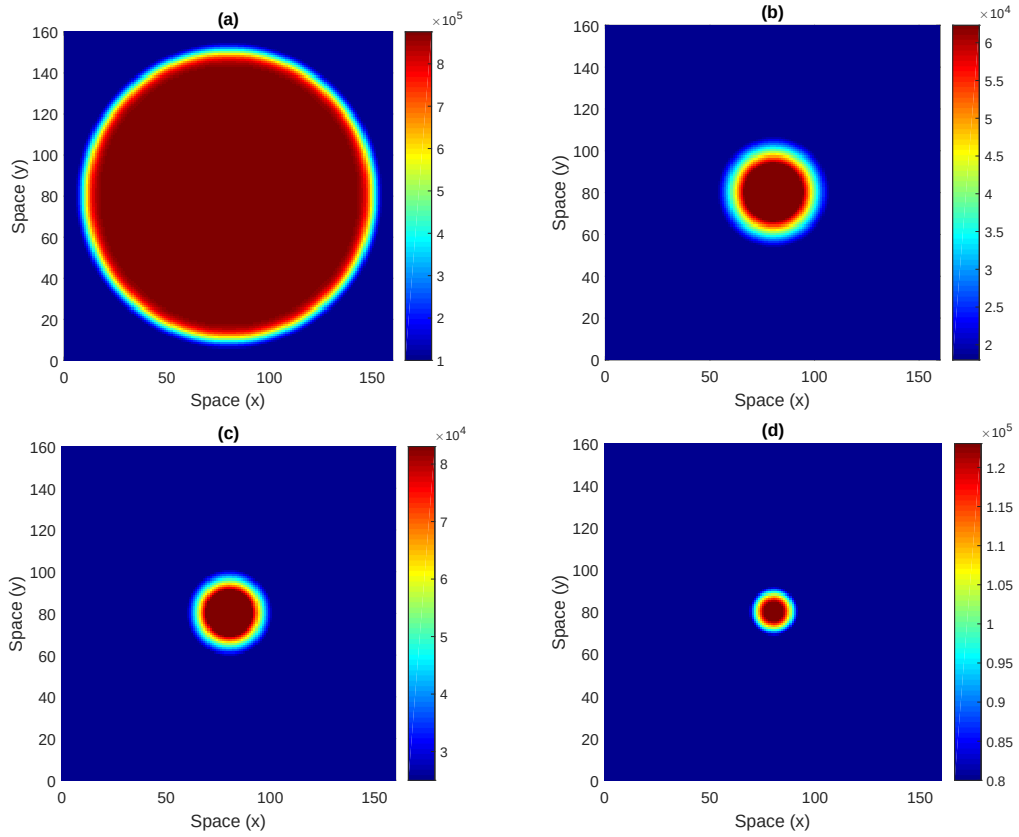

Figure 3.9: *The glioma cells density $G(t, x, y)$ with T11TS. The parameter values are specified in Table 3.1.*

3.10(d,e,f)) administration of T11 target structure respectively, with increasing value of diffusion coefficient ($D_1 = 4, 7, 10$). In both the cases, the malignant gliomas fail to spread in the domain, implying that T11 target structure succeeded in controlling the growth of malignant gliomas.

3.7 Conclusion

A spatiotemporal mathematical model of interaction between malignant gliomas and immune system, namely, macrophages, cytotoxic T-lymphocytes, IFN-γ and TGF-β is studied in this chapter. To study the spatial aspect of the system, the original model studied by Banerjee et. al. [12; 79; 80] is expressed as a reaction-diffusion equation. The system is investigated before and after the administration

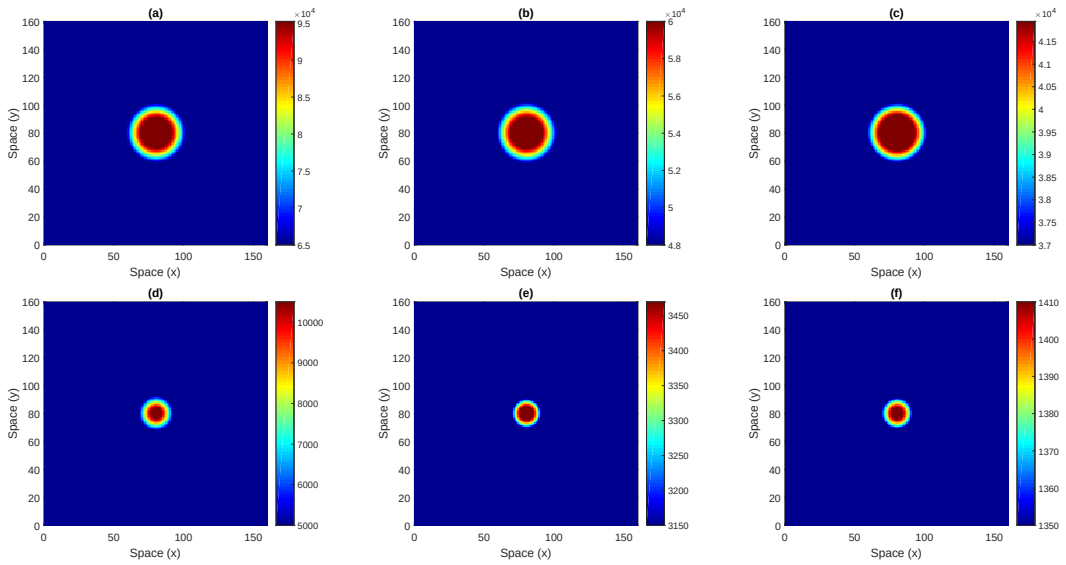

Figure 3.10: *Effect of diffusion on the glioma cells density $G(t, x, y)$ after administration of T11 target structure. The upper panel is evaluated at $T = 213$ with diffusion coefficient (D_1) of gliomas as 4, 7, 10 respectively. The lower panel is evaluated at $T = 225$ with diffusion coefficient (D_1) of gliomas as 4, 7, 10 respectively. The parameter values are specified in Table 3.1.*

of the immunotherapeutic drug T11 target structure for better understanding of the growth and invasion of glioma population.

Though extensive analytical study has been done on the proposed reaction-diffusion model, it is difficult to predict its biological implications unless the results are subjected to numerical data. Using the numerical data from Table 3.1, it is observed that no Turing zone exists for both the cases T11 $= 0$ and T11 $\neq 0$, implying that the system will have no Turing bifurcation and hence no Turing pattern. Without the administration of T11 target structure, the non-Turing patterns for gliomas indicate that the body's own defense mechanism, that is, the natural immune responses is too weak to control the growth and spread of malignant gliomas, which leads to glioma invasion of the entire domain. This aggressive motility of the gliomas restrict the propagation of the immune components, namely, macrophages and cytotoxic T-lymphocytes. After the administration of T11 target structure, the glioma cell proliferation is controlled by activating the phagocytic activity of macrophages as well as cytotoxic efficacy of the cytotoxic T-lymphocytes.

The spatiotemporal study of the effect of the immunotherapeutic drug T11 target structure on malignant gliomas is relatively new and our study show that it may be a promising therapeutic method to eradicate malignant gliomas. We sincerely hope that mathematical technique, numerical simulations and biological interpretations presented in this chapter would be helped to immunotherapy research with T11 target structure.

Chapter 4

Spatial aspects of hunting cooperation in predators with Holling type II functional response

4.1 Introduction

Spatial patterns formation in nature are ubiquitous, with illustrations like zebra stripe patterns on animals skin, Turing patterns in a coherent quantum field, or diffusive patterns in predator–prey models [7; 8; 122; 157]. The spatial factors of species interplay has been recognized as a vital component as how ecological communities are created and ecological interplay occurs over a broad limit of temporal and spatial scale [51]. Spatial population distribution is of major importance in the study of ecological systems [98; 104; 158]. Mechanisms and scenarios characterizing the spatial population distribution of ecological species in spatial habitat are a focus of special interest in population dynamics. The spatial population distribution is affected by the proliferation capacity of the species and interactions between individuals [184].

Spatial pattern formation of predator–prey systems have started based upon the elementary work of A. M. Turing on morphogenesis [179]. The spatial predator–prey systems are studied to comprehend the role of random mobility of the prey and predator, inside their residence. A fully comprehensive elucidation of the spatial

impact on ecological species interplays can be observed in the book, written by Okubo et.al. [125].

Spatial mathematical model is an appropriate tool for investigating fundamental mechanism of complex spatiotemporal population dynamics. An appropriate mathematical structure to explain the spatial aspect of population dynamics is specified by reaction-diffusion equations. Reaction-diffusion models were initially applied to describe the ecological pattern formation by Segel and Jackson in 1972 [157], based on the primary work of Turing [179]. Over the last several decades, a lot of articles have been published on the spatial dynamics of predator–prey model based on reaction-diffusion equations and different types of patterns have emerged for these models [8; 9; 10; 15; 18; 70; 104; 105; 114; 117; 120; 125; 141; 142; 157; 187; 193; 197].

Cooperative behavior can stimulate a relation among the population density and per capita population growth rate [45; 162]. Ecologists have accepted several mechanisms for stimulating cooperative behavior in prey, namely cooperating reproduction, foraging capacity, etc. The cooperative behavior in prey may be generated by predation or by procedure inborn to the prey lifespan history [162]. Theory has pervasively pay attention to cooperative behavior in preys [2; 37; 54; 66; 67; 116; 150; 185; 195] and cooperative behavior in predators are less studied and poorly understood [24; 48; 183], in particular when space is considered explicitly. A mathematical model of prey and predator population interplay with cooperative behavior in predators through the system of nonlinear ordinary differential equations has been studied in non-spatial domain by Alves et.al. [5]. Motivated from their work, we modify and extend the model in a spatial domain to study its spatial dynamics.

The objective of this current investigation is to create deep intuition into methods of spatial pattern formation in predator–prey model with cooperative behavior in predators. Here, we investigate how distinct intensity of cooperation rate, basic reproduction number of the predator and diffusion coefficients affect the spatial patterns of predator–prey interaction.

4.2 Model description

By incorporating diffusion and Holling type II functional response in the predator–prey system with cooperative behavior in predators [5], we obtain the following diffusive predator–prey model as

$$\begin{aligned} \frac{\partial X}{\partial t'} &= rX\left(1-\frac{X}{K}\right)-\frac{(\lambda+aY)\,XY}{1+h_1\,(\lambda+aY)\,X}+d_1\nabla^2 X, \\ \frac{\partial Y}{\partial t'} &= \frac{e\,(\lambda+aY)\,XY}{1+h_1\,(\lambda+aY)\,X}-mY+d_2\nabla^2 Y, \end{aligned} \tag{4.1}$$

where $X(t^{'})$ and $Y(t^{'})$ are the densities of prey and predator population at time $t^{'}$ and location (X_1, X_2), respectively. Here, r is the intrinsic growth rate of the prey and K is its carrying capacity. We consider a Holling type II functional response of the form

$$\frac{(\lambda+aY)\,X}{1+h_1\,(\lambda+aY)\,X}, \tag{4.2}$$

which depends on both prey and predator densities, thereby reflecting hunting cooperation (handling-driven). The parameter λ ($\lambda > 0$) is the attack rate per predator and prey, a ($a > 0$) describes the predator cooperation in hunting (aY is cooperation term) and h_1 is the predator's handling time of a prey. The parameter e is conversion efficiency and m is the per capita mortality rate of predators. The non-negative constants d_1 and d_2 are the diffusion coefficients for prey and predator densities respectively.

We now non-dimensionalized the model (4.1) by introducing the dimensionless variables

$$u=\frac{e\lambda}{m}X, \quad v=\frac{\lambda}{m}Y, \quad t=mt^{'}, \quad x=X_1\sqrt{\frac{m}{d_2}}, \quad y=X_2\sqrt{\frac{m}{d_2}},$$

and dimensionless parameters

$$h=\frac{m}{e}h_1, \quad \sigma=\frac{r}{m}, \quad C=\frac{e\lambda}{m}K, \quad \alpha=\frac{am}{\lambda^2}, \quad D=\frac{d_1}{d_2},$$

and obtain the modified model as

$$\begin{aligned} \frac{\partial u}{\partial t} &= \sigma u\left(1-\frac{u}{C}\right)-\frac{(1+\alpha v)\,uv}{1+h\,(1+\alpha v)\,u}+D\,\nabla^2 u, \\ \frac{\partial v}{\partial t} &= \frac{(1+\alpha v)\,uv}{1+h\,(1+\alpha v)\,u}-v+\nabla^2 v, \end{aligned} \tag{4.3}$$

where the positive constant D is the ratio of diffusion coefficients of prey and predator densities and $\nabla^2\big(=\frac{\partial^2}{\partial x^2}+\frac{\partial^2}{\partial y^2}\big)$ is the usual Laplacian operator in two dimensional space $\mathbf{R}=(x,y)$. To make certain that spatial patterns are governed by reaction-diffusion equations, model (4.3) is to be analyzed with the following non-zero initial conditions

$$2\mathrm{D}:\ u(x,y,0)>0,\quad v(x,y,0)>0,\quad (x,y)\in\Omega=[0,L]\times[0,L] \tag{4.4}$$

and zero-flux (Neumann) boundary conditions

$$\frac{\partial u}{\partial N}=\frac{\partial v}{\partial N}=0, \tag{4.5}$$

where L denotes the size of the system in the direction of u and v. N is outward unit normal on the boundary $\partial\Omega$. Condition (4.5) implies that no individual species leave the domain.

4.3 Analysis of the non-spatial model

In absence of diffusion the equilibrium points of the system are given by

$$\begin{aligned}\sigma u\left(1-\frac{u}{C}\right)-\frac{(1+\alpha v)\,uv}{1+h\,(1+\alpha v)\,u} &= 0,\\ \frac{(1+\alpha v)\,uv}{1+h\,(1+\alpha v)\,u}-v &= 0.\end{aligned} \tag{4.6}$$

Clearly $(0,0)$, $(C,0)$ and (u^*,v^*) are the steady state solutions, where $u^*=\frac{1}{(1-h)(1+\alpha v^*)}$ and v^* is the solution of

$$A_0v^3+A_1v^2+A_2v+A_3=0, \tag{4.7}$$

where
$A_0=(h-1)^2\,C\alpha^2$,
$A_1=2\,(h-1)^2\,C\alpha$,
$A_2=(h-1)\,C\,(h-1+\sigma\alpha)$,
$A_3=\sigma\,(1+hC-C)$.
Note: Clearly, A_0 and A_1 are positive. We use Descartes' rule of sign to find the number of positive roots of equation (4.7), we get the following variations in signs

of cubic polynomial are as follows:

$+ \quad + \quad + \quad + \quad \rightarrow \quad$ 0 positive roots

$+ \quad + \quad + \quad - \quad \rightarrow \quad$ 1 positive roots

$+ \quad + \quad - \quad + \quad \rightarrow \quad$ 2 positive roots

$+ \quad + \quad - \quad - \quad \rightarrow \quad$ 1 positive roots.

Therefore, the condition for one positive roots is $A_3 < 0$ imply $h < 1 - \frac{1}{C}$, which is the condition for uniqueness of (u^*, v^*).

The existence of non zero equilibrium point implies $h < 1$. The variational matrix about the equilibrium point (u^*, v^*) is given by

$$\left[\begin{array}{cc} \sigma - \frac{2\sigma u}{C} - \frac{v(1+\alpha v)}{(1+h(u+\alpha uv))^2} & -\frac{u(1+2\alpha v+hu(1+\alpha v)^2)}{(1+h(u+\alpha uv))^2} \\ \frac{v(1+\alpha v)}{(1+h(u+\alpha uv))^2} & \frac{-1-(-1+h)h(u+\alpha uv)^2+u(1+2\alpha v-2h(1+\alpha v))}{(1+h(u+\alpha uv))^2} \end{array} \right]_{(u^*,v^*)}.$$

(i) At $(0, 0)$, the variational matrix is

$$\mathbf{J}_1 = \left[\begin{array}{cc} \sigma & 0 \\ 0 & -1 \end{array} \right],$$

whose eigenvalues are -1 and $\sigma(> 0)$. Hence, the system is unstable at the origin.

(ii) At $(C, 0)$, the variational matrix is

$$\mathbf{J}_2 = \left[\begin{array}{cc} -\sigma & -\frac{C}{1+hC} \\ 0 & \frac{C(1-2h)-(h-1)hC^2-1}{(1+hC)^2} \end{array} \right],$$

whose eigenvalues are $-\sigma$ and $-1+\frac{C}{1+hC}$. Hence, the system is asymptotically stable if $\frac{C}{1+hC} < 1$.

(iii) At (u^*, v^*), variational matrix is

$$\mathbf{J}^* = \left[\begin{array}{cc} -(-1+h)^2 v^*(1+v^*\alpha) + \frac{(2+(-1+h)C(1+v^*\alpha))\sigma}{(-1+h)C(1+v^*\alpha)} & \frac{-1+(-2+h)v^*\alpha}{1+v^*\alpha} \\ (-1+h)^2 v^*(1+v^*\alpha) & -\frac{(-1+h)v^*\alpha}{(1+v^*\alpha)} \end{array} \right],$$

and the corresponding characteristic equation is

$$\lambda^2 + B_1\lambda + B_2 = 0,$$

where

$$B_1 = \frac{-2\sigma+(-1+h)C((-1+h)v^*(-1+h(1+v^*\alpha)^2-\alpha(-1+v^*(2+v^*\alpha)))-(1+v^*\alpha)\sigma)}{(-1+h)C(1+v^*\alpha)},$$

$$B_2 = (-1+h)^2 v^*(1+v^*\alpha) + \frac{v^*\alpha(-2-(-1+h)C(1+v^*\alpha))\sigma}{C(1+v^*\alpha)^2}.$$

By Routh-Hurwitz criterion, system (4.3) will be asymptotically stable about (u^*, v^*) if for all $B_i > 0$ $(i = 1, 2)$. In the numerical simulation section, the specific steady state under study has been mentioned.

4.4 Analysis of the spatiotemporal model

Interior equilibrium point (u^*, v^*) of non-spatial system (4.3) is spatially homogenous steady state, that is, constant in space and time for the reaction-diffusion system (4.3) (spatiotemporal model). We assume that (u^*, v^*) is stable in non-spatial system (4.3) which means the spatially homogenous steady state is stable with respect to spatially homogenous perturbations. Though the diffusion is often consider as a stabilizing process, it is a well known fact that diffusion can make a spatially homogenous steady state linearly unstable (Turing instability) with respect to heterogenous perturbations in a system of two interacting species [111; 157; 179]. The condition for Turing instability may be obtained by introducing a small heterogenous perturbation of the homogenous steady state as follows:

$$\begin{aligned} u(t,x,y) &= u^* + \epsilon_1 \exp(\lambda_k t)\cos(k_x x)\cos(k_y y), \\ v(t,x,y) &= v^* + \epsilon_2 \exp(\lambda_k t)\cos(k_x x)\cos(k_y y), \end{aligned} \tag{4.8}$$

where ϵ_1 and ϵ_2 are two non-zero reals and $k = (k_x, k_y)$, such that $k^2 = \left(k_x^2 + k_y^2\right)$, is the wave number.

Substituting (4.8) into (4.3) and then linearizing it about interior equilibrium point (u^*, v^*), we obtain the variational matrix as

$$\begin{bmatrix} -(-1+h)^2 v^*(1+v^*\alpha) + \frac{(2+(-1+h)C(1+v^*\alpha))\sigma}{(-1+h)C(1+v^*\alpha)} - Dk^2 & \frac{-1+(-2+h)v^*\alpha}{1+v^*\alpha} \\ (-1+h)^2 v^*(1+v^*\alpha) & -\frac{(-1+h)v^*\alpha}{(1+v^*\alpha)} - k^2 \end{bmatrix}.$$

The corresponding characteristic equation is

$$\lambda^2 + C_1(k^2)\lambda + C_2(k^2) = 0, \tag{4.9}$$

where

$$C_1(k^2) = \big(1+D\big)k^2 + \frac{(-1+h)^2v^*\Big(-1+\alpha-2v^*\alpha-v^{*2}\alpha^2+h(1+v^*\alpha)^2\Big)C+\sigma\Big(-2-(-1+h)(1+v^*\alpha)C\Big)}{(-1+h)(1+v^*\alpha)C},$$

$$C_2(k^2) = \frac{Dk^2\Big((-1+h)v^*\alpha+k^2(1+v^*\alpha)\Big)}{1+v^*\alpha} + \frac{(-1+h)^3C(1+k^2)v^*(1+v^*\alpha)^3-\Big(2+(-1+h)C(1+v^*\alpha)\Big)\Big((-1+h)v^*\alpha+k^2(1+v^*\alpha)\Big)\sigma}{(-1+h)C(1+v^*\alpha)^2}.$$

By Routh-Hurwitz criterion, the system (4.3) will be stable about (u^*, v^*) if $C_1(k^2) > 0$ and $C_2(k^2) > 0$. As the parameters D and k^2 are all positive and $\frac{(-1+h)^2v^*\Big(-1+\alpha-2v^*\alpha-v^{*2}\alpha^2+h(1+v^*\alpha)^2\Big)C+\sigma\Big(-2-(-1+h)(1+v^*\alpha)C\Big)}{(-1+h)(1+v^*\alpha)C} > 0$ (by the stability of the non-spatial model of (4.3)), $C_1(k^2) > 0$ is always positive. Therefore, the condition for diffusive instability is $C_2(k^2) < 0$.

The polynomial function $C_2(k^2)$ has a minimum for some value of k, say k_{min}, where

$$k_{min}^2 = \frac{\sigma\big(2+(-1+h)(1+v^*\alpha)C\big) - (-1+h)^2v^*\big(D\alpha-(1+v^*\alpha)^2+h(1+v^*\alpha)^2\big)C}{2CD(h-1)(1+v^*\alpha)}.$$

For this minimum value of k, Turing instability will occur when $C_2(k_{min}^2) < 0$. Therefore, substituting k_{min}^2 in $C_2(k^2)$, we get the sufficient condition for Turing instability as

$$\frac{2\sigma - C(h-1)\big(D(h-1)v^*\alpha + (1+v^*\alpha)\left((h-1)^2v^*(1+v^*\alpha)-\sigma\right)\big)}{C(h-1)(1+v^*\alpha)} - \frac{2C(h-1)\sqrt{D}(1+v^*\alpha)\sqrt{\frac{C(h-1)^2v^*(1+v^*\alpha)^3+v^*\alpha(-2-C(h-1)(1+v^*\alpha))\sigma}{C(1+v^*\alpha)^2}}}{C(h-1)(1+v^*\alpha)} > 0. \tag{4.10}$$

The interval of the wave number for which Turing instability take place is (k_-, k_+) and in this interval, we have $C_2(k^2) < 0$, where

$$k_- = \frac{\sigma}{CD(h-1)(1+v^*\alpha)} - \frac{A}{2D(1+v^*\alpha)} - \frac{1}{2D}\sqrt{\frac{B^2+4CD(h-1)^2v^*E}{C^2(h-1)^2(1+v^*\alpha)^2}},$$

$$k_+ = \frac{\sigma}{CD(h-1)(1+v^*\alpha)} - \frac{A}{2D(1+v^*\alpha)} + \frac{1}{2D}\sqrt{\frac{B^2+4CD(h-1)^2v^*E}{C^2(h-1)^2(1+v^*\alpha)^2}},$$

and

$A = (2\alpha\sigma + C(h-1)(1+v^*\alpha)\,(-(h-1)(1+v^*\alpha)^2 + \alpha\sigma))$,

$B = C(h-1)\,(D(h-1)v^*\alpha + (1+v^*\alpha)\,((h-1)^2 v^*(1+v^*\alpha) - \sigma)) - 2\sigma$,

$E = 2\alpha\sigma + C(h-1)(1+v^*\alpha)\,(-(h-1)(1+v^*\alpha)^2 + \alpha\sigma)$.

4.5 Numerical simulations

We will now investigate the numerical results of both non-spatial as well as spatiotemporal models, namely (4.3). For numerical simulation, we set σ and h as $\sigma = 10.0$, $h = 0.1$, and consider C and α, as controlling parameters. For these values of parameters, the positive equilibrium points are (0, 0), (0.8, 0), (0.5909, 1.5442) and (0.6287, 1.3459). The steady state (0.5909, 1.5442) is stable and (0.6287, 1.3459) is unstable. Hence, throughout our study in the spatiotemporal domain, we have considered the stable steady state (0.5909, 1.5442). Figure 4.1 shows the dynamics of preys and predators in the non-spatial domain.

Please note that the non-dimensional parameter $C = \frac{e\lambda}{m}K$, comprising of the dimensional carrying capacity, attack rate, per capita mortality rate of predators and the conversion efficiency, can also be interpreted as the basic reproduction number of the predator, which is defined as the average number of offspring produced by a single predator during its life time, when introduced into the prey population at carrying capacity. If $C > 1$, then the predator population survives and coexist with prey (see the upper panel of Figure 4.1). However, if $C < 1$, then the predators go extinct (see the lower panel of Figure 4.1). Both of these results are true for $\alpha = 0$, that is, without hunting cooperation. When $C > 1$ and with increasing α, the predator density increases and the prey density decreases due to predation pressure. With small values of cooperation rate ($\alpha = 0.05$, 0.1, 0.4), predator population increases due to better forage on prey and consequently the prey population decreases (see the upper panel of Figure 4.1). However, the predator population decreases with large values of cooperation rate ($\alpha = 0.7$, 1.2) due to decrease in prey density (see the upper panel of Figure 4.1). If $C < 1$ and the cooperation coefficient ($\alpha = 0.4$) is small, then the predator population go to extinct as the prey population is too small to sustain them. However, for large value of cooperation rate ($\alpha = 0.7$, 1.2), the

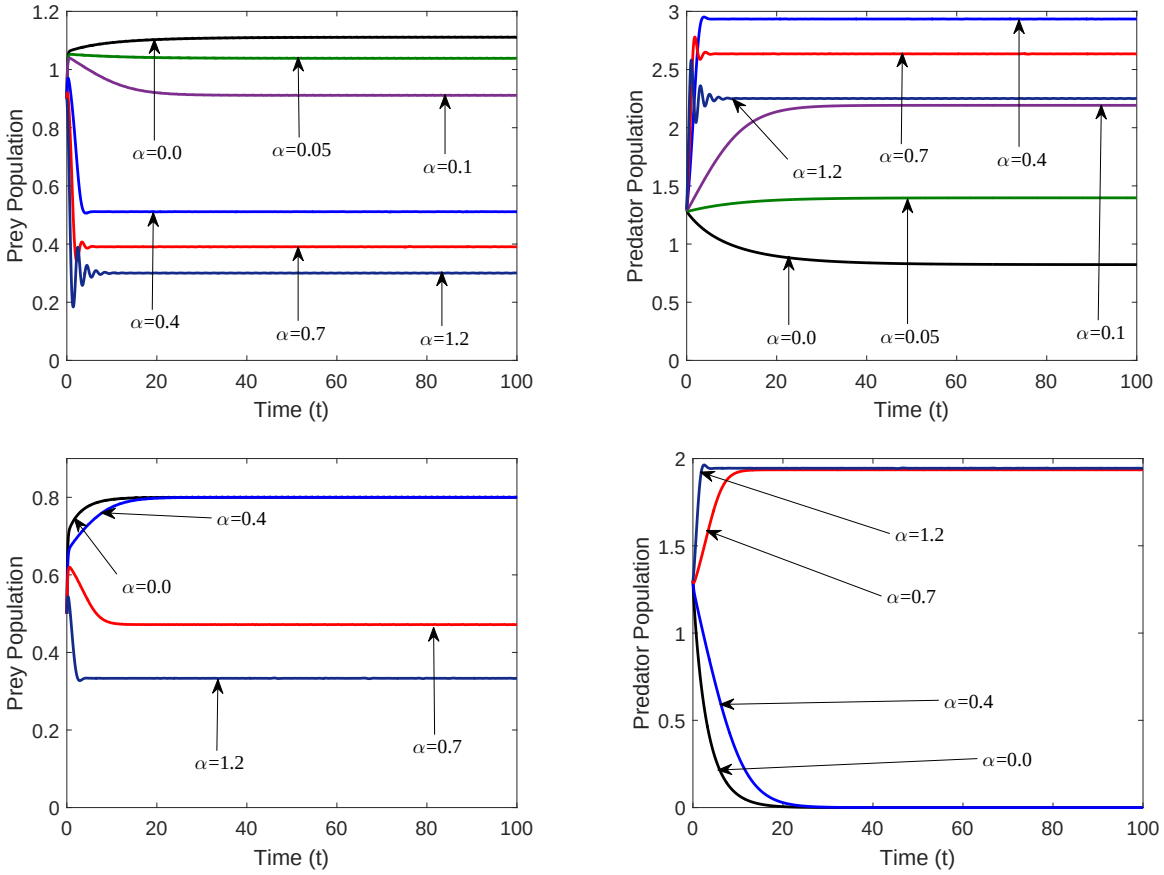

Figure 4.1: Dynamics of preys(u) and predators(v) in the non-spatial domain of the model (4.3) for fixed parameters $\sigma = 10.0$, $h = 0.1$ and different parameter values of hunting cooperation rates (α) which are mentioned in figures. Upper panel for C=1.2 and lower panel for C=0.8.

predator survives due to hunting cooperation behavior in predators (see the lower panel of Figure 4.1).

We now simulate the spatiotemporal model in two dimensional space with the help of finite difference scheme for spatial derivatives. The forward Euler's numerical method is used for the non-spatial part of model (4.3) and general finite difference scheme of five point is used for the spatial part. The reaction-diffusion partial differential equations, given by (4.3), is numerically solved by using splitting method [49; 97]. The numerical values for the step sizes of time and space have been selected adequately small for avoiding the numerical artifacts. In this study, we have employed statistically uncorrelated Gaussian white noise perturbation in space, which

is mathematically denoted in two dimensional case as

$$\begin{aligned} u(x_i, y_j, 0) &= u^* + \gamma_1 \epsilon_{ij}, \\ v(x_i, y_j, 0) &= v^* + \gamma_2 \eta_{ij}, \end{aligned} \tag{4.11}$$

where γ_1 and γ_2 are very small real numbers and ϵ_{ij} and η_{ij} are statistically uncorrelated Gaussian white noise perturbations with zero mean and fixed variance in two dimensional space.

For spatiotemporal model, we perform all the numerical simulations of the system (4.3) over the non-zero initial condition and zero-flux boundary conditions, in two dimensional spatial domain. The domain size is 70×70 with time-step $\Delta t = 0.001$ and space-step $\Delta x = \Delta y = 0.5$. The parameter values of σ and h remain same ($\sigma = 10$, $h = 0.1$) and C, α are used as the controlling parameter (just like the non-spatial case).

Note: The Neumann zero-flux conditions are placed at boundary of the numerical domain in two dimensional problems. The size of the domain is chosen large enough so that the impact of the boundaries has been kept as small as possible during the simulation time.

We now demonstrate diffusive induced instability (Turing instability) and the corresponding pattern formation for the system (4.3). Although, the sufficient conditions for Turing instability were obtained analytically in previous section, whether they are satisfied with our corresponding set of parameter values, is yet to be tested. In order to do so, we sketch the Turing instability condition (4.10) for distinct values of D (other parameter values are fixed, namely, $\sigma = 10.0$, $\alpha = 0.57$, $C = 0.8$, $h = 0.1$). The left snapshot of Figure 4.2 shows the zone for the emergence of spatial patterns corresponding to Turing instability condition against the ratio of diffusion coefficients (D). We observe that the sufficient condition of the diffusive instability, that is, equation (4.10) holds, when D is adequately large, starting from $D = 32.76$ (see the left panel of Figure 4.2). The spatial dispersion curve for this particular model is shown in the right snapshot of Figure 4.2, and the dispersion relation is represented by the real part of the largest eigenvalues of the spatial model. The corresponding plot of real part of largest eigenvalue $Re(\lambda)$ against the wave number (k) is shown in the right panel of Figure 4.2. The real part of largest

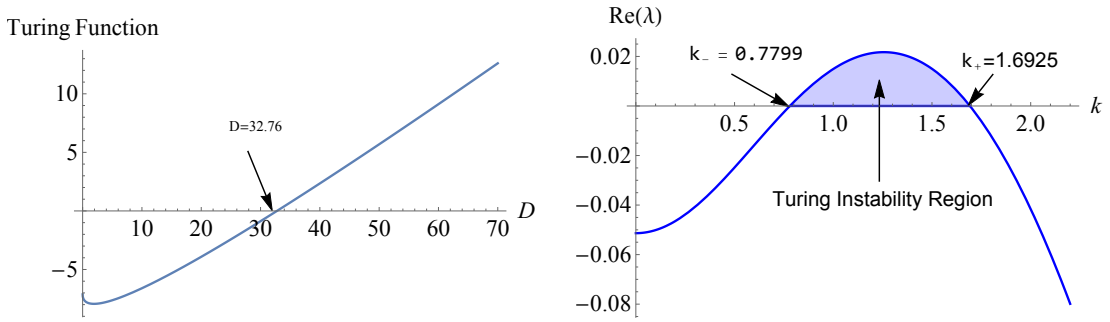

Figure 4.2: Emergence of spatial pattern corresponding to Turing instability condition; Characterization of the dispersal relation for D=40.

eigenvalue $Re(\lambda) > 0$ holds, the wave number (k) fit in the interval (k_-, k_+), that is, (0.7799, 1.6925). Also, we obtain the controlling parameter space for Turing instability via sufficient condition, which is shown in Figure 4.3.

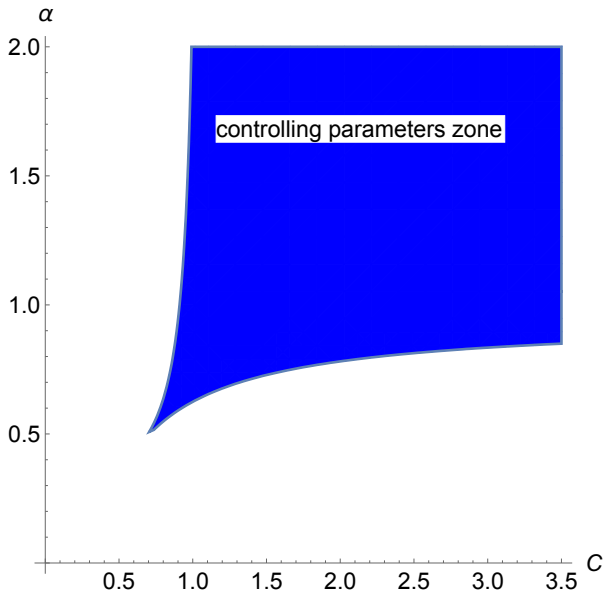

Figure 4.3: Controlling parameters space for Turing patterns corresponding to Turing instability condition in the region.

Figure 4.4 shows the non-Turing spatial distribution of densities of the prey and predator population when $C > 1$ at time $t = 500$ with different cooperation rates (α). With increase in the hunting cooperation rate $(\alpha = 0.7, 1.2)$, the prey

density always decline (Figure 4.4(a,c)). With high hunting cooperation rates, the predator population succeed in killing more preys, thereby resulting in the decrease of spread of prey population and hence their population also decreases due to non-availability of preys (Figure 4.4(b,d)). Figure 4.5 shows the Turing patterns for prey and predator population distributed over two dimensional spatial domain obtain at $t = 500$, for $C > 1$ and different values of α. The patterns arising in the large time limit are shown in the Figure 4.5, which are typical results of Turing instability, namely the spot (patch) like patterns.

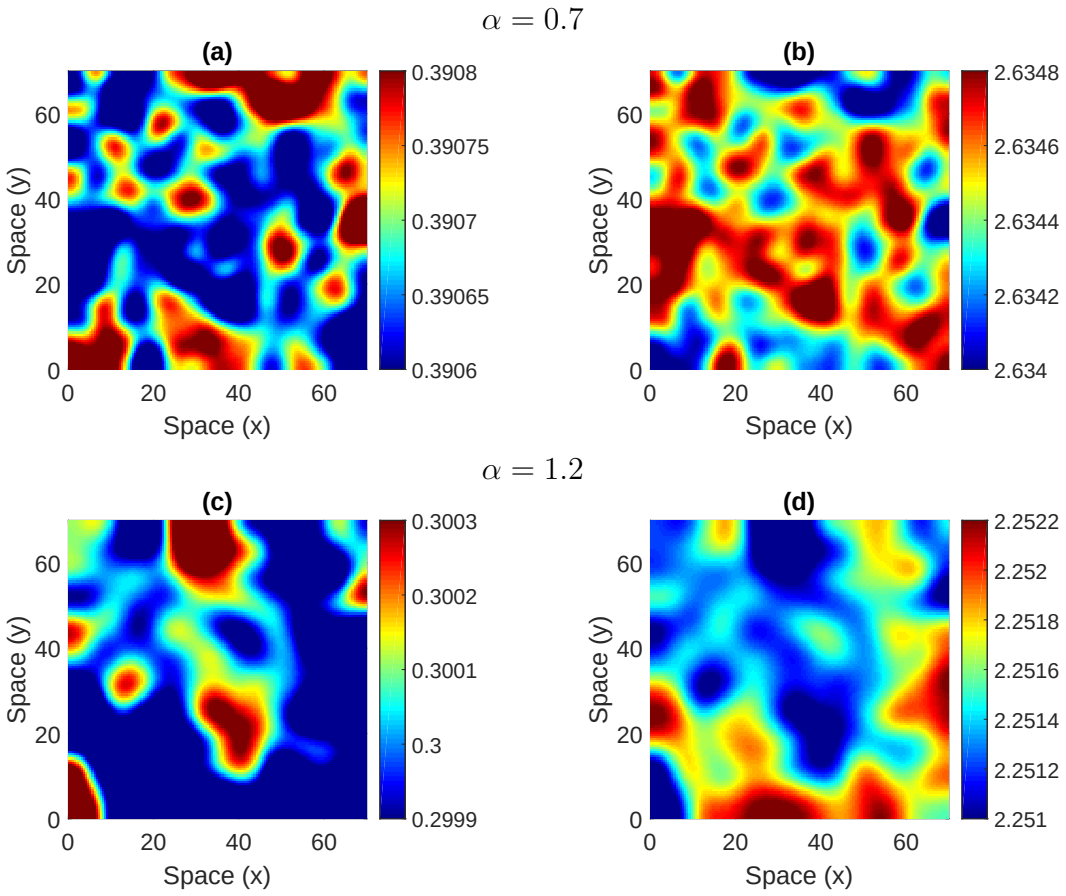

Figure 4.4: Non-Turing spatial distribution of densities of prey (left column) and predator (right column) when $C > 1$ at time $t = 500$ with different cooperation rates (α). Other parameter values are $\sigma = 10.0$, $C = 1.2$, $h = 0.1$, $D = 1$ and initial distribution is given by (4.11).

Figure 4.6 shows the Non-Turing spatial distribution of densities of the prey and predator population when $C\ (= 0.8) < 1$ at time $t = 500$ with different cooperation

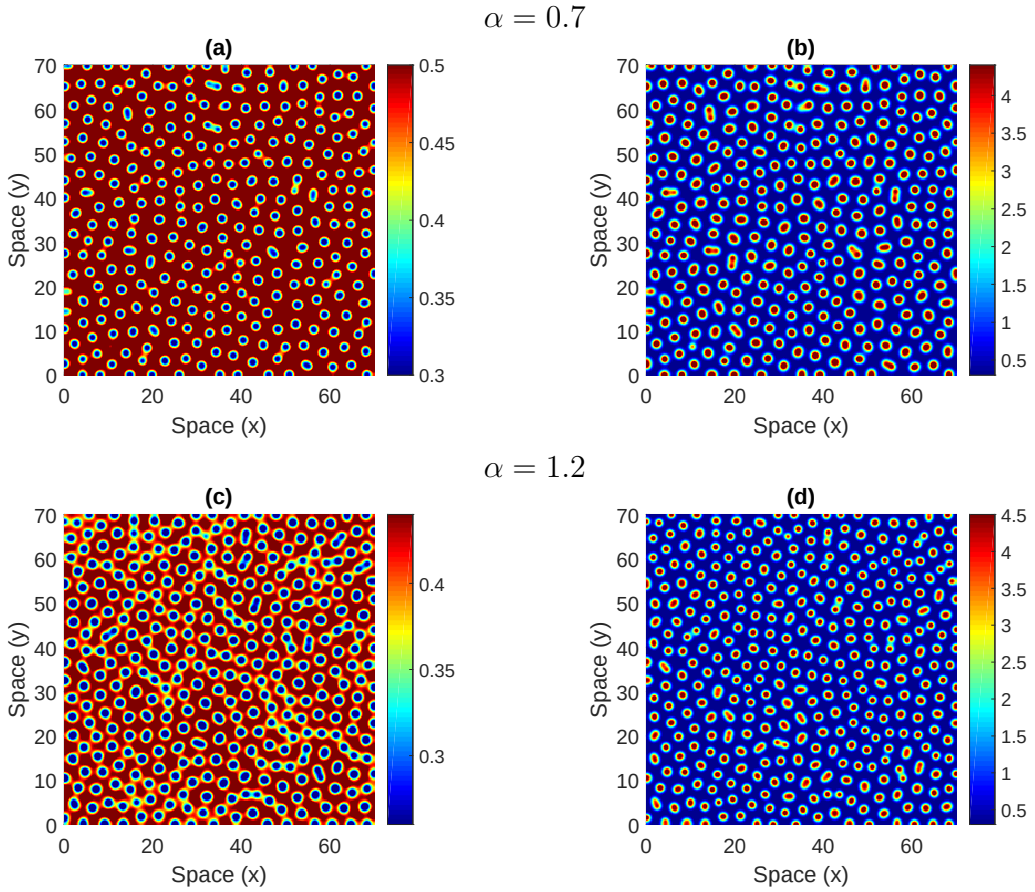

Figure 4.5: Turing spatial distribution of densities of prey (left column) and predator (right column) when $C > 1$ at time $t = 500$ with different cooperation rates (α). Other parameter values are $\sigma = 10.0$, $C = 1.2$, $h = 0.1$, $D = 40$ and initial distribution is given by (4.11).

rates (α). Other parameter values are $\sigma = 10.0$, $h = 0.1$ and initial distribution is given by (4.11). For small values of cooperation rates ($\alpha = 0.0, 0.4$), the predator population go extinct (no figure is drawn as the spatial scale is negligible), which means that the predator population can not be sustained even if the hunting cooperation is present (but small). However, for $\alpha = 0.7, 1.2$, the hunting cooperation behavior in predators is large enough to make their survival possible (Figure 4.6(b,d)). For all the values of hunting cooperation coefficients, the prey population exist with steady decline (see non-spatial results in Figure 4.1, and spatial results in the Figure 4.6(a,c)). Figure 4.7 shows the Turing patterns for prey and predator population distributed over two dimensional spatial domain obtain at $t = 500$ and

$C < 1$ and also different values of α. The patterns arising in the large time limit are shown in the Figure 4.7. For some higher values of hunting cooperation coefficient ($\alpha = 0.7,\ 1.2$), both prey and predators population coexist and form the spatial pattern of stripes type.

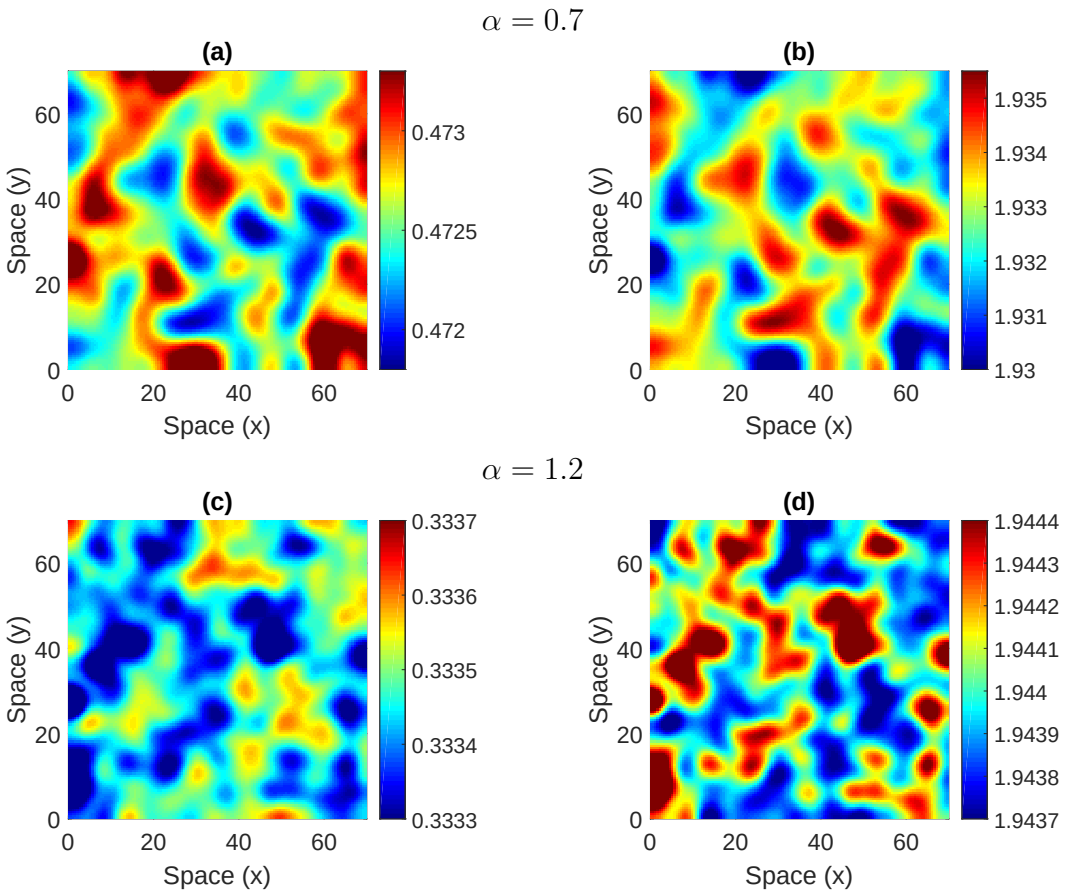

Figure 4.6: Non-Turing spatial distribution of densities of prey (left column) and predator (right column) when $C < 1$ at time $t = 500$ with different cooperation rates (α). Other parameter values are $\sigma = 10.0$, $C = 0.8$, $h = 0.1$, $D = 1$ and initial distribution is given by (4.11).

In Figure 4.8, we have illustrated the density distributions of prey (left column) and predator (right column) which covers three kinds of spatial pattern namely spots, mixed (spots-stripes) and stripes. The first two snapshots (upper panel) in Figure 4.8 show the two dimensional stationary diffusive patterns of the model (4.3) at time $t = 500$ and $C = 0.8$ with diffusion coefficient ratio $D = 40$ for the prey and predator population respectively. In these snapshots, hexagonal patterns

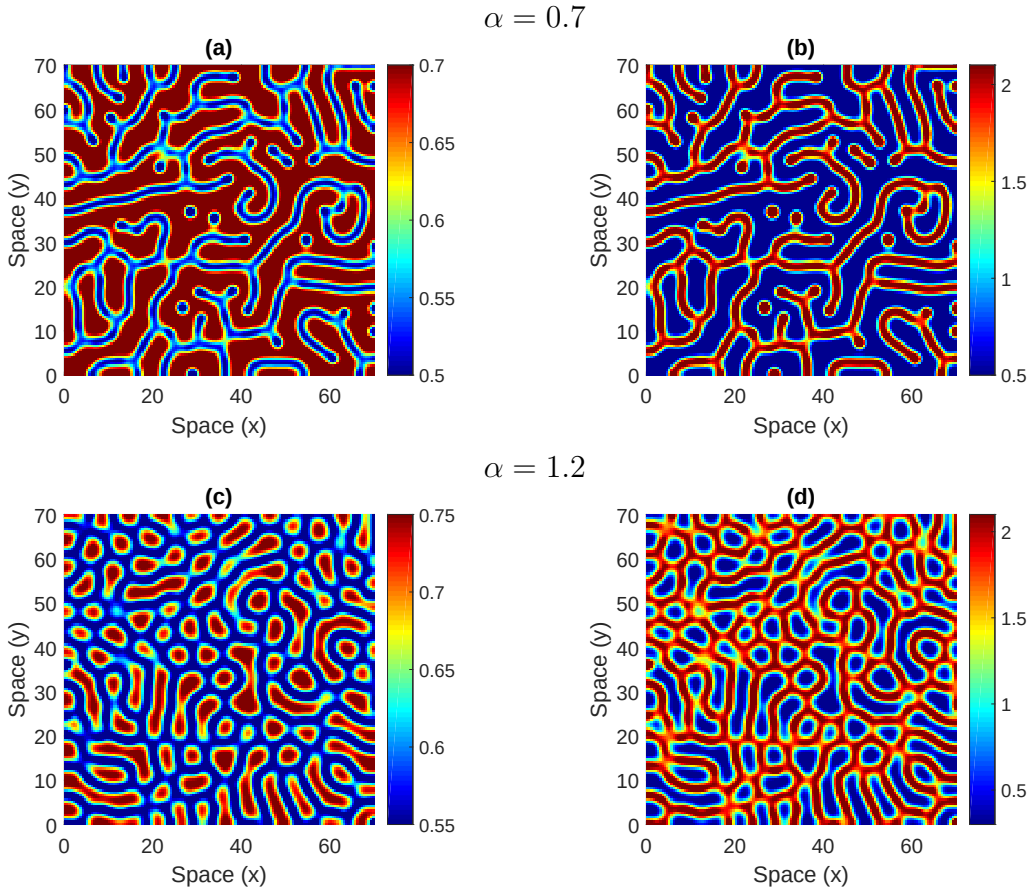

Figure 4.7: Turing spatial distribution of densities of prey (left column) and predator (right column) when $C < 1$ at time $t = 500$ with different cooperation rates (α). Other parameter values are $\sigma = 10.0$, $C = 0.8$, $h = 0.1$, $D = 40$ and initial distribution is given by (4.11).

(spots) prevail over the entire habitat eventually. In Figure 4.8(a), it is observed that the blue spots (minimum density of u) are distributed on a reddish background (maximum density of u), that is, the preys are segregated with low population density. On the other hand, Figure 4.8(b) consists of red spots on a blue background, that is, the predators are isolated with high population density. As the C is increased to 0.802, some patches split into stripes resulting in spots-stripes patterns in both prey and predator population (Figure 4.8(c,d)). When C is increased to 0.804, the dynamics of the model exhibits a decay in the spot and emergence in stripes pattern only (Figure 4.8(e,f)). Thus, by increasing the control parameter C, a sequence spots $\rightarrow$ spot-stripes $\rightarrow$ stripes is observed.

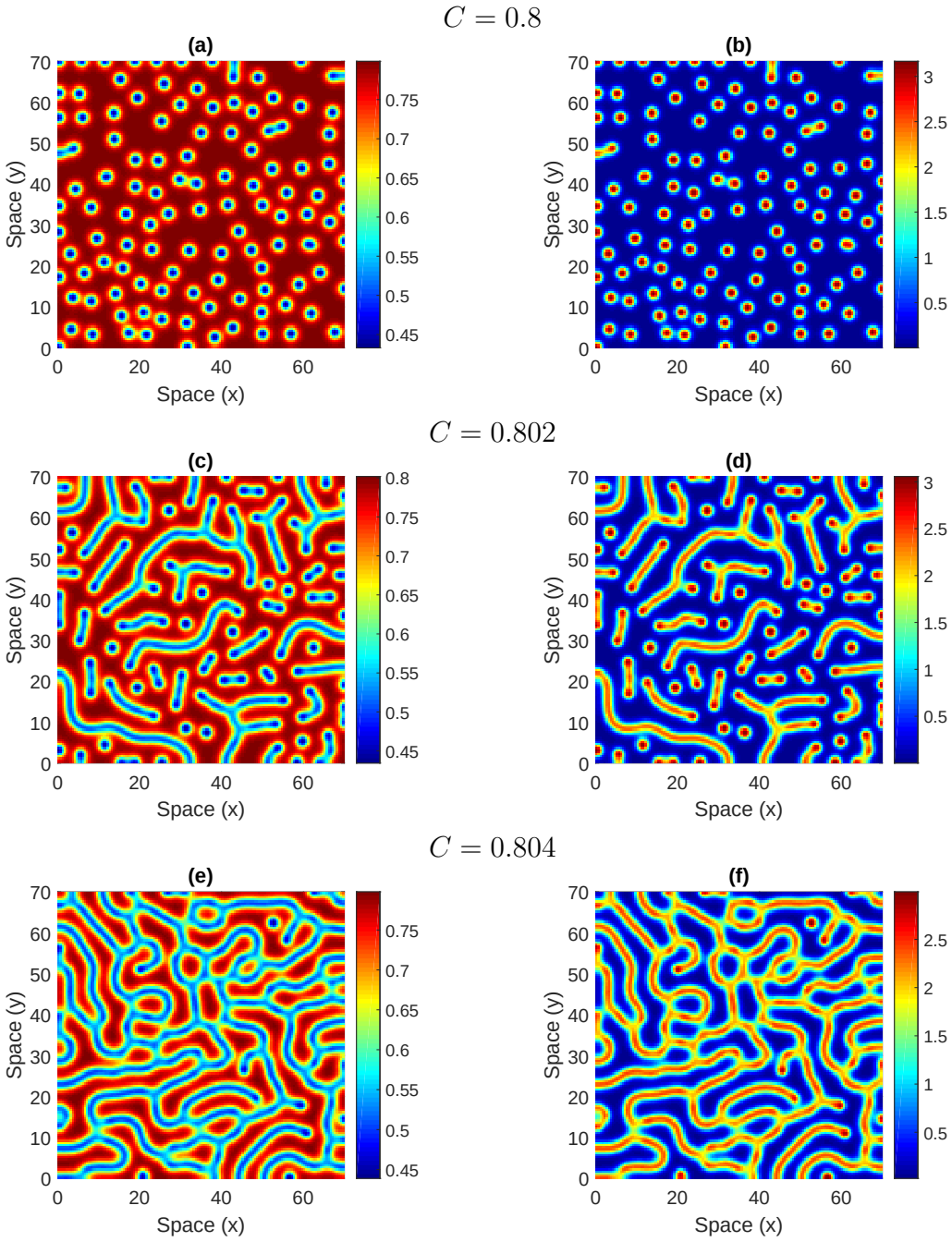

Figure 4.8: 2D-spatial patterns of the prey (left column) and predator (right column) at time moment $t = 500$ for different values of C. Other parameter values are $\sigma = 10$, $\alpha = 0.57$, $h = 0.1$, $D = 40$.

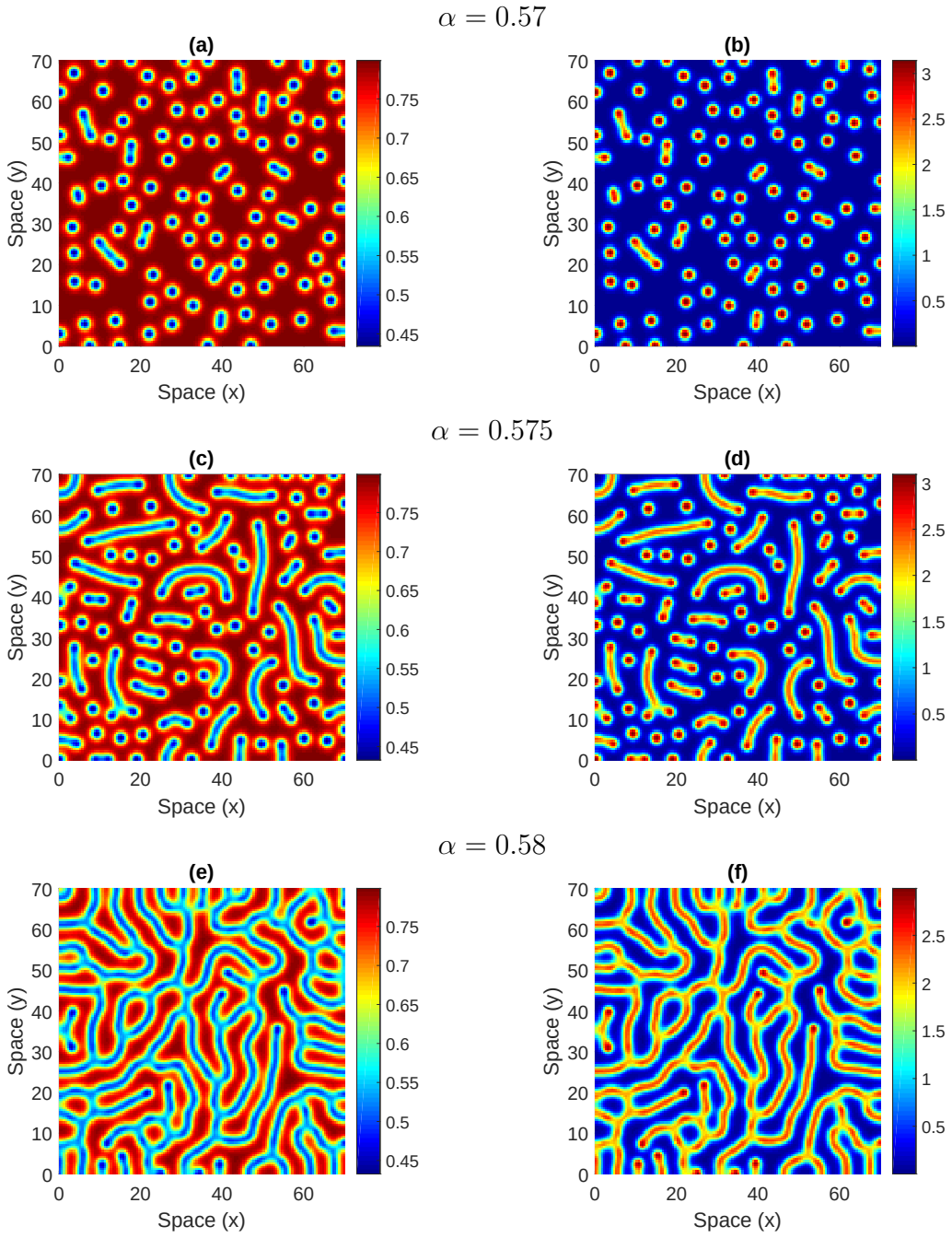

Figure 4.9: 2D-spatial patterns of the prey (left column) and predator (right column) at time moment $t = 500$ for different values of α. Other parameter values are $\sigma = 10$, $C = 0.8$, $h = 0.1$, $D = 40$.

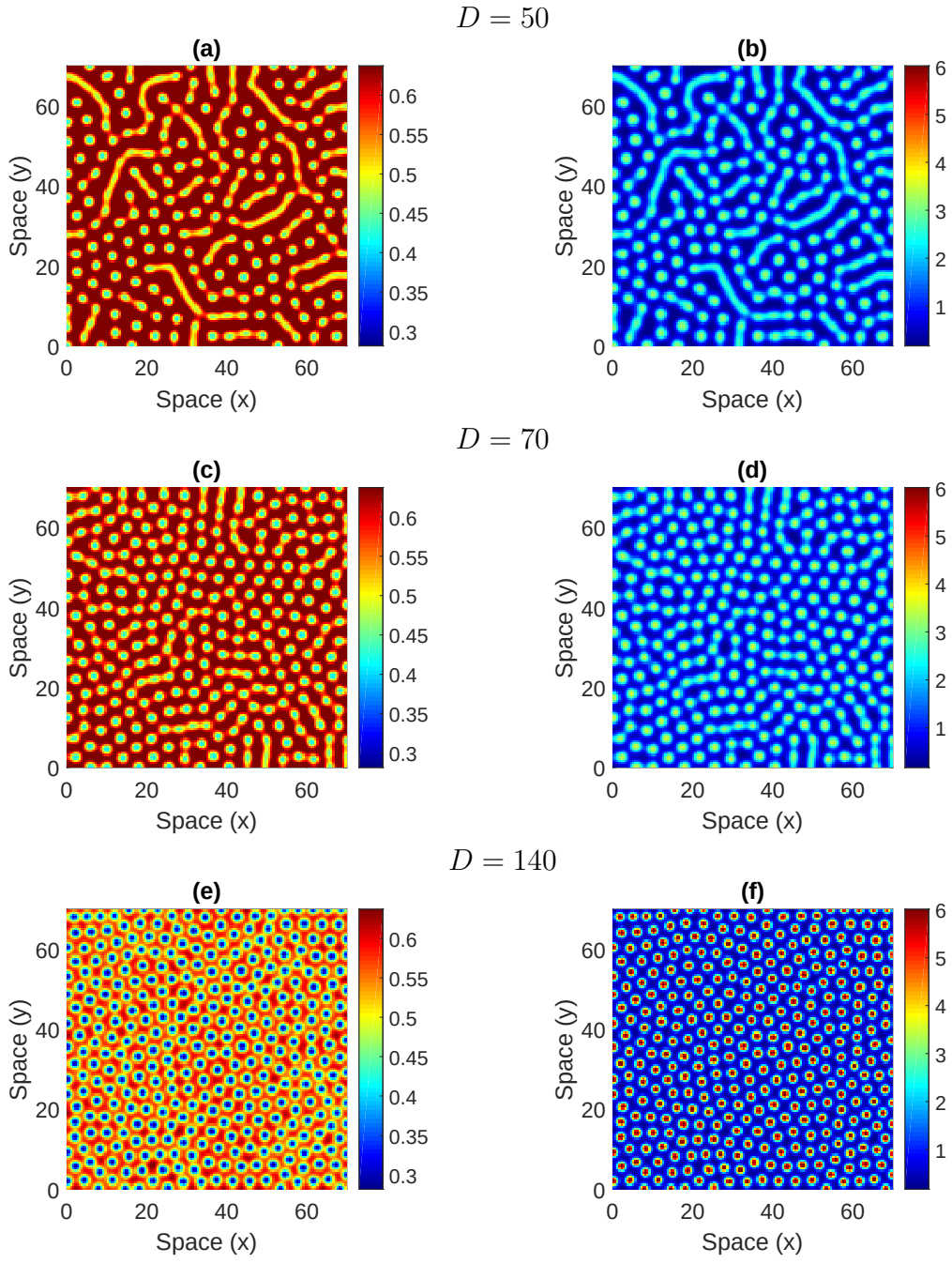

Figure 4.10: 2D-spatial patterns of the prey (left column) and predator (right column) at time moment $t = 500$ for different values of diffusion coefficient D. Other parameter values are $\sigma = 10$, $\alpha = 0.58$, $C = 0.8$, $h = 0.1$.

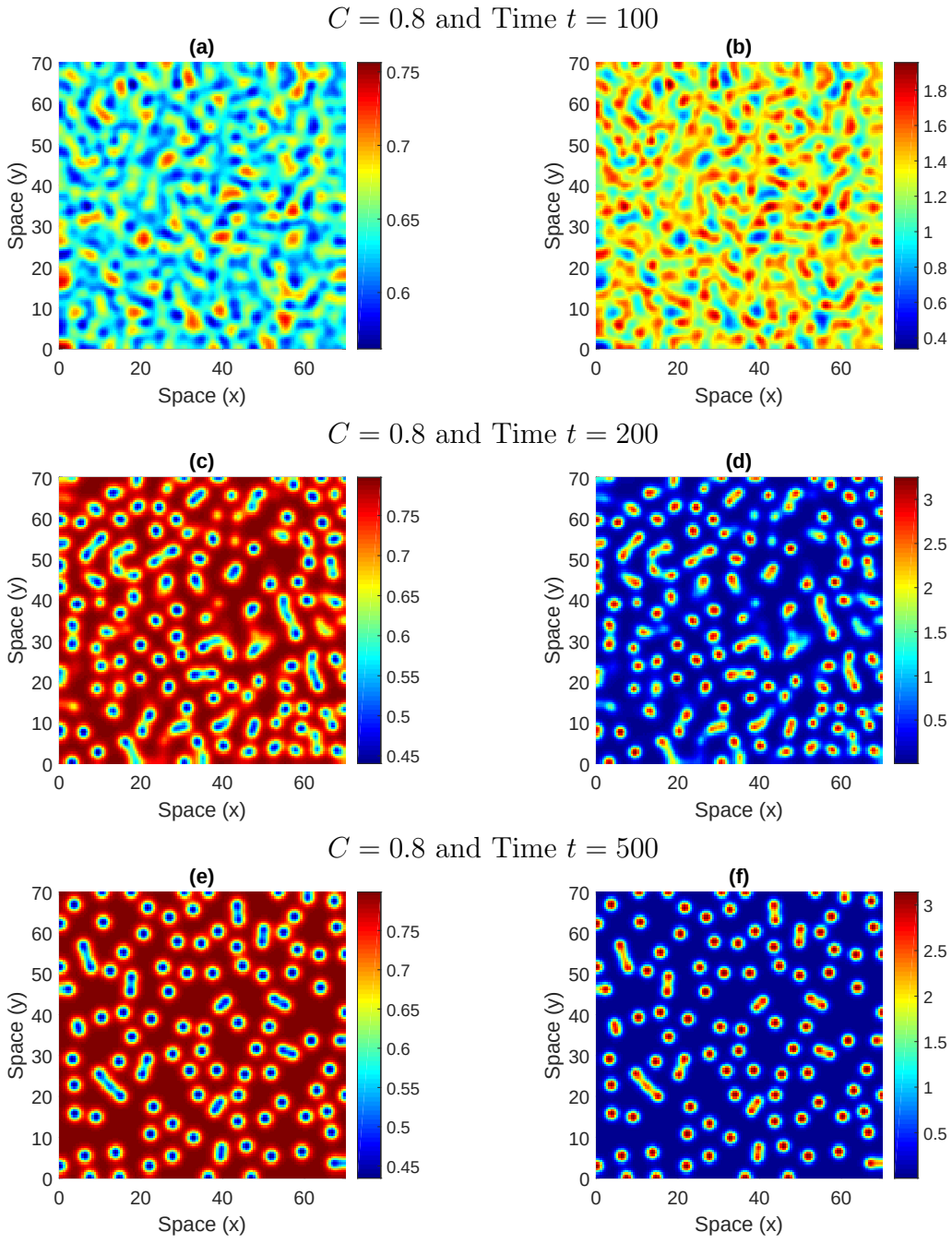

Figure 4.11: Time evolution of patterns of the prey (left column) and predator (right column) with parameters $\sigma = 10$, $\alpha = 0.57$, $h = 0.1$, $D = 40$.

Figure 4.9 demonstrates the spatial patterns of prey (left column) and predator (right column) with respect to different cooperation rates α. The first two snapshots (upper panel) of Figure 4.9 show the two dimensional spatial patterns of the model (4.3) at time $t = 500$ with cooperation rate $\alpha = 0.57$ for the prey and predator population respectively. In these snapshots, the spots pattern prevail over the entire habitat. In Figure 4.9(a), it is observe that blue spots (minimum density of u) are distributed on a reddish background (maximum density of u), that is, the preys are segregated with low population density. On the other hand, in Figure 4.9(b) consists of red spots on a blue background, that is, the predators are isolated with high population density. As the cooperation rate α is increases to 0.575, some spots split into stripes resulting in spots-stripes patterns in both prey and predator population (Figure 4.9(c,d)). When α is increases to 0.58, the dynamics of the model exhibits a decay in the spot and emergence in stripes pattern (Figure 4.9(e,f)). Thus, by increasing the α (rate of hunting cooperation), a sequence spots $\rightarrow$ spot-stripes $\rightarrow$ stripes is observed. Density distributions of prey (left column) and predator (right column) have been illustrated in Figure 4.10 with changing D, the ratio of diffusion coefficients. Figure 4.10 shows the two dimensional stationary diffusive patterns of the model (4.3) at time $t = 500$ for the prey and predator population with different values of D, other parameter values are $\sigma = 10$, $\alpha = 0.58$, $c = 0.8$ and $h = 0.1$. As D is changed to 50, 70 and 140, a sequence of mixed patterns is observed, which ultimately gives rise to spot for large values of the diffusion coefficient D. It is interesting to note that with increasing D, the patterns changes from stripes to spots (Figure 4.10(a–f)).

Figure 4.11 shows the time evolution of spatial densities distribution of preys (left column) and predators (right column) at different times, namely $t = 100$, $t = 200$ and $t = 500$ with varying controlling parameter C. Figure 4.11 (left column) shows the distribution of preys for fixed value of controlling parameter $C = 0.8$ at times 100, 200 and 500 respectively. Similarly, Figures 4.11 (right column) show the distribution of predators for fixed value of controlling parameter $C = 0.8$ at times 100, 200 and 500 respectively. We observe that the competitiveness between spots and stripes for prey and predator population densities. The simulation begins with uniform steady state $(u^*,\ v^*) = (0.5909,\ 1.5442)$ and the random Gaussian white

noise perturbations result in emergence of patterns, like, stripes and spots for both the prey and predator densities. Ultimately, the spatial pattern becomes stationary spots after a long time (Figure 4.11(e,f)). We now change the value of controlling parameter C to 0.802 and then observe that the change in dynamics in the densities of prey (left column) and predator (right column) at times, namely $t = 100$, $t = 200$ and $t = 500$. The random perturbations lead to the formation of spots-stripes ending with the time independent spots-stripes patterns for both the prey (see left column of Figure 4.12) and predator (see right column of Figure 4.12) densities. Figure 4.13 demonstrates the spatial patterns of both the prey and predator densities for the fixed value of controlling parameter $C = 0.804$. The random perturbations leads to the formation of stripes patterns only in both the species and with time these stripes are time independent.

In Figures 4.14, 4.15, 4.16, we show the time evolution of spatial patterns of preys and predators at different times with varying controlling parameter α. Figure 4.14 (left column) show the spatial distribution of preys for controlling parameter $\alpha = 0.57$ at times 100, 200 and 500 respectively. Similarly, Figure 4.14 (right column) show the distribution of predators for controlling parameter $\alpha = 0.57$ at times 100, 200 and 500 respectively. We observe that the competitiveness between spots and stripes for prey and predator population densities. The simulation begins with uniform steady state $(u^*,\ v^*) = (0.5909,\ 1.5442)$ and the random Gaussian white noise perturbations result in emergence of patterns, like, stripes and spots for both the prey and predator densities. Ultimately, the spatial pattern becomes stationary spots after a long time (see lower panel of Figure 4.14). We now change the value of controlling parameter α to 0.575 and then observe that the change in dynamics in the densities of prey and predator at times, namely $t = 100$, $t = 200$ and $t = 500$. The random perturbations lead to the formation of spots-stripes ending with the time independent spots-stripes patterns for both the prey (see left column of Figure 4.15) and predator (see right column of Figure 4.15) densities. Figure 4.16 demonstrates the spatial patterns of both the prey and predator densities for the fixed value of controlling parameter $\alpha = 0.58$. The random perturbations leads to the formation of stripes patterns only in both the species and with time these stripes are time independent.

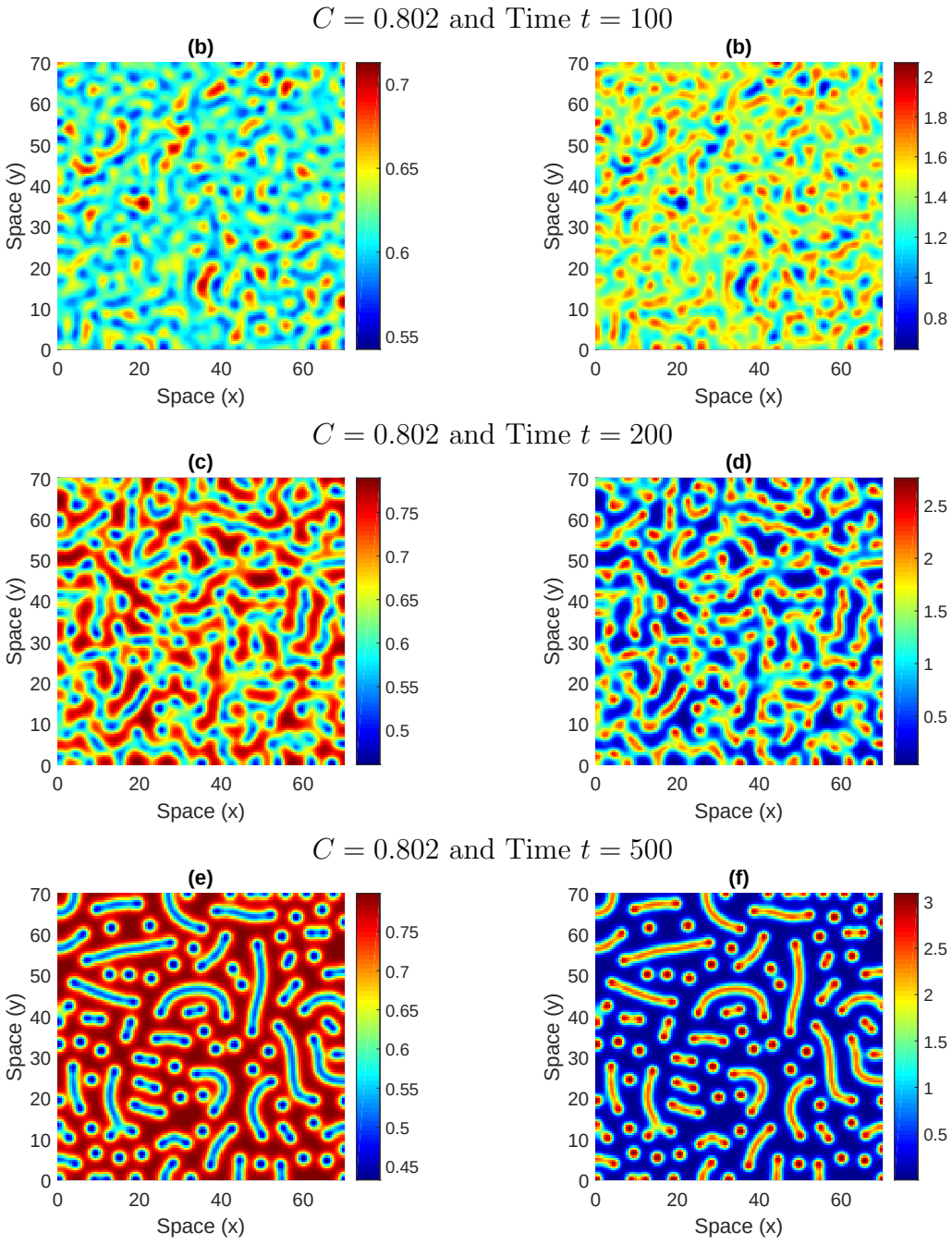

Figure 4.12: Time evolution of patterns of the prey (left column) and predator (right column) with parameters $\sigma = 10$, $\alpha = 0.57$, $h = 0.1$, $D = 40$.

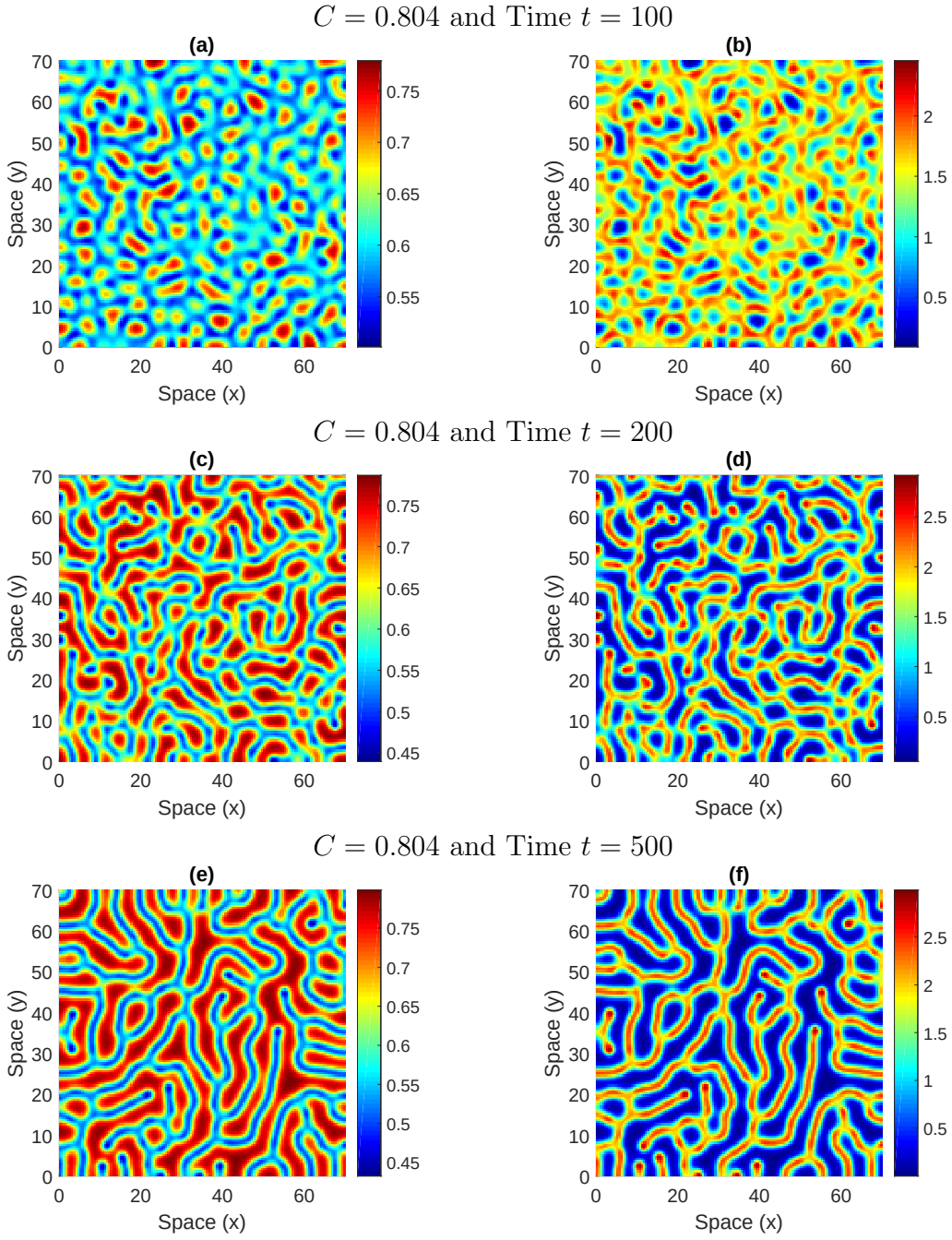

Figure 4.13: Time evolution of patterns of the prey (left column) and predator (right column) with parameters $\sigma = 10$, $\alpha = 0.57$, $h = 0.1$, $D = 40$.

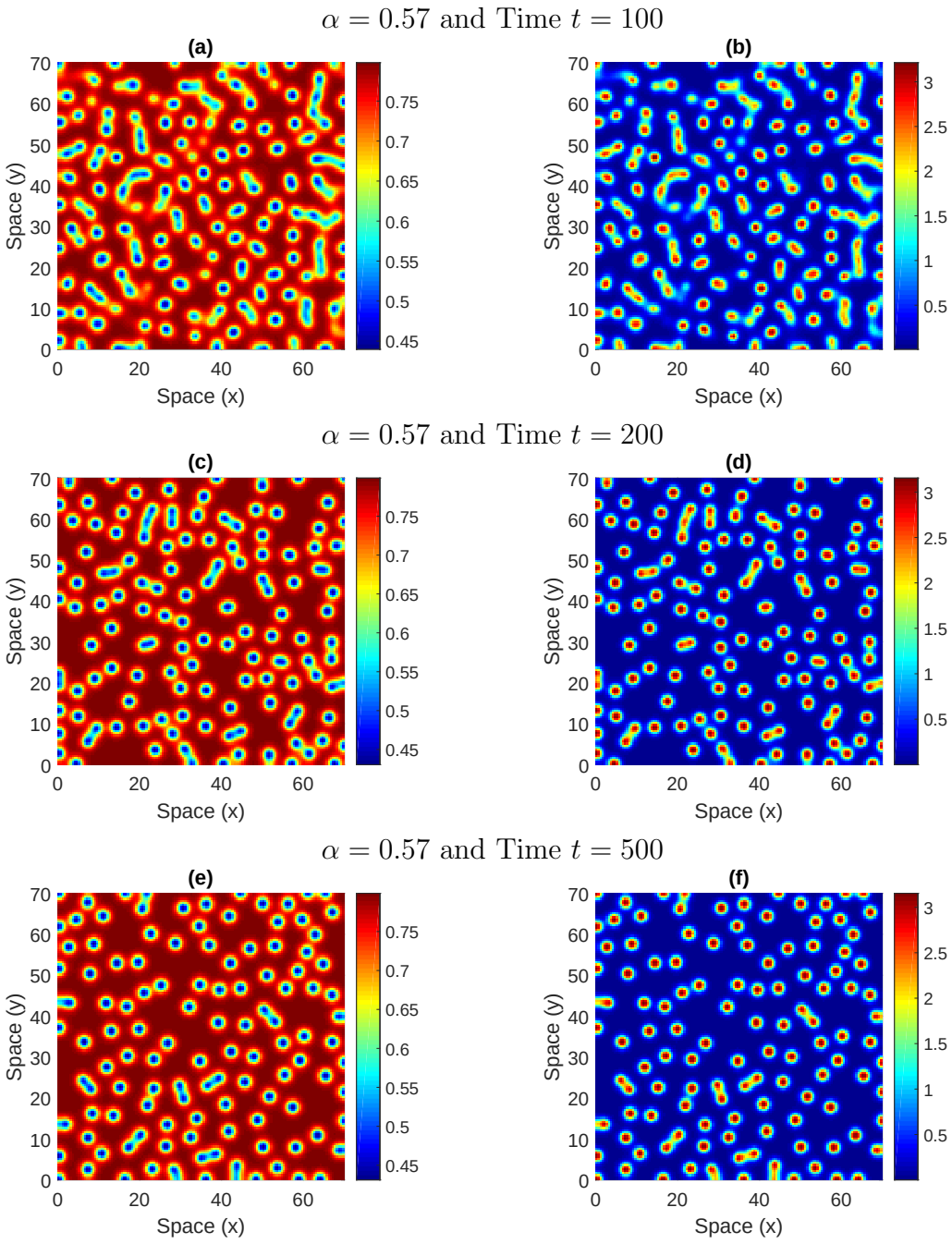

Figure 4.14: Time evolution of patterns of the prey (left column) and predator (right column) with parameters $\sigma = 10$, $C = 0.8$, $h = 0.1$, $D = 40$.

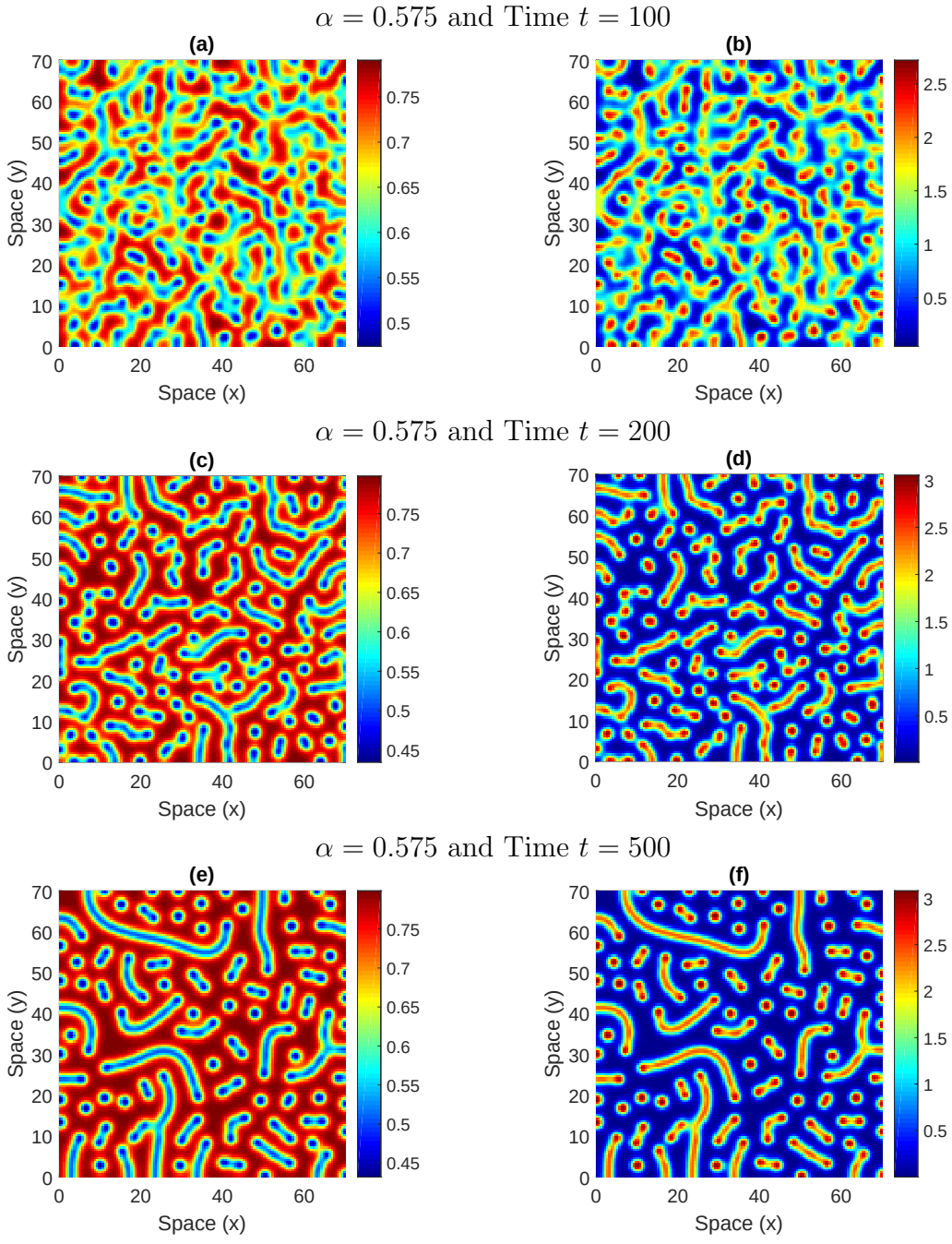

Figure 4.15: Time evolution of patterns of the prey (left column) and predator (right column) with parameters $\sigma = 10$, $C = 0.8$, $h = 0.1$, $D = 40$.

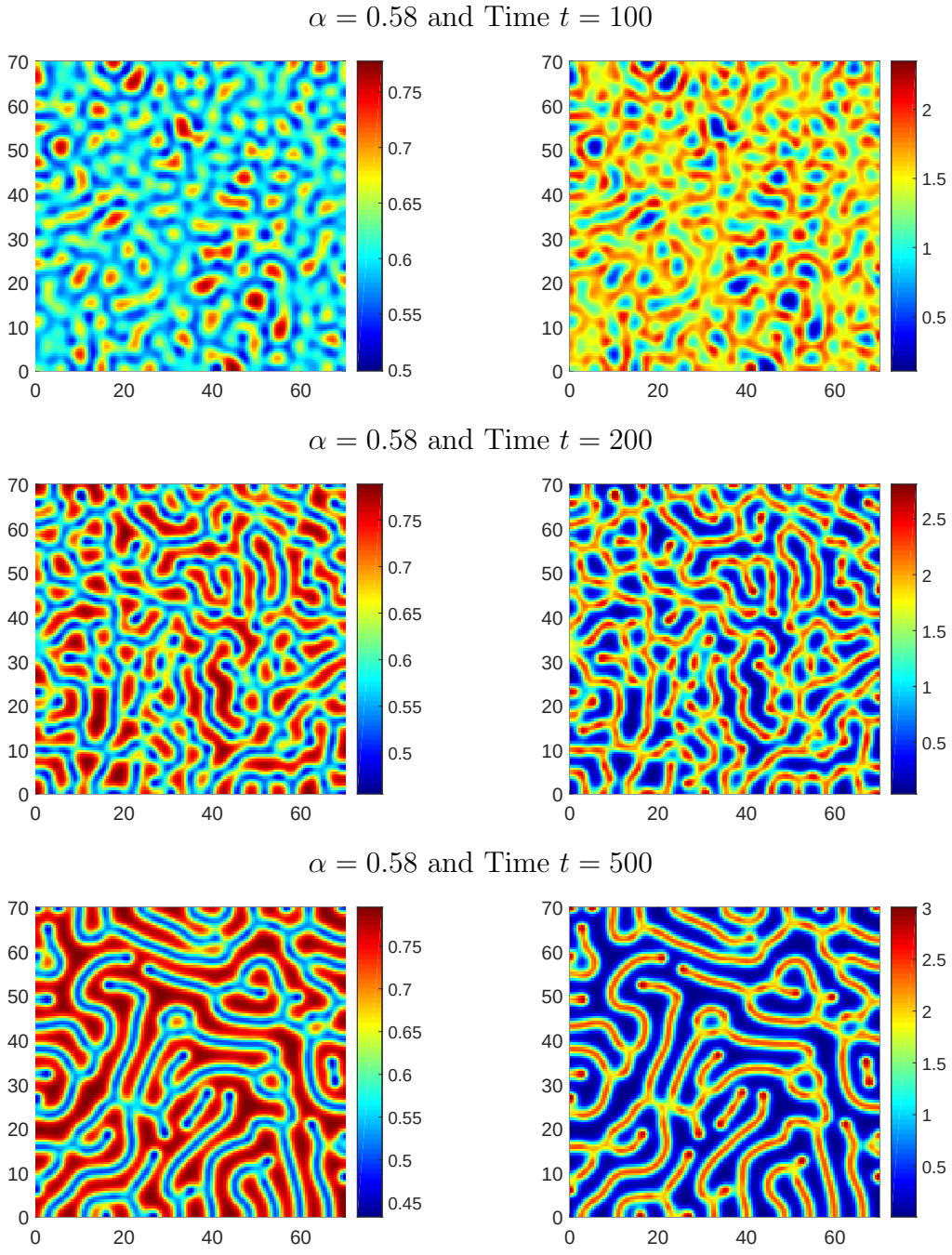

Figure 4.16: Time evolution of patterns of the prey (left column) and predator (right column) with parameters $\sigma = 10$, $C = 0.8$, $h = 0.1$, $D = 40$.

4.6 Conclusion

In theoretical ecology, intensive studies of the mechanisms and scenarios of pattern formation, in models of interacting populations, have always been an attraction, as their perception help to enhance the understanding of real-world ecological systems. In this chapter, we have considered a diffusive predator–prey model with hunting cooperation in predators and type II functional response under non-zero initial conditions and zero-flux boundary conditions. We have provided elaborate analysis of both non-spatial and spatiotemporal models and studied possible scenarios of pattern formation in the diffusive predator–prey model with hunting cooperation in predators. While studying the spatiotemporal model, we first obtain the condition for diffusive instability and identified the corresponding domain in the space of controlling parameters. The hunting cooperation coefficient α, the basic reproduction number of the predator (C) and the ratio of diffusion coefficient (D) are the controlling parameters in our study. Using the parameter values from both Turing and non-Turing domain, we investigate the properties of the system using extensive numerical simulations.

Our model simulation has been categorized in two separate domains, namely, the non-Turing and the Turing domains. We have highlighted the effect of hunting cooperation in predators along with the basic reproduction number of the predators. After simulated numerically, we confirmed that in the non-Turing domain, with $C > 1$, the predator population increased with slight hunting cooperation and decreased with the increase in the hunting cooperation coefficient. Also, for $C < 1$, the increase in the hunting cooperation in the predators, help them to survive. In the Turing domain, with $C < 1$, the hunting cooperation in predators play a crucial role in the coexistence. By varying the values of cooperation coefficient and basic reproduction number, we get dissimilar types of diffusive patterns, namely, patchy pattern (spots), stripe pattern and mixed pattern (spot-stripe). From the point of view of population dynamics, one can observe that there exists the pattern formation (spot) for preys implying that the preys are scattered with low density and the remaining region is high dense, which means that the preys have segregated in very small groups over the large area and are safe. Similarly, spot formation in predators convey that with hunting cooperation, the predators are scattered and isolated but

still survives. Large African predators like cheetah (Acinonyx jubatus), leopard (Panthera pardus) and lion (Pathera leo) regularly predate ungulates, double their mass with the possibility of injury or death to the predator during prey capture but can easily be overcome by cooperative hunting, that may improve hunting success rate [36].

The methods and consequences in the study may amplify the systematic investigation of spatial pattern formation in the predator–prey systems, and may nicely enforce in some different research dimensions. Further analysis are important to study the patterns dynamics of some more diffusive ecological models. It would be interesting to study the traveling waves in the spatial predator–prey models with hunting cooperation in predators with type III or type IV functional responses. This work highlights a number of research areas for future consideration in spatial pattern formation.

Chapter 5

Spatiotemporal model of a predator–prey system with herd behavior and quadratic mortality

5.1 Introduction

Predator–prey models in which the prey exhibits herd behavior, have been an area of great interest in the last few years [3; 21; 22; 25; 65; 102; 107; 170; 189]. In herd behavior, the predator interacts with prey along the outer corridor of the herd of prey, as a mathematical consequence of which the interaction term for predator–prey is the square root of prey population.

The herd behavior of the preys is related to group defence, in which the preys at the boundary of the group hurt most, from the attacks of the predators. The number of preys remaining on the border of the group is proportional to the length of the perimeter of the ground region occupied by the group [25], which in turn is directly proportional to the square root of the area of that grounded region. Hence, it is reasonable and logical to use square root term for the prey population to portray the model with herd behavior [170]. Also, herd behavior is about local interaction, which is taken care by the power response function, basically it takes care of the sort range interaction. By adding diffusion to the model, we are looking into the dynamics when the herd is changing the habitat, basically the effect of long range

diffusion.

Of many components that affect the dynamics of predator–prey interaction, one of the vital component is the functional response. Extensively, the functional response can be categorized into many distinct variants: Holling I–III variants [75; 76], Crowley–Martin variant [40], Beddington–DeAngelis variant [20; 41] and the converted structures of these types [77; 89; 196]. The functional response with square root term for the prey population motivates us to study the spatial dynamics of predator–prey system with herd behavior in prey, where we have considered Holling type II functional response.

Mechanisms of spatial dynamics in predator–prey models with herd in predators have been comparatively new and to the best of our knowledge, studied by few [170; 193]. The objective of this current investigation is to create deep intuition into methods of spatial pattern formation in predator–prey model with herd behavior in preys. Here, we investigate how the rate of the biomass of the predators, handling time of preys and mortality rate of predators, affect the spatial dynamics of predator–prey interaction.

5.2 Model description

By incorporating diffusion and Holling type II functional response in the general predator–prey system with herd behavior [3; 25; 102; 171], we obtain the following diffusive predator–prey model as

$$\begin{aligned} \frac{\partial U}{\partial t} &= rU\left(1-\frac{U}{K}\right)-\frac{\alpha\sqrt{U}V}{1+t_h\alpha\sqrt{U}}+D_1\nabla^2U, \\ \frac{\partial V}{\partial t} &= \frac{c\alpha\sqrt{U}V}{1+t_h\alpha\sqrt{U}}-sV+D_2\nabla^2V, \end{aligned} \tag{5.1}$$

where $U(t)$ and $V(t)$ are the densities of prey and predator population at time t and location (X, Y) respectively. Here, r is the intrinsic growth rate of the prey and K is its carrying capacity. We consider a Holling type II functional response with herd behavior in prey of the form

$$\frac{\alpha\sqrt{U}}{1+t_h\alpha\sqrt{U}},$$

which depends on prey densities. The parameter α is the search efficiency of predator for preys, and t_h is predator's average handling time of prey. The parameter s is the natural mortality rate of the predator in the absence of prey, and c is the rate of conversion of prey biomass to predator biomass. The non-negative constants D_1 and D_2 are the diffusion coefficients for prey and predator densities respectively.

We now non-dimensionalized the model (5.1) by introducing the dimensionless variables

$$u = \frac{U}{K}, \quad v = \frac{\alpha V}{r\sqrt{K}}, \quad \tau = rt, \quad x = X\sqrt{\frac{r}{D_2}}, \quad y = Y\sqrt{\frac{r}{D_2}},$$

and dimensionless parameters

$$m = \frac{s}{r}, \quad \gamma = t_h\alpha\sqrt{K}, \quad \beta = c\frac{\alpha\sqrt{K}}{r}, \quad D = \frac{D_1}{D_2}.$$

We get the modified model as

$$\begin{aligned} \frac{\partial u}{\partial \tau} &= u\,(1-u) - \frac{\sqrt{u}v}{1+\gamma\sqrt{u}} + D\ \nabla^2 u, \\ \frac{\partial v}{\partial \tau} &= \frac{\beta\sqrt{u}v}{1+\gamma\sqrt{u}} - mv + \nabla^2 v, \end{aligned} \tag{5.2}$$

and in the line of the following references [19; 26; 64], we select the quadratic death rate for predator population.

Note: In herd behavior of preys, group defence is involved. The predators could not easily catch their preys which results in stress, overcrowding and intra-specific as well as inter-specific competitions. Hence, it is justified to take quadratic mortality in predators.

Then the above model (5.2) will be modified to the following form:

$$\begin{aligned} \frac{\partial u_1}{\partial \tau} &= u_1\,(1-u_1) - \frac{\sqrt{u_1}v_1}{1+\gamma\sqrt{u_1}} + D\ \nabla^2 u_1, \\ \frac{\partial v_1}{\partial \tau} &= \frac{\beta\sqrt{u_1}v_1}{1+\gamma\sqrt{u_1}} - m{v_1}^2 + \nabla^2 v_1, \end{aligned} \tag{5.3}$$

where the positive constant D is the ratio of diffusion coefficients of prey and predator densities for models (5.2) and (5.3) respectively, and $\nabla^2\big(=\frac{\partial^2}{\partial x^2}+\frac{\partial^2}{\partial y^2}\big)$ is the usual Laplacian operator in two dimensional space $\mathbf{R} = (x, y)$. To make certain that spatial patterns are governed by reaction-diffusion equations, models (5.2) and (5.3)

are to be analyzed with the following non-zero initial conditions

for model with linear mortality (model 5.2)

$$\begin{aligned}
&\text{1D}: \ u(x,0) > 0, \quad v(x,0) > 0, \quad x \in \Omega = [0, L], \\
&\text{2D}: \ u(x,y,0) > 0, \quad v(x,y,0) > 0, \quad (x,y) \in \Omega = [0, L] \times [0, L],
\end{aligned}$$

for model with quadratic mortality (model 5.3)

$$\begin{aligned}
&\text{1D}: \ u_1(x,0) > 0, \quad v_1(x,0) > 0, \quad x \in \Omega_1 = [0, L_1], \\
&\text{2D}: \ u_1(x,y,0) > 0, \quad v_1(x,y,0) > 0, \quad (x,y) \in \Omega_1 = [0, L_1] \times [0, L_1],
\end{aligned}$$

and zero-flux (Neumann) boundary conditions

$$\begin{aligned}
&\frac{\partial u}{\partial \nu} = \frac{\partial v}{\partial \nu} = 0 \text{ (for model with linear mortality)}, \\
&\frac{\partial u_1}{\partial \nu_1} = \frac{\partial v_1}{\partial \nu_1} = 0 \text{ (for model with quadratic mortality)}, \qquad (5.4)
\end{aligned}$$

where L and L_1 denotes the size of the system in the direction of (u, v) and (u_1, v_1) respectively. ν and ν_1 are outward unit normal on the boundary $\partial\Omega$ and $\partial\Omega_1$ respectively. Conditions (5.4) implies that no individual species leave the domain.
Note: Both the models (5.2) and (5.3) fail to maintain the positivity condition at all the future time.

5.3 Analysis of the non-spatial model

5.3.1 Non-spatial dynamics of the predator–prey system with linear mortality

In absence of diffusion, the equilibrium points of the system (5.2) are given by

$$\begin{aligned}
u\,(1-u) - \frac{\sqrt{u}v}{1+\gamma\sqrt{u}} &= 0, \\
\frac{\beta\sqrt{u}v}{1+\gamma\sqrt{u}} - mv &= 0.
\end{aligned}$$

Clearly $(0,\ 0)$, $(1,\ 0)$ and $(u^*,\ v^*)$ are the steady state solutions, where

$$u^* = \frac{m^2}{(\beta - m\gamma)^2}, \quad v^* = \sqrt{u^*}(1-u^*)(1+\gamma\sqrt{u^*}).$$

The variational matrix about the equilibrium point $(u^*,\ v^*)$ is given by

$$\left[\begin{array}{cc} 1-2u-\frac{v}{2\sqrt{u}\left(1+\gamma\sqrt{u}\right)^2} & -\frac{\sqrt{u}}{1+\gamma\sqrt{u}} \\ \frac{\beta v}{2\sqrt{u}\left(1+\gamma\sqrt{u}\right)^2} & \frac{\beta\sqrt{u}}{1+\gamma\sqrt{u}}-m \end{array}\right]_{(u^*,v^*)}.$$

(i) At $(1,\ 0)$, the variational matrix is

$$\left[\begin{array}{cc} -1 & -\frac{1}{1+\gamma} \\ 0 & \frac{\beta}{1+\gamma}-m \end{array}\right],$$

whose eigenvalues are -1 and $\frac{\beta}{1+\gamma}-m$. Therefore, the system is asymptotically stable if $\frac{\beta}{1+\gamma}<m$.

(ii) At $(u^*,\ v^*)$, the variational matrix is

$$\left[\begin{array}{cc} 1-2u^*-\frac{1-u^*}{2(1+\gamma\sqrt{u^*})} & -\frac{\sqrt{u^*}}{1+\gamma\sqrt{u^*}} \\ \frac{\beta(1-u^*)}{2(1+\gamma\sqrt{u^*})} & \frac{\beta\sqrt{u^*}}{1+\gamma\sqrt{u^*}}-m \end{array}\right],$$

and the corresponding characteristic equation is

$$\lambda^2+A_1\lambda+A_2=0,$$

where

$$A_1=\frac{3u^*-1+4\gamma u^{*\frac{3}{2}}-2(\beta+\gamma)\sqrt{u^*}+2m(1+\gamma\sqrt{u^*})}{2(1+\gamma\sqrt{u^*})} \quad \text{and}$$

$$A_2=\frac{2\beta\sqrt{u^*}(1-2u^*)+m(3u^*-1-2\gamma\sqrt{u^*}+4\gamma u^{*\frac{3}{2}})}{2(1+\gamma\sqrt{u^*})}.$$

By Routh-Hurwitz criterion, system (5.2) will be asymptotically stable about $(u^*,\ v^*)$ if all $A_i>0$ $(i=1,2)$. In the numerical simulation section, the specific steady state under study has been mentioned.

5.3.2 Non-spatial dynamics of the model predator–prey system with quadratic mortality

In absence of diffusion, the equilibrium points of the system (5.3) are given by

$$\begin{aligned} u_1\left(1-u_1\right)-\frac{\sqrt{u_1}v_1}{1+\gamma\sqrt{u_1}} &= 0, \\ \frac{\beta\sqrt{u_1}v_1}{1+\gamma\sqrt{u_1}}-m{v_1}^2 &= 0. \end{aligned}$$

Clearly (0, 0), (1, 0) and (${u_1}^*$, ${v_1}^*$) are the steady state solutions, where ${v_1}^* = \frac{\beta}{m}\left(\frac{\sqrt{{u_1}^*}}{1+\gamma\sqrt{{u_1}^*}}\right)$ and ${u_1}^*$ is the solution of

$$m\gamma^2 {{u_1}^*}^2 - m(\gamma^2-1){u_1}^* + 2m\gamma\sqrt{{u_1}^*}({u_1}^* - 1) + (\beta - m) = 0.$$

The variational matrix about the equilibrium point (${u_1}^*$, ${v_1}^*$) is given by

$$\left[\begin{array}{cc} 1 - 2u_1 - \frac{v_1}{2\sqrt{u_1}\left(1+\gamma\sqrt{u_1}\right)^2} & -\frac{\sqrt{u_1}}{1+\gamma\sqrt{u_1}} \\ \frac{\beta v_1}{2\sqrt{u_1}\left(1+\gamma\sqrt{u_1}\right)^2} & \frac{\beta\sqrt{u_1}}{1+\gamma\sqrt{u_1}} - 2mv_1 \end{array}\right]_{({u_1}^*,\ {v_1}^*)}.$$

(i) At (1, 0), the variational matrix is

$$\left[\begin{array}{cc} -1 & -\frac{1}{1+\gamma} \\ 0 & \frac{\beta}{1+\gamma} \end{array}\right],$$

whose eigenvalues are -1 and $\frac{\beta}{1+\gamma}$. Therefore, the system is unstable (since $\frac{\beta}{1+\gamma}$ is always positive).

(ii) At (${u_1}^*$, ${v_1}^*$), the variational matrix is $\left(\text{ since } {v_1}^* = \frac{\beta}{m}\frac{\sqrt{{u_1}^*}}{1+\gamma\sqrt{{u_1}^*}}\ \right)$

$$\left[\begin{array}{cc} 1 - 2{u_1}^* - \frac{\beta}{2m(1+\gamma\sqrt{{u_1}^*})^3} & -\frac{\sqrt{{u_1}^*}}{1+\gamma{u_1}^*} \\ \frac{\beta^2}{2m(1+\gamma{u_1}^*)^3} & -\frac{\beta\sqrt{{u_1}^*}}{1+\gamma{u_1}^*} \end{array}\right],$$

and the corresponding characteristic equation is

$$\lambda^2 + B_1\lambda + B_2 = 0,$$

where

$$B_1 = \frac{\beta + 2m(1+\gamma\sqrt{{u_1}^*})^2\left(2{u_1}^* - 1 + (\beta-\gamma)\sqrt{{u_1}^*} + 2\gamma{{u_1}^*}^{\frac{3}{2}}\right)}{2m(1+\gamma\sqrt{{u_1}^*})^3} \quad \text{and}$$

$$B_2 = \frac{\beta\sqrt{{u_1}^*}\left(\beta + m(2{u_1}^* - 1)(1+\gamma\sqrt{{u_1}^*})^3\right)}{m(1+\gamma\sqrt{{u_1}^*})^4}.$$

By Routh-Hurwitz criterion, system (5.3) will be asymptotically stable about (${u_1}^*$, ${v_1}^*$) if all $B_i > 0$ $(i = 1, 2)$. In the numerical simulation section, the specific steady state under study has been mentioned.

Note: The variational matrix is indeterminate at (0, 0) for both the models.

5.4 Analysis of the spatiotemporal model

5.4.1 Spatial dynamics of the predator–prey system with linear mortality

Interior equilibrium point $(u^*,\ v^*)$ of non-spatial system is spatially homogenous steady state, that is, constant in space and time for the reaction-diffusion system (5.2) (spatiotemporal model). We assume that $(u^*,\ v^*)$ is stable in non-spatial system, which means the spatially homogenous steady state is stable with respect to spatially homogenous perturbations. Though the diffusion is often consider as a stabilizing process, it is a well known fact that diffusion can make a spatially homogenous steady state linearly unstable (Turing instability) with respect to heterogenous perturbations in a system of two interacting species [111; 157; 179]. The condition for Turing instability may be obtained by introducing a small heterogenous perturbation of the homogenous steady states as follows:

$$\begin{aligned} u\left(x,y,\tau\right) &= u^* + \epsilon_1 \exp\left(\lambda_k \tau\right) \cos\left(k_x x\right) \cos\left(k_y y\right), \\ v\left(x,y,\tau\right) &= v^* + \epsilon_2 \exp\left(\lambda_k \tau\right) \cos\left(k_x x\right) \cos\left(k_y y\right), \end{aligned} \tag{5.5}$$

where ϵ_1 and ϵ_2 are two non-zero reals and $k = (k_x, k_y)$, such that $k^2 = \left(k_x^2 + k_y^2\right)$, is the wave number.

Substituting (5.5) into (5.2) and then linearizing it about interior equilibrium $(u^*,\ v^*)$, we obtain the variational matrix as

$$\begin{bmatrix} 1 - 2u^* - \frac{1-u^*}{2(1+\gamma\sqrt{u^*})} - Dk^2 & -\frac{\sqrt{u^*}}{1+\gamma\sqrt{u^*}} \\ \frac{\beta(1-u^*)}{2(1+\gamma\sqrt{u^*})} & \frac{\beta\sqrt{u^*}}{1+\gamma\sqrt{u^*}} - m - k^2 \end{bmatrix}, \tag{5.6}$$

and the corresponding characteristic equation is

$$\lambda^2 + C_1(k^2)\lambda + C_2(k^2) = 0, \tag{5.7}$$

where

$$C_1(k^2) = \left(1 + D\right)k^2 + \frac{3u^* - 1 + 4\gamma {u^*}^{\frac{3}{2}} - 2(\beta+\gamma)\sqrt{u^*} + 2m(1+\gamma\sqrt{u^*})}{2(1+\gamma\sqrt{u^*})}$$

and

$$C_2(k^2) = \frac{D\Big(2k^4(1+\gamma\sqrt{u^*})+2k^2(m-\beta\sqrt{u^*}+m\gamma\sqrt{u^*})\Big)+k^2(3u^*-1)}{2(1+\gamma\sqrt{u^*})} + \frac{2\beta\sqrt{u^*}(1-2u^*)+2k^2\gamma\sqrt{u^*}(2u^*-1)+m(3u^*-1-2\gamma\sqrt{u^*}+4\gamma {u^*}^{\frac{3}{2}})}{2(1+\gamma\sqrt{u^*})}.$$

By Routh-Hurwitz criterion, system (5.2) will be asymptotically stable about $(u^*,\ v^*)$ if $C_1(k^2) > 0$ and $C_2(k^2) > 0$. As the parameters D and k^2 are all positive and $\frac{3u^*-1+4\gamma {u^*}^{\frac{3}{2}}-2(\beta+\gamma)\sqrt{u^*}+2m(1+\gamma\sqrt{u^*})}{2(1+\gamma\sqrt{u^*})} > 0$ (by the stability of the non-spatial model of (5.2)), $C_1(k^2)$ is always positive. Therefore, the condition for diffusive instability is $C_2(k^2) < 0$.

The polynomial function $C_2(k^2)$ has a minimum for some value of k, say k_{min}, where

$$k^2_{min} = \frac{1-3u^*+2\gamma\sqrt{u^*}(1-2u^*)-2D(m-\beta\sqrt{u^*}+m\gamma\sqrt{u^*})}{4D(1+\gamma\sqrt{u^*})}.$$

Hence, the minimum value of k for which Turing instability will occur is $C_2(k^2_{min}) < 0$. Therefore, substituting k^2_{min} in $C_2(k^2)$, we get the sufficient condition for Turing instability as

$$\frac{1-3u^*+2\gamma\sqrt{u^*}(1-2u^*)-2D(m-\beta\sqrt{u^*}+m\gamma\sqrt{u^*})}{2(1+\gamma\sqrt{u^*})} - \sqrt{\frac{D\Big(4\beta\sqrt{u^*}(1-2u^*)+2m(3u^*-1-2\gamma\sqrt{u^*}+4\gamma {u^*}^{\frac{3}{2}})\Big)}{1+\gamma\sqrt{u^*}}} > 0. \quad (5.8)$$

The interval of the wave number for which Turing instability take place is (k_-, k_+) and in this interval, we have $C_2(k^2_{min}) < 0$, where

$$k_- = \frac{A}{4D(1+\gamma\sqrt{u^*})} - \frac{1}{4D}\sqrt{\frac{A^2-8DB}{(1+\gamma\sqrt{u^*})^2}},$$

$$k_+ = \frac{A}{4D(1+\gamma\sqrt{u^*})} + \frac{1}{4D}\sqrt{\frac{A^2-8DB}{(1+\gamma\sqrt{u^*})^2}},$$

$$A = 1-3u^*+2\gamma\sqrt{u^*}(1-2u^*)-2D(m-\beta\sqrt{u^*}+m\gamma\sqrt{u^*}) \quad \text{and}$$

$$B = (1+\gamma\sqrt{u^*})(2\beta\sqrt{u^*}(1-2u^*)+m(3u^*-1-2\gamma\sqrt{u^*}+4\gamma {u^*}^{\frac{3}{2}})).$$

5.4.2 Spatial dynamics of the predator–prey system with quadratic mortality

Same analysis follows as discussed in the previous section, by introducing a small heterogenous perturbation of the homogenous steady states (${u_1}^*,\ {v_1}^*$), namely,

$$\begin{aligned} u_1(x,y,\tau) &= {u_1}^* + \xi_1 \exp(\lambda_k \tau)\cos(k_x x)\cos(k_y y), \\ v_1(x,y,\tau) &= {v_1}^* + \xi_2 \exp(\lambda_k \tau)\cos(k_x x)\cos(k_y y), \end{aligned} \tag{5.9}$$

where ξ_1 and ξ_2 are non-zero real numbers and $k = (k_x, k_y)$, such that $k^2 = \left(k_x^2 + k_y^2\right)$, is the wave number.

Substituting (5.9) into (5.3) and linearizing it about interior equilibrium (${u_1}^*$, ${v_1}^*$), we obtain the variational matrix as

$$\begin{bmatrix} 1 - 2{u_1}^* - \frac{\beta}{2m(1+\gamma\sqrt{{u_1}^*})^3} - Dk^2 & -\frac{\sqrt{{u_1}^*}}{1+\gamma{u_1}^*} \\ \frac{\beta^2}{2m(1+\gamma{u_1}^*)^3} & -\frac{\beta\sqrt{{u_1}^*}}{1+\gamma{u_1}^*} - k^2 \end{bmatrix}, \tag{5.10}$$

and the corresponding characteristic equation is

$$\lambda^2 + D_1(k^2)\lambda + D_2(k^2) = 0, \tag{5.11}$$

where

$$D_1(k^2) = \big(1+D\big)k^2 + \frac{\beta\sqrt{{u_1}^*}}{1+\gamma\sqrt{{u_1}^*}} + \frac{\beta + 2m(2{u_1}^* - 1)(1+\gamma\sqrt{{u_1}^*})^3}{2m(1+\gamma\sqrt{{u_1}^*})^3}$$

and

$$\begin{aligned} D_2(k^2) = {} & \frac{\beta\sqrt{{u_1}^*}(2{u_1}^* - 1) + k^2(2{u_1}^* - 1 + (D\beta - \gamma)\sqrt{{u_1}^*} + 2\gamma {{u_1}^*}^{\frac{3}{2}})}{1+\gamma\sqrt{{u_1}^*}} \\ & + \frac{\beta^2\sqrt{{u_1}^*}}{m(1+\gamma\sqrt{{u_1}^*})^4} + \frac{\beta k^2}{2m(1+\gamma\sqrt{{u_1}^*})^3} + Dk. \end{aligned}$$

Using Routh-Hurwitz criterion, system (5.3) will be asymptotically stable about (${u_1}^*,\ {v_1}^*$) if $D_1(k^2) > 0$ and $D_2(k^2) > 0$. As the parameters D and k^2 are all positive and $\left(\frac{\beta+2m(2{u_1}^*-1)(1+\gamma\sqrt{{u_1}^*})^3}{2m(1+\gamma\sqrt{{u_1}^*})^3} + \frac{\beta\sqrt{{u_1}^*}}{1+\gamma\sqrt{{u_1}^*}}\right) > 0$ (by the stability of the non-spatial model of (5.3)), $D_1(k^2)$ is always positive. Therefore, the condition for diffusive instability is $D_2(k^2) < 0$.

The polynomial function $D_2(k^2)$ has a minimum for some value of k, is obtained as

$$k^2_{min} = \frac{1}{4}\left(\frac{2 - 4{u_1}^* - \frac{\beta}{m(1+\gamma\sqrt{{u_1}^*})^3}}{D} - \frac{2\beta\sqrt{{u_1}^*}}{1+\gamma\sqrt{{u_1}^*}}\right).$$

Hence, the minimum value of k for which Turing instability will occur is $D_2(k^2_{min}) < 0$ in the interval $(k_-,\ k_+)$ and we get the sufficient condition for Turing instability as

$$\frac{2m(1-2{u_1}^*)(1+\gamma\sqrt{{u_1}^*})^3 - \beta}{2m(1+\gamma\sqrt{{u_1}^*})^3} - \frac{D\beta\sqrt{{u_1}^*}}{1+\gamma\sqrt{{u_1}^*}} - \sqrt{\frac{4D\Big(\beta\sqrt{{u_1}^*}(\beta + m(2{u_1}^* - 1)(1+\gamma\sqrt{{u_1}^*})^3)\Big)}{m(1+\gamma\sqrt{{u_1}^*})^4}} > 0, \quad (5.12)$$

where

$$\begin{aligned}
k_- &= \frac{A}{4Dm(1+\gamma\sqrt{{u_1}^*})^3} - \frac{1}{4Dm(1+\gamma\sqrt{{u_1}^*})^3}\sqrt{B^2 - 16DC},\\
k_+ &= \frac{A}{4Dm(1+\gamma\sqrt{{u_1}^*})^3} + \frac{1}{4Dm(1+\gamma\sqrt{{u_1}^*})^3}\sqrt{B^2 - 16DC},\\
A &= 2m(1-2{u_1}^*)(1+\gamma\sqrt{{u_1}^*})^3 - 2Dm\beta\sqrt{{u_1}^*}(1+\gamma\sqrt{{u_1}^*})^2 - \beta,\\
B &= \beta + 2Dm\beta\sqrt{{u_1}^*}(1+\gamma\sqrt{{u_1}^*})^2 + 2m(2{u_1}^* - 1)(1+\gamma\sqrt{{u_1}^*})^3,\\
C &= m\beta\sqrt{{u_1}^*}(1+\gamma\sqrt{{u_1}^*})^2(\beta + m(2{u_1}^* - 1)(1+\gamma\sqrt{{u_1}^*})^3).
\end{aligned}$$

5.5 Numerical simulations

We will now investigate the numerical results of both non-spatial as well as spatiotemporal models, namely, (5.2) and (5.3). For numerical simulation, we set $\gamma = 0.01$, $\beta = 0.8$, and consider m as controlling parameter in both models. For these values of parameters, equilibrium points of model (5.2) are (0, 0), (1, 0) and (0.7792, 0.1966) (m=0.7), and the equilibrium points of model (5.3) are (0, 0), (1, 0) and (0.1822, 0.3506) (m=0.97). The system (5.2) is stable about the positive equilibrium point (0.7792, 0.1966) and predator free steady state (1, 0) with this set of parameters is asymptotically stable. Also, the steady state solution (0.1822, 0.3506) of system (5.3) is asymptotically stable but the predator free steady state (1, 0) is always unstable. Figure 5.1 shows the dynamics of prey and predator densities

in the non-spatial domain for linear and quadratic mortality respectively. When mortality is linear, the predators go to extinction with increasing m (Figure 5.1(a)). On the other hand, in the case of quadratic mortality, the prey and predator species always exist (coexist), even when mortality rate is increased. However, the predator density decreases as the mortality rate crosses the numerical value 1.28, but never goes extinct (Figure 5.1(b)).

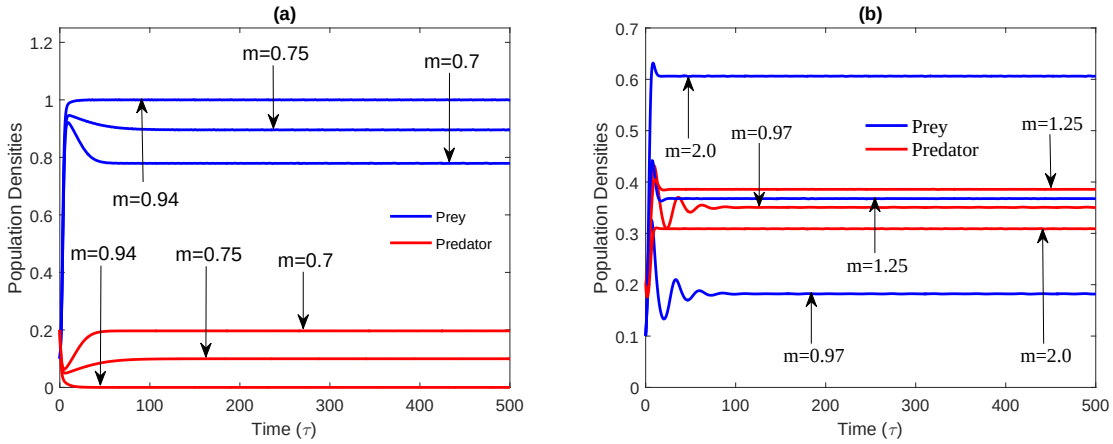

Figure 5.1: (a) Dynamics of preys (u) and predators (v) in the non-spatial domain of the model with linear mortality (model 5.2) for different mortality rate m; (b) Dynamics of preys (u) and predators (v) in the non-spatial domain of the model with quadratic mortality (model 5.3) for different mortality rate m. Other parameter values are $\beta = 0.8$ and $\gamma = 0.01$.

We now simulate the spatiotemporal models (both with linear and quadratic mortality) in one and two dimensional spaces with the help of finite difference scheme for spatial derivatives. The forward Euler's numerical method is used for the non-spatial part of models and general finite difference scheme of five point is used for the spatial part. The reaction-diffusion partial differential equations, given by (5.2), is numerically solved by using splitting method [49; 97]. The numerical values for the step sizes of time and space have been selected adequately small for avoiding the numerical artifacts. In this study, we have employed (for both the models) statistically uncorrelated Gaussian white noise perturbation in space, which is mathematically denoted in one and two dimensional cases as

$$\begin{aligned} u(x_i, 0) &= u^* + \eta_1 \xi_i, \\ v(x_i, 0) &= v^* + \eta_2 \chi_i, \end{aligned} \tag{5.13}$$

and

$$\begin{aligned} u(x_i, y_j, 0) &= u^* + \gamma_1 \epsilon_{ij}, \\ v(x_i, y_j, 0) &= v^* + \gamma_2 \eta_{ij}, \end{aligned} \tag{5.14}$$

where η_1, η_2, γ_1 and γ_2 are very small real numbers and ξ_i, χ_i, ϵ_{ij} and η_{ij} are statistically uncorrelated Gaussian white noise perturbations with zero mean and fixed variance, in one and two dimensional spaces respectively. Similar approach is also considered for model (5.3) with quadratic mortality.

For spatiotemporal models, we perform numerical simulations of the systems (5.2) as well as (5.3) over the non-zero initial condition and zero-flux boundary conditions, in one and two dimensional spatial domain. The domain size for simulation of model (5.2) (with linear mortality) in one dimension is [0, 4000] and in two dimension is 500×500 units. For the model with quadratic mortality, the domain size for simulation in one dimension is [0, 1000] and for two dimensional space is 100×100 units with time-step $\Delta t = 0.001$ and space-step $\Delta x = \Delta y = 1$. The Neumann zero-flux conditions are placed at boundary of the numerical domain in one and two dimensional problems. The size of the domain is chosen large enough so that the impact of the boundaries has been kept as small as possible during the simulation time.

Figure 5.2 shows the one dimensional non-Turing spatial distribution of densities of the prey and predator population of model (5.2) at time $t = 2500$ with different values of per capita mortality rate (m) of predator. With decrease in the per capita mortality rate of predators ($m = 0.47,\ 0.46,\ 0.45,\ 0.434$), the amplitude of the periodic solutions increases rapidly as m decreases from the Hopf-bifurcation value ($m = 0.46188$), and the periodic solution branch terminates at some critical value m^* (> 0) of m. Note that the periodic solution branch only occurs over a narrow range of the parameter m. Figure 5.2(a) shows non-spatial behavior of the predator and prey with a smooth spatial population. Here, the approximations have evolved into the spatially homogeneous stationary states. For a slightly changed value of the mortality rate ($m = 0.46,\ 0.45$), a formation of a strongly irregular *jagged* dynamics pattern inside a subdomain of the system is observed (Figures 5.2(b, c)). For further decrease in the rate of mortality ($m = 0.434$), the size of the region occupied

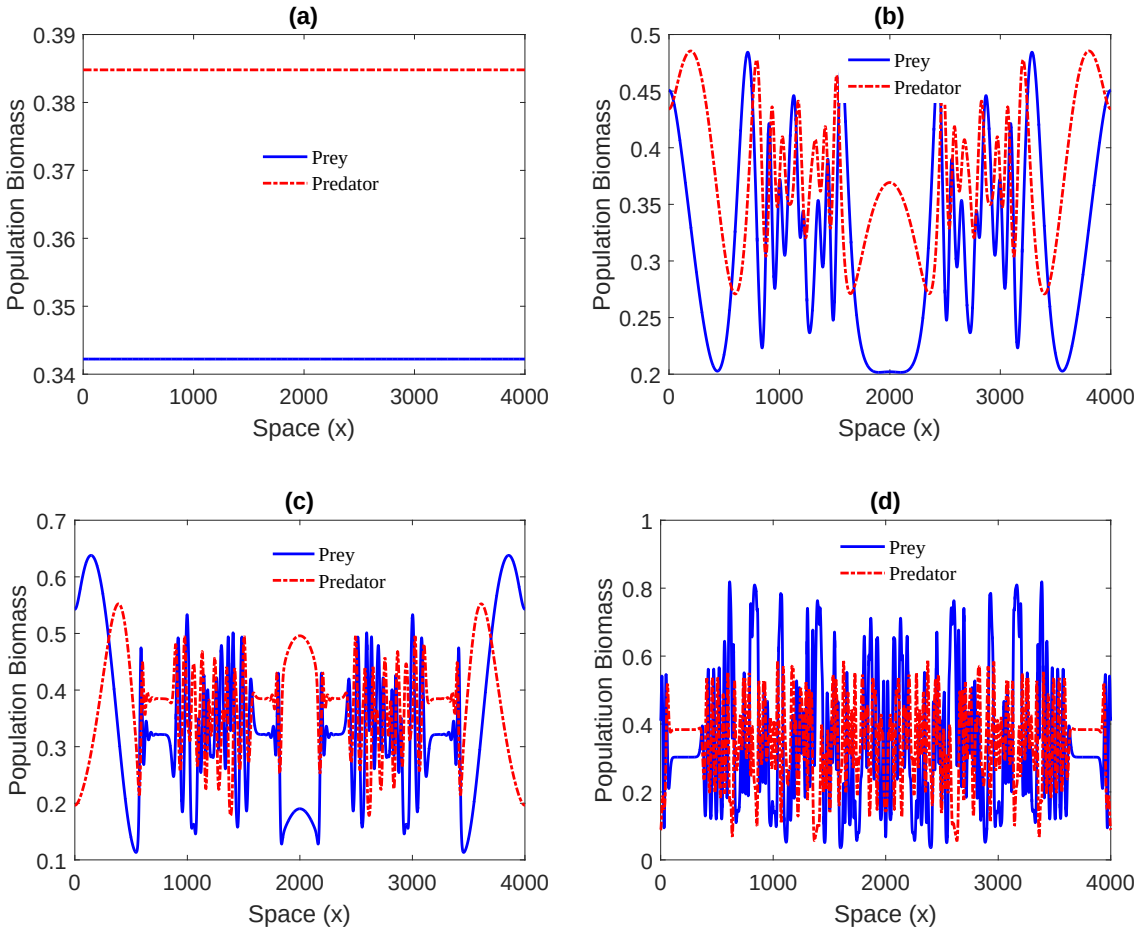

Figure 5.2: One dimensional non-Turing dynamic patterns of the model with linear mortality (model 5.2) at time moment $\tau = 2500$; solid blue line for prey and dashed red line for predator. (a) $m = 0.47$; (b) $m = 0.46$; (c) $m = 0.45$; (d) $m = 0.434$. Other parameter values are $\beta = 0.8$, $\gamma = 0.01$ and $D = 1.0$.

by this pattern steadily grows with time, so that finally irregular spatiotemporal oscillations invade over the whole domain, pertaining to chaotic dynamics (Figure 5.2(d)), which is always growing until it occupies the entire domain. Figure 5.3 shows the snapshots of two dimensional non-Turing spatial distribution of densities of the prey and predator population at time $t = 2500$ with different values of per capita mortality rate (m) of predator. The system dynamics follows a series of patterns which qualitatively resembles the one dimensional case. At $m = 0.46$, the population distribution is smooth and regular (Figures 5.3(a, d)), at $m = 0.45$ it forms semi-spiral like structures (Figures 5.3(b, e)). The domain grows gradually and finally chaotic pattern invades over the entire space, for both the preys and the

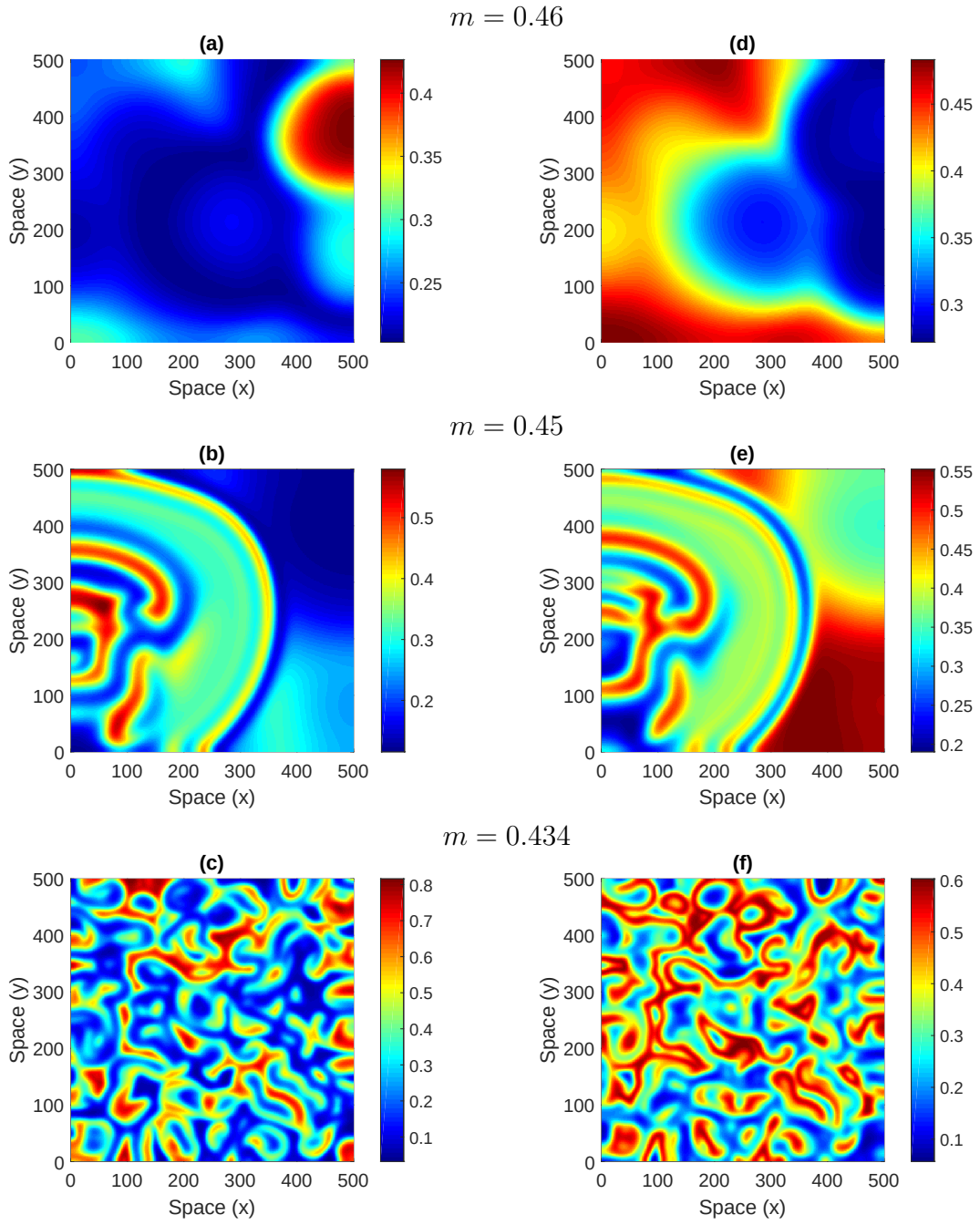

Figure 5.3: Two dimensional non-Turing dynamic patterns of the model with linear mortality (model 5.2) for prey (left panel) and predator (right panel) at time moment $\tau = 2500$. (a) and (d) $m = 0.46$; (b) and (e) $m = 0.45$; (c) and (f) $m = 0.434$. Other parameter values are $\beta = 0.8$, $\gamma = 0.01$ and $D = 1.0$.

predators (Figures 5.3(c, f)).

We now demonstrate diffusive induced instability (Turing instability) and the corresponding pattern formation for the system (5.3) with quadratic mortality. Although, the sufficient conditions for Turing instability were obtained analytically in previous section, whether they are satisfied with our corresponding set of parameter values, is yet to be tested. In order to do so, we sketch the Turing instability condition (5.12) for distinct values of D (other parameter values are fixed, namely, $\gamma = 0.01$, $\beta = 0.8$). Figure 5.4(a) shows the zone for the emergence of spatial patterns corresponding to Turing instability condition against the ratio of diffusion coefficients (D). We observe that the sufficient condition of the diffusive instability, that is, equation (5.12) holds, when D is adequately small ($D = 0.102318$) (see Figure 5.4(a)). The spatial dispersion curve for this particular model, and the corresponding plot of real part of largest eigenvalue $Re(\lambda)$ against the wave number (k) is shown in Figure 5.4(b). The real part of largest eigenvalue $Re(\lambda) > 0$ holds, the wave number (k) fit in the interval (k_-, k_+), that is, $(0.591509, 4.44236)$. Also, the controlling parameter space, namely $m - \beta$ spaces and $m - \gamma$ spaces, for Turing instability via sufficient condition, is shown in Figures 5.5(a) and 5.5(b).

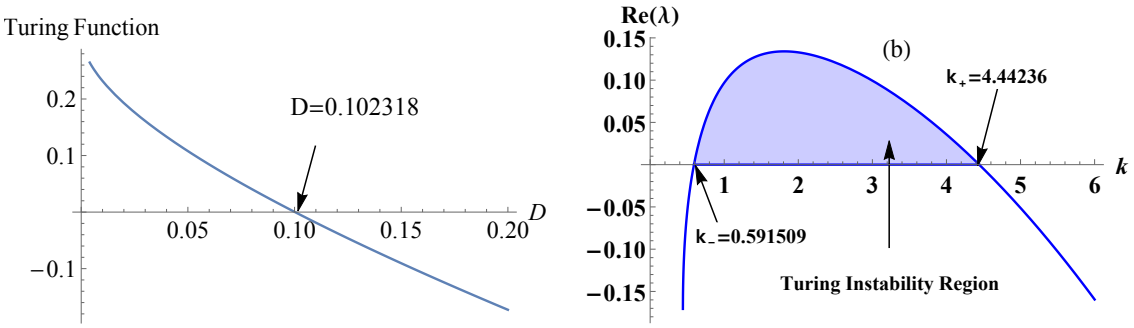

Figure 5.4: (a) Emergence of spatial pattern corresponding to Turing instability condition of the model with quadratic mortality (model 5.3); (b) Characterization of the dispersal relation for D=0.08 of the model with quadratic mortality (model 5.3).

In Figure 5.6, we have illustrated the one dimensional Turing dynamics of densities distribution of the prey and predator population of model (5.3) at time $t = 2500$ with different per capita mortality rate (m) of predator. In Figure 5.6(a), the approximations have evolved into the spatially homogenous stationary values $u_1{}^*$ and

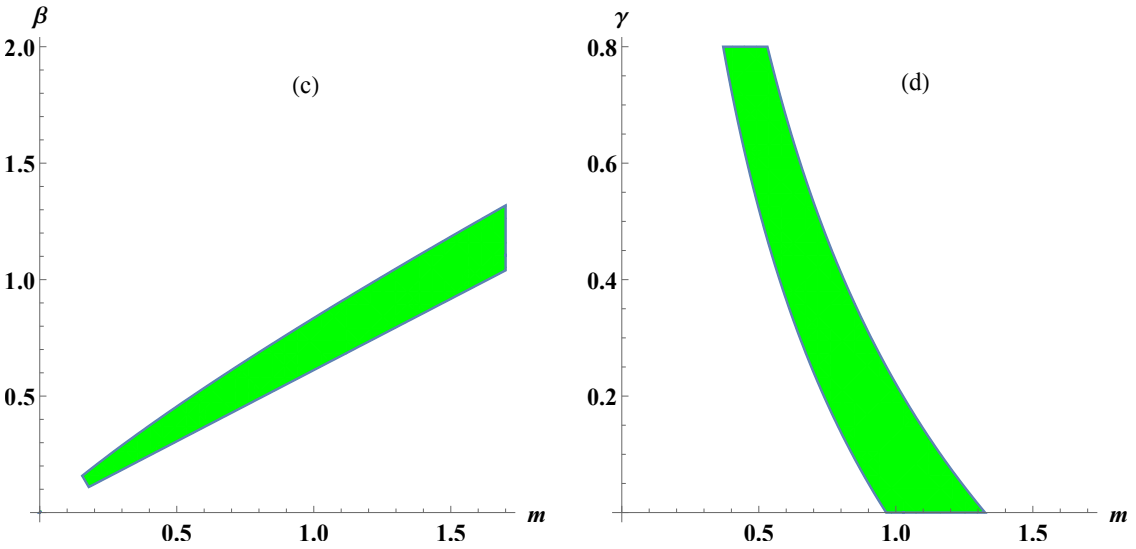

Figure 5.5: (a) Parameters zone for Turing pattern of the model with quadratic mortality (model 5.3) with $D = 0.08$: $m - \beta$ space; (b) Parameters zone for Turing pattern of the model with quadratic mortality (model 5.3) with $D = 0.08$: $m - \gamma$ space.

$v_1{}^*$. Figure 5.6(b, c, d) show the response of the system after m is changed to 0.97, 1.25 and 2.0 at the moment $t = 2500$. For the parameter values allowing for Turing instability, the periodic patterns begin to emerge in a certain subdomain, which amplifies and then decay, and eventually spreads over the whole area. Figure 5.7 shows the Turing patterns for prey and predator population of the system (5.3) distributed over two dimensional spatial domain obtain at $t = 2500$ for different values of m. The patterns arising in the large time limits are shown in the Figures 5.7(a–f). For some values of per capita mortality rate of predator m (= 0.97, 1.25, 2.0), both prey and predators population coexist and form the spatial pattern of two types, namely, mixture of spots and stripes and then spots. Some values of per capita mortality rate of predator m (=0.97, 1.25, 2.0), both prey and predators population coexist and form the spatial pattern of two types, namely, mixture of spots and stripes and then spots.

Figure 5.8 shows the Turing patterns for prey and predator population of the system (5.3) distributed over two dimensional spatial domain obtain at $t = 2500$ for different values of γ, the search efficacy of predators for preys. The pattern shows, namely, a mixture of stripe-spots (Figure 5.8(a, d)) and then spots (Figure

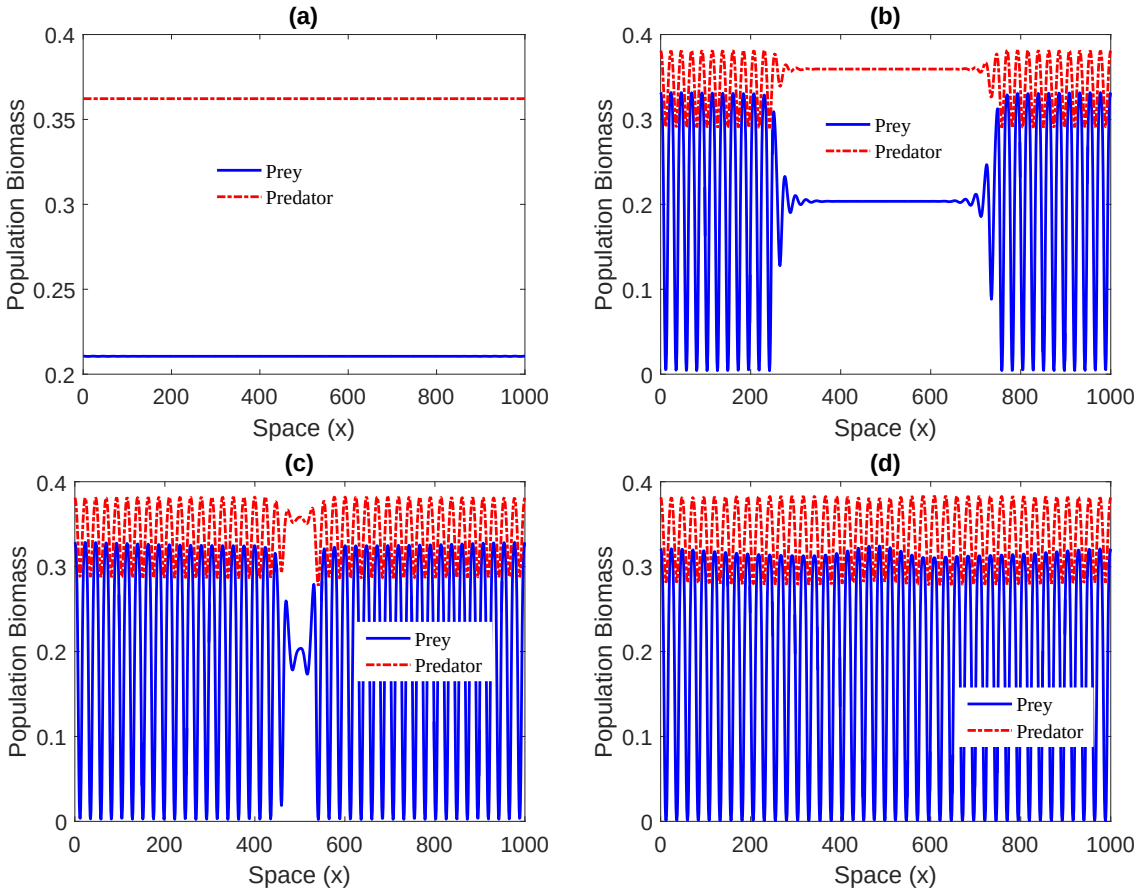

Figure 5.6: One dimensional Turing dynamic patterns of the model with quadratic mortality (model 5.3) for prey and predator at time moment $\tau = 2500$; solid blue line for prey and dashed red line for predator. (a) $m = 0.93$; (b) $m = 0.97$; (c) $m = 1.25$; (d) $m = 2.0$. Other parameter values are $\beta = 0.8$, $\gamma = 0.01$ and $D = 0.08$.

5.8(b, e)). For $\gamma = 0.02$, the system is very close to the boundary that separates the Turing zone from the non-Turing zone. It is a transition state from spots to smooth and regular patterns. Figure 5.9 shows the Turing patterns of the system (5.3) distributed over spatial domain obtain at $t = 2500$ for different values of β, the rate of conversion of prey biomass to predator biomass. The patterns arising in the large time limits are shown in the Figures 5.9(a–f). For some values of β (β = 0.76, 0.78, 0.80), both prey and predators population coexist and show patchy spatial pattern (spots).

Having thus established the Turing patterns in the system (5.3), by changing the values of control parameters (m, γ, β), we proceed with the numerical simulation of system (5.3), by changing the ratio of diffusion coefficients (D). Figure 5.10 shows

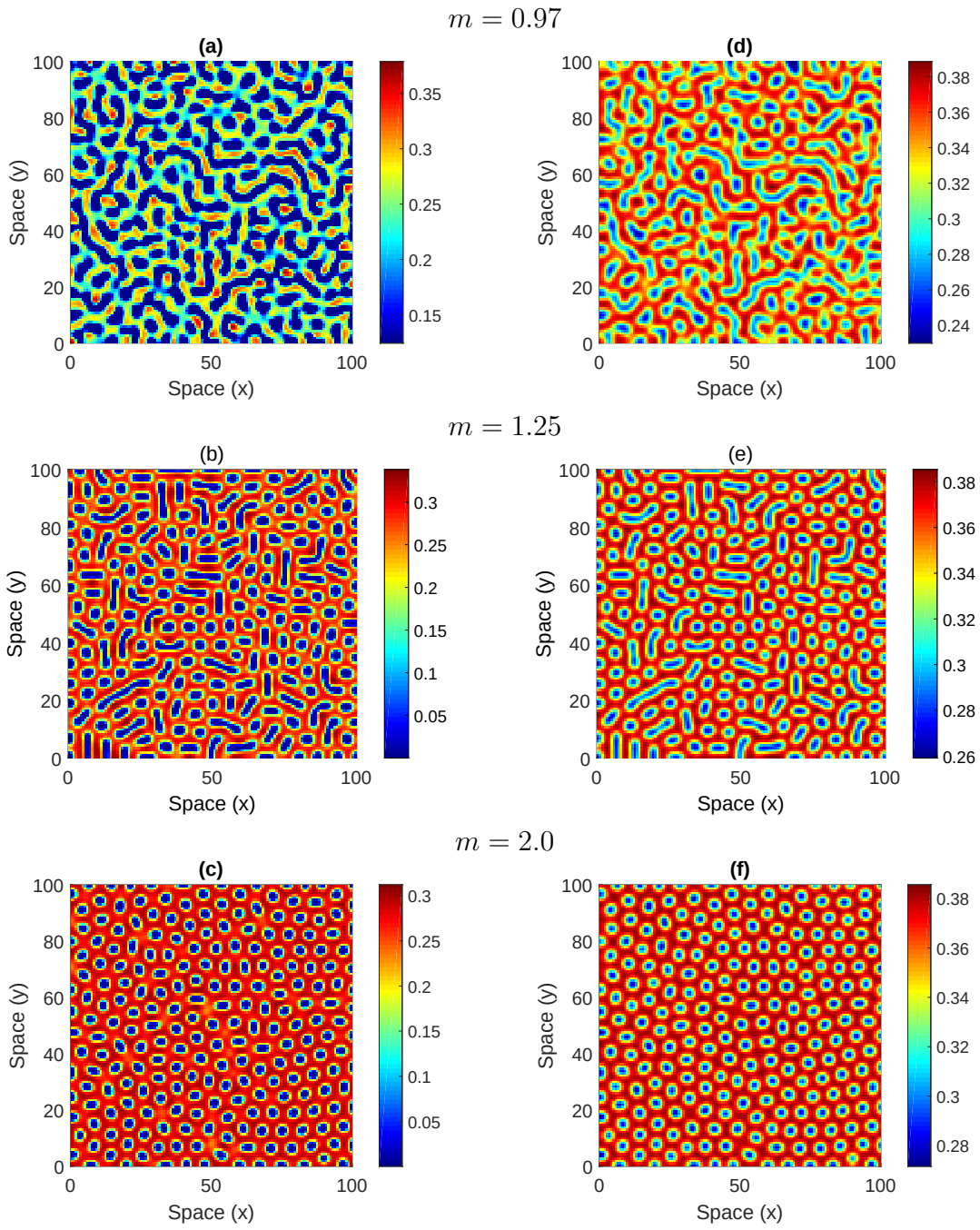

Figure 5.7: Two dimensional Turing dynamic patterns of the model with quadratic mortality (model 5.3) for prey (left panel) and predator (right panel) at time moment $\tau = 2500$. (a) and (d) $m = 0.97$; (b) and (e) $m = 1.25$; (c) and (f) $m = 2.0$. Other parameter values are $\beta = 0.8$, $\gamma = 0.01$ and $D = 0.08$.

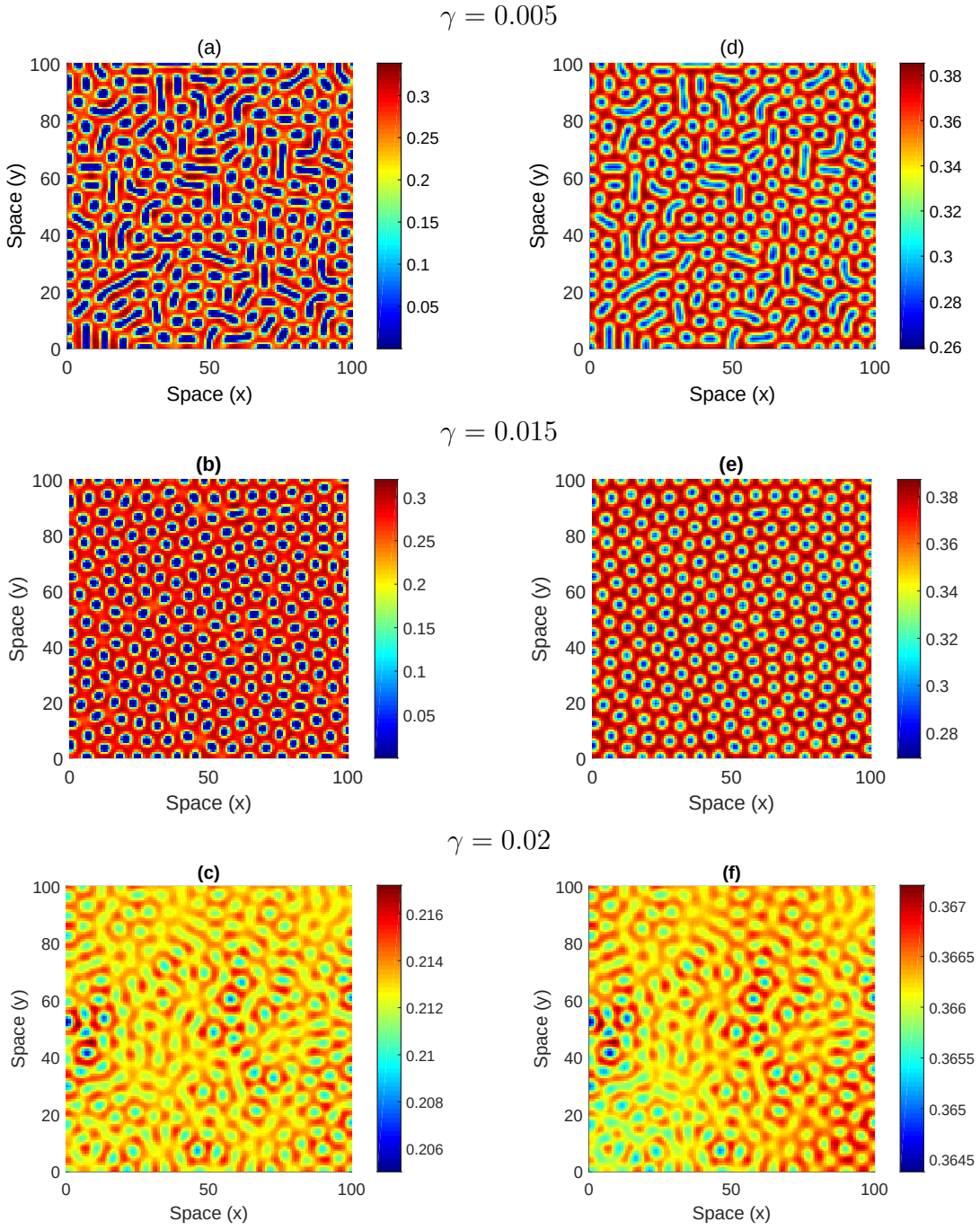

Figure 5.8: Two dimensional Turing dynamic patterns of the model with quadratic mortality (model 5.3) for prey (left panel) and predator (right panel) at time moment $\tau = 2500$. (a) and (d) $\gamma = 0.005$; (b) and (e) $\gamma = 0.015$; (c) and (f) $\gamma = 0.02$. Other parameter values are $\beta = 0.8$, $m = 1.25$ and $D = 0.08$.

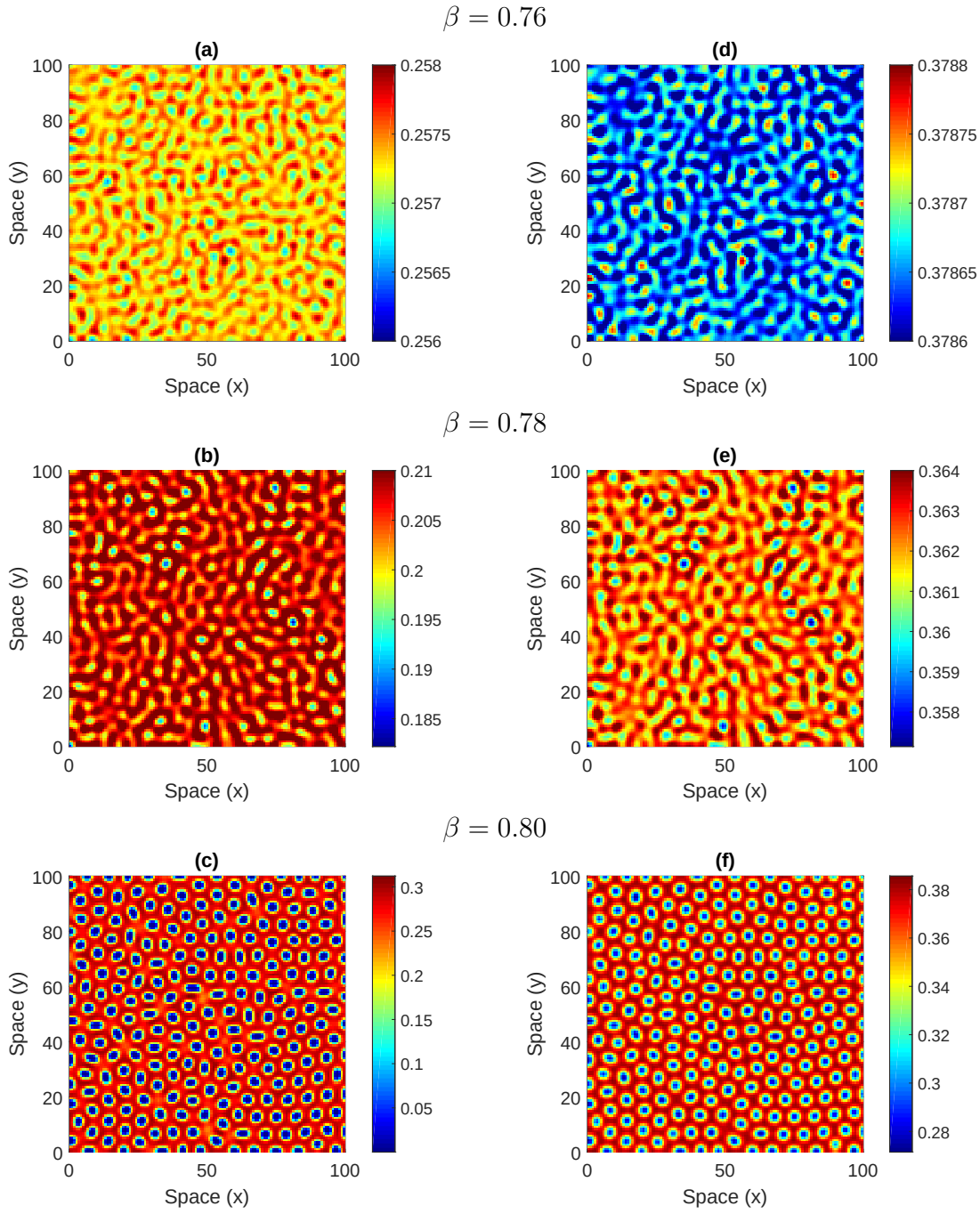

Figure 5.9: Two dimensional Turing dynamic patterns of the model with quadratic mortality (model 5.3) for prey (left panel) and predator (right panel) at time moment $\tau = 2500$. (a) and (d) $\beta = 0.76$; (b) and (e) $\beta = 0.78$; (c) and (f) $\beta = 0.8$. Other parameter values are $\gamma = 0.01$, $m = 1.25$ and $D = 0.08$.

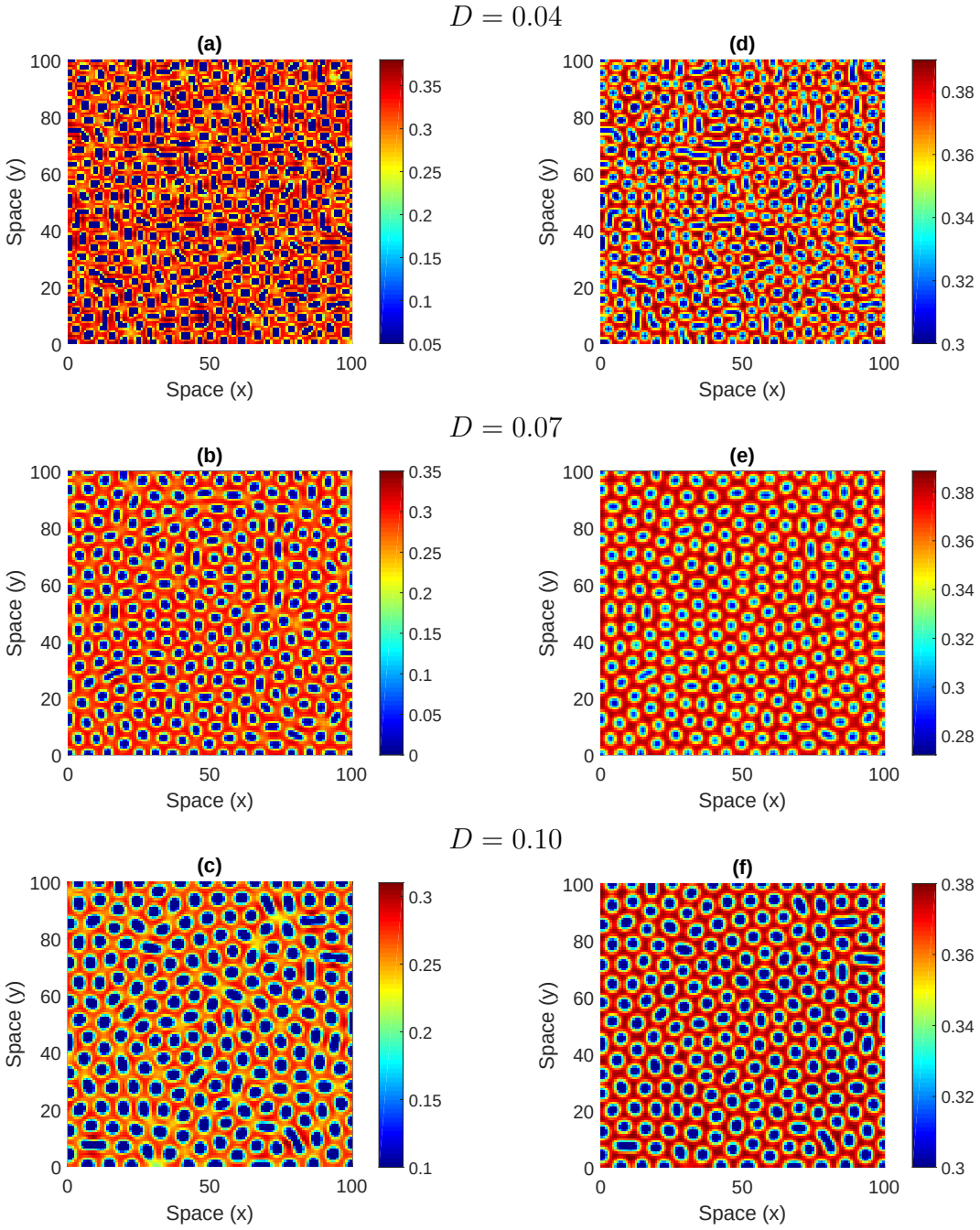

Figure 5.10: Two dimensional Turing dynamic patterns of the model with quadratic mortality (model 5.3) for prey (left panel) and predator (right panel) at time moment $\tau = 2500$. (a) and (d) $D = 0.04$; (b) and (e) $D = 0.07$; (c) and (f) $D = 0.1$. Other parameter values are $\gamma = 0.01$, $\beta = 0.8$ and $m = 1.25$.

the Turing patterns for prey and predator population over the two dimensional spatial domain at $\tau = 2500$ for different D, the ratio of the diffusion coefficients. In this case, the Turing patterns have already approached to their sizeable time stationary limit. Although the spatial patterns stay qualitatively identical over the span of parameters considered in Figure 5.10, it is easily seen that the size of the patches tends to become elongated with an increase in D. The amplitude of the density of the population shifts in the spatial patterns tends to rise slightly with the diffusion coefficient D.

5.6 Discussion and conclusion

For several decades, factors and mechanisms resulting in complex spatiotemporal population dynamics and ecological pattern formation have been a major focus in ecology [9; 10; 17; 19; 52; 53; 99; 100; 109; 110; 116; 117; 143; 157; 170; 185; 187; 193; 197]. The aim of this chapter is to investigate the effect of linear and quadratic mortality in a predator–prey system with herd behavior. The non-spatial study reveals that the system with increasing linear mortality become extinct whereas the system with quadratic mortality always coexist. In spatiotemporal model, the predator–prey system with linear mortality display four basic dynamics, namely, stationary, smooth oscillatory, intermittent chaos and chaos covering most of the domain. The non-Turing pattern is smooth and regular, which grows gradually and a chaotic pattern is observed for both the preys and the predators. No Turing pattern is observed in this case. However, the system with quadratic mortality demonstrate diffusive induced instability resulting in Turing patterns. By varying the mortality rate, we get dissimilar types of diffusive patterns, namely, mixed pattern (spot-stripe) and patchy pattern (spots), implying that there is a spot pattern replication, where the prey is in a isolated zone with low density and remainder region is in high density.

With increasing D, the rate of the diffusion coefficients, the pattern changes from spot-stripe to spots, implying that the prey and the predator populations are flocking together. The mobility of individuals for both species within their habitat can promote the coexistence between the prey and the predators. The methods

and results in the present chapter may enrich the research of pattern formation in the predator–prey model with herd behavior and quadratic mortality and may will explain many field observations.

Chapter 6

Conclusions and Future Research Scope

6.1 Concluding Remarks

This thesis has primarily focused on the spatiotemporal analysis, namely, Turing and non-Turing spatial distribution patterns, of tumor–immune and ecological systems through mathematical modeling and numerical simulations, where an attempt has been made to understand the effects of controlling parameters on the spatiotemporal pattern formation of different mathematical models. The summary of the results are given sequentially as follows:

- First, we have focused our attention on a spatiotemporal mathematical model describing the growth of a solid tumor in presence of an immune responses, which is termed as effector cells. The proposed model is a modification of the non-spatial model by Kuznetsov et al. [91] by extending it to a spatiotemporal one.

- Local stability analysis of the spatiotemporal model reveals that the tumor free equilibrium exists and is stable, when the intrinsic growth rate of the tumor is less then the ratio of constant input of the effector cells and its decay rate ($\alpha < \frac{\sigma}{\delta}$). The interior equilibrium does not exist in this case. However, when $\alpha > \frac{\sigma}{\delta}$, three interior equilibria (u^*, v^*) exist, of which two of them are stable. The immune system fails to control the tumor growth in this case.

- The system is also subjected to higher order spatiotemporal perturbation terms for stability check, but the results remains same as obtained from linear stability analysis.

- One interesting phenomenon of evolution of carrying capacity and expansion of tumor cell population is observed. This observation allows us to relate the tumor's volumetric growth rate to the host organs's functionality conveying composite infrastructure. When the carrying capacity of the primary host organ is about to be exceeded, metastasis will be triggered. While the biological processes involved in cancer expansion may lead to some upward adjustment of the carrying capacity, presumably these parenchymal and stromal compensation mechanisms are limited and tumor cells will eventually spread to distant sites.

- Next, a spatiotemporal mathematical model of interaction between malignant gliomas and immune system, namely, macrophages, cytotoxic T-lymphocytes, IFN-γ and TGF-β is studied. The system is investigated before and after the administration of the immunotherapeutic drug T11 target structure for better understanding of the growth and invasion of glioma population.

- It is observed that no Turing zone exists for both the cases T11 = 0 and T11 $\neq$ 0, implying that the system will have no Turing bifurcation and hence no Turing pattern.

- Without the administration of T11 target structure, the non-Turing patterns for gliomas indicate that the body's own defense mechanism, that is, the natural immune responses is too weak to control the growth and spread of malignant gliomas, which leads to glioma invasion of the entire domain.

- The aggressive motility of the gliomas restrict the propagation of the immune components, namely, macrophages and cytotoxic T-lymphocytes. After the administration of T11 target structure, the glioma cell proliferation is controlled by activating the phagocytic activity of macrophages as well as cytotoxic efficacy of the cytotoxic T-lymphocytes.

- The spatiotemporal study of the effect of the immunotherapeutic drug T11 target structure on malignant gliomas shows that it may be a promising therapeutic method to eradicate malignant gliomas.

- Next, we have investigated a spatial predator–prey model with hunting cooperation in predators.

- Using linear stability analysis, we obtain the condition for diffusive instability and identify the corresponding domain in the space of controlling parameters. Using extensive numerical simulations, we obtain complex patterns, namely, spotted pattern, stripe pattern and mixed pattern in the Turing domain, by varying the hunting cooperation in predators and carrying capacity of prey parameters. The results focus on the effect of hunting cooperation in pattern dynamics of a diffusive predator–prey model and help us in better understanding of the dynamics of the predator–prey interaction in real environment.

- In our last problem, we have investigated a diffusive predator–prey model exhibiting herd behavior for preys with linear and quadratic mortality term for predators.

- Using linear stability analysis, we obtain the conditions for diffusive instability and identify the corresponding Turing as well as non-Turing zone in the space of control parameters. Using extensive numerical simulations, we obtain spatiotemporal patterns for both non-Turing (model with linear mortality) and Turing (model with quadratic mortality) cases by varying mortality rates, the search efficacy of predators for preys and the rate of conversion of prey biomass to predator biomass.

- The non-Turing pattern exhibits spatiotemporal chaos whereas the Turing patterns focuses in many pattern dynamics and help us in the better understanding of the dynamics of the predator–prey interaction.

6.2 Future Research Scope

The mathematical models proposed in this thesis has many forthcoming possibilities. Some of the future perspectives are as follows:

- The entire thesis is focused on spatiotemporal dynamics through reaction-diffusion partial differential equations. The stochastic aspect of the model system is not introduced at all. How will the stochasticity has effect on the dynamics of the tumor–immune and predator–prey systems? Will it generate some new dynamics which may be able to explain the complex interactions?

- The cross–diffusion spatial aspect of the system can be studied by introducing cross–diffusion terms to the model equations.

- Amplitude equations for pattern forming system, which describe slow modulations in space and time of patterns occurring can be derived. Also, the physical interpretation of more complicated solutions of the amplitude equations can be discussed.

Bibliography

[1] Adams D. O. and Hamilton T. A., *The cell biology of macrophage activation*, Annual Review of Immunology, 2(1)(1984), 283–318.

[2] Aguirre P., González-Olivares E., Torres S., Sysavathdy S., *Stochastic predator–prey model with Allee effect on prey*, Nonlinear Analysis: Real World Applications, 14(1)(2013), 768–779.

[3] Ajraldi V., Pittavino M., Venturino E., *Modeling herd behavior in population systems*, Nonlinear Analysis: Real World Applications, 12(4)(2011), 2319–2338.

[4] Albert A., Freedman M., Perelson A. S., *Tumors and the immune system: The effects of a tumor growth modulator*, Mathematical Biosciences, 50(2)(1980), 25–58.

[5] Alves M. T. and Hilker F. M., *Hunting cooperation and Allee effects in predators*, Journal of Theoretical Biology, 419(1)(2017), 13–22.

[6] Alvord Jr. E. C. and Shaw C. M., *Neoplasms Affecting the Nervous System of the Elderly*, In: The Pathology of the Aging Human Nervous System, 210–286, 1991.

[7] Aragón J. L., Torres M., Gil D., Barrio R. A., Maini P. K., *Turing patterns with pentagonal symmetry*, Physical Review E, 65(5)(2002), 051913–051922.

[8] Ardizzone V., Lewandowski P., Luk M. H., Tse Y. C., Kwong N. H., Lücke A., Abbarchi M., Baudin E., Galopin E., Bloch J., Lemaitre A., Leung P. T., Roussignol P., Binder R., Tignon J., Schumacher S., *Formation and control of Turing patterns in a coherent quantum fluid*, Scientific Reports, 3(1)(2013), 1–6.

[9] Banerjee M. and Banerjee S., *Turing instabilities and spatiotemporal chaos in ratio-dependent Holling–Tanner model*, Mathematical Biosciences, 236(1)(2012), 64–76.

[10] Banerjee M. and Petrovskii S. V., *Self-organised spatial patterns and chaos in a ratio-dependent predator–prey system*, Theoretical Ecology, 4(1)(2011), 37–53.

[11] Banerjee S., *Immunotherapy with interleukin–2: a study based on mathematical modeling*, International Journal of Applied Mathematics and Computer Science, 18(3)(2008), 389–398.

[12] Banerjee S., Khajanchi S., Chaudhuri S., *A mathematical model to elucidate brain tumor abrogation by immunotherapy with T11 Target structure*, PloS One, 10(5)(2014), 0123611–0123632.

[13] Banerjee S. and Sarkar R. R., *Delay–induced model for tumor–immune interaction and control of malignant tumor growth*, Biosystems, 91(1)(2008), 268–288.

[14] Banerjee T., Dutta P. S., Gupta A., *Mean-field dispersion-induced spatial synchrony, oscillation and amplitude death, and temporal stability in an ecological model*, Physical Review E, 91(5)(2015), 052919–052931.

[15] Banerjee T., Dutta P. S., Zakharova A., Schöll E., *Chimera patterns induced by distance-dependent power-law coupling in ecological networks*, Physical Review E, 94(3)(2016), 032206–032213.

[16] Barrio R. A., Leppänen T., Karttunen M., Kaski K., *Morphological transitions and bistability in Turing systems*, Physical Review E, 70(6)(2004), 066202–066211.

[17] Barrio R. A., Varea C., Aragón J. L., Maini P. K., *A two–dimensional numerical study of spatial pattern formation in interacting Turing systems*, Bulletin of Mathematical Biology, 61(3)(1999), 483–505.

[18] Bascompte J. and Solé R. V., *Spatiotemporal patterns in nature*, Trends in Ecology and Evolution, 13(5)(1998), 173–174.

[19] Baurmann M., Gross T., Feudel U., *Instabilities in spatially extended predator–prey systems: spatiotemporal patterns in the neighborhood of Turing–Hopf bifurcations*, Journal of Theoretical Biology, 245(2)(2007), 220–229.

[20] Beddington J. R., *Mutual interference between parasites or predators and its effect on searching efficiency*, Journal of Animal Ecology, 44(3)(1975), 331–340.

[21] Belvisi S. and Venturino E., *An ecoepidemic model with diseased predators and prey group defense*, Simulation Modelling Practice and Theory, 34(1)(2013), 144–155.

[22] Bera S. P., Maiti A., Samanta G. P., *Modelling herd behavior of prey: analysis of a prey–predator model*, World Journal of Modelling and Simulation, 11(1)(2015), 3–14.

[23] Berezhnaya N. M., Yakimovich L. V., Kobzar R. A. S., Lyulkin V. D., Papivets A. Y., *The effect of interleukin–2 on proliferation of explants of malignant soft–tissue tumours in diffusion chambers*, Experimental Oncology, 8(1)(1986), 39–42.

[24] Bompard A., Amat I., Fauvergue X., Spataro T., *Host-parasitoid dynamics and the success of biological control when parasitoids are prone to Allee effects*, PloS One, 8(10)(2013), 076768–076779.

[25] Braza P. A., *Predator–prey dynamics with square root functional responses*, Nonlinear Analysis: Real World Applications, 13(4)(2012), 1837–1843.

[26] Brentnall S. J., Richards K. J., Brindley J., Murphy E., *Plankton patchiness and its effect on larger-scale productivity*, Journal of Plankton Research, 25(1)(2003), 121–140.

[27] Burton A. C., *Rate of growth of solid tumours as a problem of diffusion*, Growth, 30(2)(1966), 157–176.

[28] Byrne H. M. and Chaplain M. A. J., *Modelling the role of cell-cell adhesion in the growth and development of carcinomas*, Mathematical and Computer Modelling, 24(12)(1996), 1–17.

[29] Callewaert D. M., Meyers P., Hiernaux J., Radcliff G., *Kinetics of cellular cytotoxicity mediated by cloned cytotoxic T lymphocytes*, Immunobiology, 178(3)(1988), 203–214.

[30] Camara B. I., Mokrani H., Afenya E., *Mathematical modelling of gliomas therapy using oncolytic viruses*, Mathematical Biosciences and Engineering, 10(3)(2013), 565–578.

[31] Chakrabarty S. P. and Hanson F. B., *Optimal Control of Drug Delivery to Brain Tumors for a Test of PDE Driven Models Using The Galerkin Finite Element Method*, Proceedings of the 44th IEEE Conference on Decision and Control, IEEE, 1613–1618, 2005.

[32] Chakrabarty S. P. and Hanson F. B., *Distributed parameters deterministic model for treatment of brain tumors using Galerkin finite element method*, Mathematical Biosciences, 219(2)(2009), 129–141.

[33] Chaplain M. and Matzavinos A., *Mathematical Modelling of Spatiotemporal Phenomena in Tumour Immunology*, Springer–Verlag, 2006.

[34] Chattopadhyay J. and Pal S., *Viral infection on phytoplankton–zooplankton system–a mathematical model*, Ecological Modelling, 151(1)(2002), 15–28.

[35] Chattopadhyay J. and Tapaswi P. K., *A mathematical model of tumor growth with spatially decreasing diffusion coefficient of mitotic inhibitor*, Journal of Biological Systems, 2(1)(1994), 1–12.

[36] Clements H. S., Tambling C. J., Kerley G. I. H., *Prey morphology and predator sociality drive predator prey preferences*, Journal of Mammalohgy, 97(1)(2016), 919–927.

[37] Courchamp F., Clutton-Brock T., Grenfell B., *Inverse density dependence and the Allee effect*, Trends in Ecology and Evolution, 14(10)(1999), 405–410.

[38] Cross M. C. and Hohenberg P. C., *Pattern formation outside of equilibrium*, Reviews of Modern Physics, 65(3)(1993), 1–273.

[39] Cross M. C. and Hohenberg P. C., *Spatiotemporal chaos*, Science, 263(5153)(1994), 1569–1569.

[40] Crowley P. H. and Martin E. K., *Functional responses and interference within and between year classes of a dragonfly population*, Journal of the North American Benthological Society, 8(2)(1989), 211–221.

[41] DeAngelis D. L., Goldstein R. A., O'Neill R. V., *A model for tropic interaction*, Ecology, 56(4)(1975), 881–892.

[42] DeBoer R. J. and Hogeweg P., *Tumor escape from immune elimination: Simplified precursor bound cytotoxicity models*, Journal of Theoretical Biology, 113(4)(1985), 719–736.

[43] DeBoer R. J. and Hogeweg P., *Interactions between macrophages and T–lymphocytes: Tumor sneaking through intrinsic to helper T cell dynamics*, Journal of Theoretical Biology, 120(3)(1986), 331–354.

[44] DeLisi C. and Rescigno A., *Immune surveillance and neoplasia–I. A minimal mathematical model*, Bulletin of Mathematical Biology, 39(2)(1977), 201–221.

[45] Dennis B. and Couchamp J., *Allee effects in ecology and conservation*, Environmental Conservation, 36(1)(2009), 80–80.

[46] DePillis L. G., Gu W., Fister K. R., Head T. A., Maples K., Murugan A., Neal T., Yoshida K., *Chemotherapy for tumors: An analysis of the dynamics and a study of quadratic and linear optimal controls*, Mathematical Biosciences, 209(1)(2007), 292–315.

[47] DePillis L. G., Mallet D. G., Radunskaya A. E., *Spatial tumor–immune modeling*, Computational and Mathematical Methods in Medicine, 7(2)(2006), 159–176.

[48] DeRoos A., Persson L., Thieme H. R., *Emergent Allee effects in top predators feeding on structured prey populations*, Proceedings of the Royal Society of London B: Biological Sciences, 270(1515)(2003), 611–618.

[49] Descombes S. and Massot M., *Operator splitting for nonlinear reaction-diffusion systems with an entropic structure: singular perturbation and order reduction*, Numerische Mathematik, 97(1)(2004), 667–698.

[50] DeVisser K. E. and Kast W. M., *Effects of TGF–β on the immune system: implications for cancer immunotherapy*, Leukemia, 13(8)(1999), 1188–1199.

[51] Dieckmann U., Richard L., Metz J. A. J., *The Geometry of Ecological Interactions: Simplifying Spatial Complexity*, Cambridge University Press, 2000.

[52] Dubey B., Das B., Hussain J., *A predator–prey interaction model with self and cross-diffusion*, Ecological Modelling, 141(1)(2001), 67–76.

[53] Dubey B., Kumari N., Upadhyay R. K., *Spatiotemporal pattern formation in a diffusive predator-prey system: an analytical approach*, Journal of Applied Mathematics and Computing, 31(2)(2009), 413–432.

[54] Dugatkin L. A., *Cooperation Among Animals: An Evolutionary Perspective*, Oxford University Press, 1997.

[55] Dutta P. S. and Banerjee T., *Spatial coexistence of synchronized oscillation and death: A chimeralike state*, Physical Review E, 92(4)(2015), 042919–042925.

[56] Dutta S., Riaz S. S., Ray D. S., *Noise–induced instability: An approach based on higher–order moments*, Physical Review E, 71(3)(2005), 036216–036223.

[57] Edelstein-Keshet L., *Mathematical Models in Biology*, SIAM, 48, 1988.

[58] Erkintalo M., Hammani K., Kibler B., Finot C., Akhmediev N., Dudley J. M., Genty G., *Higher–order modulation instability in nonlinear fiber optics*, Physical Review Letters, 107(25)(2011), 253901–253905.

[59] Ferreira Jr. S. C., Martins M. L., Vilela M. J., *Reaction-diffusion model for the growth of avascular tumor*, Physical Review E, 65(2)(2002), 021907–021915.

[60] Finlay D. and Cantrell D. A., *Metabolism, migration and memory in cytotoxic T cells*, Nature Reviews Immunology, 11(2)(2011), 109–117.

[61] Finn O. J., *Molecular origins of cancer: cancer immunology*, The New England Journal of Medicine, 358(25)(2008), 2704–2715.

[62] Fish L., Pencheva N., Goodarzi H., Tran H., Yoshida M., Tavazoie S. F., *Muscleblind-like 1 suppresses breast cancer metastatic colonization and stabilizes metastasis suppressor transcripts*, Genes and Development, 30(4)(2016), 386–398.

[63] Foryś U., *Marchuk's model of immune system dynamics with application to tumour growth*, Computational and Mathematical Methods in Medicine, 4(1)(2002), 85–93.

[64] Fulton E. A., Smith A. D. M., Johnson C. R., *Mortality and predation in ecosystem models: is it important how these are expressed?*, Ecological Modelling, 169(1)(2003), 157–178.

[65] Gimmelli G., Kooi B. W., Venturino E., *Stability, Ecoepidemic models with prey group defense and feeding saturation*, Ecological Complexity, 22(2)(2015), 50–58.

[66] González-Olivares E., Mena-Lorca J., Rojas-Palma A., Flores J., *Dynamical complexities in the Leslie–Gower predator–prey model as consequences of the Allee effect on prey*, Applied Mathematical Modelling, 35(1)(2011), 366–381.

[67] González-Olivares E., Meneses-Alcay H., González-Yañez B., Mena-Lorca J., Rojas-Palma A., Ramos-Jiliberto R., *Multiple stability and uniqueness of the limit cycle in a Gause–type predator–prey model considering the Allee effect on prey*, Nonlinear Analysis: Real World Applications, 12(6)(2011), 2931–2942.

[68] Greenspan H. P., *Models for the growth of a solid tumor by diffusion*, Studies in Applied Mathematics, 51(4)(1972), 317–340.

[69] Grossman Z. and Berke G., *Tumor escape from immune elimination*, Journal of Theoretical Biology, 83(2)(1980), 267–296.

[70] Guan X., Wang W., Cai Y., *Spatiotemporal dynamics of a Leslie–Gower*

predator–prey model incorporating a prey refuge, Nonlinear Analysis: Real World Applications, 12(4)(2011), 2385–2395.

[71] Gutierrez M., Forster F. I., McConnell S. A., Cassidy J. P., Pollock J. M., Bryson D. G., *The detection of CD2+, CD4+, CD8+, and WC1+ T lymphocytes, B cells and macrophages in fixed and paraffin embedded bovine tissue using a range of antigen recovery and signal amplification techniques*, Veterinary Immunology and Immunopathology, 71(3)(1999), 321–334.

[72] Harpold H. L. P., Alvord Jr E. C., Swanson K. R., *The evolution of mathematical modeling of glioma proliferation and invasion*, Journal of Neuropathology and Experimental Neurology, 66(1)(2007), 1–9.

[73] Hatzikirou H., Deutsch A., Schaller C., Simon M., Swanson K., *Mathematical modelling of glioblastoma tumour development: a review*, Mathematical Models and Methods in Applied Sciences, 15(11)(2005), 1779–1794.

[74] Hesaaraki M. and Moghadas S., *Existence of limit cycles for predator–prey systems with a class of functional responses*, Ecological Modelling, 142(1)(2001), 1–9.

[75] Holling C. S., *The components of predation as revealed by a study of small-mammal predation of the European pine sawfly*, The Canadian Entomologist, 91(2)(1959), 293–320.

[76] Holling C. S., *Some characteristics of simple types of predation and parasitism*, The Canadian Entomologist, 91(2)(1959), 385–398.

[77] Ji C. Y., Jiang D. Q., Li X. Y., *Qualitative analysis of a stochastic ratio-dependent predator–prey system*, Journal of Computational and Applied Mathematics, 235(4)(2011), 1326–1341.

[78] Just W., Bose M., Bose S., Engel H., Schöll E., *Spatiotemporal dynamics near a supercritical Turing–Hopf bifurcation in a two–dimensional reaction–diffusion system*, Physical Review E, 64(2)(2001), 026219–026231.

[79] Khajanchi S. and Banerjee S., *Quantifying the role of immunotherapeutic drug T11 target structure in progression of malignant gliomas: Mathematical modeling and dynamical perspective*, Mathematical Biosciences, 289(1)(2017), 69–77.

[80] Khajanchi S. and Banerjee S., *Influence of multiple delays in brain tumor and immune system interaction with T11 target structure as a potent stimulator*, Mathematical Biosciences, 302(1)(2018), 116–130.

[81] Kirschner D. and Panetta J. C., *Modeling immunotherapy of the tumor–immune interaction*, Journal of Mathematical Biology, 37(3)(1998), 235–252.

[82] Kirschner D. and Tsygvintsev A., *On the global dynamics of a model for tumor immunotherapy*, Mathematical Biosciences and Engineering, 6(3)(2009), 573–583.

[83] Klausmeier C. A., *Regular and irregular patterns in semiarid vegetation*, Science, 284(5421)(1999), 1826–1828.

[84] Kleihues P., Louis D. N., Scheithauer B. W., Rorke L. B., Reifenberger G., Burger P. C., Cavenee W. K., *The WHO classification of tumors of the nervous system*, Journal of Neuropathology and Experimental Neurology, 61(3)(2002), 215–225.

[85] Kleihues P., Soylemezoglu F., Schäuble B., Scheithauer B. W., Burger P. C., *Histopathology, classification, and grading of gliomas*, Glia, 15(3)(1995), 211–221.

[86] Konukoglu E., Clatz O., Bondiau P. Y., Delingette H., Ayache N., *Extrapolating glioma invasion margin in brain magnetic resonance images: suggesting new irradiation margins*, Medical Image Analysis, 14(2)2010, 111–125.

[87] Konukoglu E., Clatz O., Menze B. H., Stieltjes B., Weber M. A., Mandonnet E., Delingette H., Ayache N., *Image guided personalization of reaction-diffusion type tumor growth models using modified anisotropic eikonal equations*, IEEE Transactions on Medical Imaging, 29(1)2010, 77–95.

[88] Kronik N., Kogan Y., Vainstein V., Agur Z., *Improving alloreactive CTL immunotherapy for malignant gliomas using a simulation model of their interactive dynamics*, Cancer Immunology, Immunotherapy, 57(3)(2008), 425–439.

[89] Kuang Y. and Beretta E., *Global qualitative analysis of a ratio-dependent predator–prey system*, Journal of Mathematical Biology, 36(3)(1998), 389–406.

[90] Kuznetsov V. A. and Knott G. D., *Modeling tumor regrowth and immunotherapy*, Mathematical and Computer Modelling, 33(12)(2001), 1275–1287.

[91] Kuznetsov V. A., Makalkin I. A., Taylor M. A., Perelson A. S., *Nonlinear dynamics of immunogenic tumours: parameter estimation and global bifurcation analysis*, Bulletin of Mathematical Biology, 56(2)(1994), 295–321.

[92] Lancaster P., *Theory of Matrices*, Academic Press, New York, 1969.

[93] Laskowski M., Mostaço-Guidolin L. C., Greer A. L., Wu J., Moghadas S., *The impact of demographic variables on disease spread: influenza in remote communities*, Scientific Reports, 1(1)(2011), 105–111.

[94] Lefever R., Hiernaux J., Urbain J., Meyers P., *On the kinetics and optimal specificity of cytotoxic reactions mediated by T–Iymphocyte clones*, Bulletin of Mathematical Biology, 54(5)(1992), 839–873.

[95] Lejeune O., Chaplain M. A. J., Akili I. El., *Oscillations and bistability in the dynamics of cytotoxic reactions mediated by the response of immune cells to solid tumours*, Mathematical and Computer Modelling, 47(5)(2008), 649–662.

[96] Lejeune O., Tlidi M., Couteron P., *Localized vegetation patches: a self–organized response to resource scarcity*, Physical Review E, 66(1)(2002), 010901–010904.

[97] LeVeque R. J., *Time-Split Methods for Partial Differential Equations*, Stanford University CA Department of Computer Science, 1982.

[98] Levin S. A. and Segel L. A., *Hypothesis for origin of planktonic patchiness*, Nature, 259(5545)(1976), 659–659.

[99] Li X., Jiang W., Shi J., *Hopf bifurcation and Turing instability in the reaction–diffusion Holling–Tanner predator-prey model*, IMA Journal of Applied Mathematics, 78(2)(2013), 287–306.

[100] Liu R. T., Liaw S. S., Maini P. K., *Two–stage Turing model for generating pigment patterns on the leopard and the jaguar*, Physical Review E, 74(1)(2006), 011914–011922.

[101] Look A. T., Schriber T. J., Nawrocki J. F., Murphy W. H., *Computer simulation of the cellular immune response to malignant lymphoid cells: Logic of approach, model design and laboratory verification*, Immunology, 43(4)(1981), 677–690.

[102] Ma X., Shao Y., Wang Z., Luo M., Fang X., Ju, Z., *An impulsive two-stage predator–prey model with stage-structure and square root functional responses*, Mathematics and Computers in Simulation, 119(1)(2016), 91–107.

[103] Macken C. A. and Perelson A. S., *A multistage model for the action of cytotoxic T lymphocytes in multicellular conjugates*, The Journal of Immunology, 132(4)(1984), 1614–1624.

[104] Maini P. K., Benson D. L., Sherratt J. A., *Pattern formation in reaction–diffusion models with spatially inhomogeneous diffusion coefficients*, Mathematical Medicine and Biology: A Journal of the IMA, 9(3)(1992), 197–213.

[105] Malchow H., Petrovskii S. V., Venturino E., *Spatiotemporal Patterns in Ecology and Epidemiology: Theory, Models, and Simulation*, Chapman and Hall/CRC, 2008.

[106] Mallet D. G. and de Pillis L. G., *A cellular automata model of tumor–immune system interactions*, Journal of Theoretical Biology, 239(3)(2006), 334–350.

[107] Matia S. N. and Alam S., *Prey–predator dynamics under herd behavior of prey*, Universal Journal of Applied Mathematics, 1(2)(2013), 251–257.

[108] Matzavinos A., Chaplain M. A., Kuznetsov V. A., *Mathematical modeling*

of the spatiotemporal response of cytotoxic T–lymphocytes to a solid tumour, Mathematical Medicine and Biology, 21(1)(2004), 1–34.

[109] McGehee E. A., Schutt N., Vasquez D. A., Peacock E. L., *Bifurcations, and temporal and spatial patterns of a modified Lotka–Volterra model*, International Journal of Bifurcatation and Chaos, 18(2)(2008), 2223–2248.

[110] Medvinsky A. B., Petrovskii S. V., Tikhonova I. A., Malchow H., Li B. L., *Spatiotemporal complexity of plankton and fish dynamics*, SIAM Review, 44(3)(2002), 311–370.

[111] Meinhardt H., *Models of biological pattern formation: from elementary steps to the organization of embryonic axes*, Current Topics in Developmental Biology, 81(1)(2008), 1–63.

[112] Merrill S. J., *Foundations of the use of enzyme kinetic analogy in cell–mediated cytotoxicity*, Mathematical Biosciences, 62(2)(1982), 219–236.

[113] Merrill S. J. and Sathananthan S., *Approximate Michaelis–Menthen kinetics displayed in a stochastic model of cell–mediated cytotoxicity*, Mathematical Biosciences, 80(2)(1986), 223–238.

[114] Mimura M. and Murray J. D., *On a diffusive prey–predator model which exhibits patchiness*, Journal of Theoretical Biology, 75(3)(1978), 249–262.

[115] Moghadas S., Alexander M. E., Corbett B. D., *A non-standard numerical scheme for a generalized Gause-type predator–prey model*, Physica D: Nonlinear Phenomena, 188(1)(2004), 134–151.

[116] Morozov A. Y., Petrovskii S. V., Li B. L., *Bifurcations and chaos in a predator–prey system with the Allee effect*, Proceedings of the Royal Society of London B: Biological Sciences, 271(1546)(2004), 1407–1414.

[117] Morozov A. Y., Petrovskii S. V., Li B. L., *Spatiotemporal complexity of patchy invasion in a predator–prey system with the Allee effect*, Journal of Theoretical Biology, 238(1)(2006), 18–35.

[118] Mukherjee J., Dutta S., Sarkar S., Begum Z., Ghosh A., Chaudhuri S., Chaudhuri S., *Preclinical changes in immunoreactivity and cellular architecture during the progressive development of intracranial neoplasms and an immunotherapeutic schedule with a novel biological response modifier, the T11TS/S–LFA3*, Asian Pacific Journal of Cancer Prevention: APJCP, 3(4)(2002), 325–337.

[119] Mukhopadhyay B. and Bhattacharyya R., *Temporal and spatiotemporal variations in a mathematical model of macrophage–tumor interaction*, Nonlinear Analysis: Hybrid Systems, 2(3)(2008), 819–831.

[120] Murray J. D., *A pre-pattern formation mechanism for animal coat markings*, Journal of Theoretical Biology, 88(1)(1981), 161–199.

[121] Murray J. D., *Mathematical Biology I. An Introduction*, Springer–Verlag, 2002.

[122] Murray J. D., *Mathematical Biology II. Spatial Models and Biomedical Applications*, Springer–Verlag, 2003.

[123] Nanda S., Moore H., Lenhart S., *Optimal control of treatment in a mathematical model of chronic myelogenous leukemia*, Mathematical Biosciences, 210(1)(2007), 143–156.

[124] Neuhauser C., *Mathematical challenges in spatial ecology*, Notices of the American Mathematical Society, 48(11)(2001), 1304–1314.

[125] Okubo A. and Levin S. A., *Diffusion and Ecological Problems: Modern Perspectives*, Springer Science and Business Media, 2013.

[126] Ouyang Q. and Swinney H. L., *Transition from a uniform state to hexagonal and striped Turing patterns*, Nature, 352(1991), 610–612.

[127] Owen M. R., Byrne H. M., Lewis C. E., *Mathematical modeling of the use of macrophages as vehicles for drug delivery to hypoxic tumor sites*, Journal of Theoretical Biology, 226(4)(2004), 377–391.

[128] Owen M. R. and Sherratt J. A., *Pattern formation and spatiotemporal irregularity in a model for macrophage–tumour interactions*, Journal of Theoretical Biology, 189(1)(1997), 63–80.

[129] Paillard F., *Commentary: immunosuppression mediated by tumor cells: A challenge for immunotherapeutic approaches*, Human Gene Therapy, 11(5)(2000), 657–658.

[130] Pal S., Chatterjee S., Das K. P., Chattopadhyay J., *Role of competition in phytoplankton population for the occurrence and control of plankton bloom in the presence of environmental fluctuations*, Ecological Modelling, 220(2)(2009), 96–110.

[131] Papadogiorgaki M., Koliou P., Kotsiakis X., Zervakis M. E., *Mathematical modelling of spatiotemporal glioma evolution*, Theoretical Biology and Medical Modelling, 10(1)(2013), 1–47.

[132] Parish C. R., *Cancer immunotherapy: the past, the present and the future*, Immunology and Cell Biology, 81(2)(2003), 106–113.

[133] Pascual M., *Diffusion–induced chaos in a spatial predator–prey system*, Proceedings of the Royal Society of London B: Biological Sciences, 251(1330)(1993), 1–7.

[134] Pascual M., Roy M., Franc A., *Simple temporal models for ecological systems with complex spatial patterns*, Ecology Letters, 5(3)(2002), 412–419.

[135] Patel A. A., Gawlinski E. T., Lemiueux S. K., Gatenby R. A., *A cellular automaton model of early tumor growth and invasion: the effects of native tissue vascularity and increased anaerobic tumor metabolism*, Journal of Theoretical Biology, 213(3)(2001), 315–331.

[136] Patriarca M. and Leppänen T., *Modeling language competition*, Physica A: Statistical Mechanics and its Applications, 338(2)(2004), 296–299.

[137] Pencheva N., Tran H., Buss C., Huh D., Drobnjak M., Busam K., Tavazoie S. F., *Convergent multi-miRNA targeting of ApoE drives LRP1/LRP8-dependent melanoma metastasis and angiogenesis*, Cell, 151(5)(2012), 1068–1082.

[138] Perelson A. S. and Bell G. I., *Delivery of lethal hits by cytotoxic T lymphocytes*

in multicellular conjugates occurs sequentially but at random, The Journal of Immunology, 129(6)(1982), 2796–2801.

[139] Perelson A. S. and Macken C. A., *Kinetics of cell–mediated cytotoxicity: stochastic and deterministic multistage models*, Mathematical Biosciences, 70(2)(1984), 161–194.

[140] Peterson P. K., Chao C. C., Hu S., Thielen K., Shaskan E. G., *Glioblastoma, transforming growth factor-β, and Candida meningitis: a potential link*, The American Journal of Medicine, 92(3)(1992), 262–264.

[141] Petrovskii S. V. and Malchow H., *A minimal model of pattern formation in a prey–predator system*, Mathematical and Computer Modelling, 29(8)(1999), 49–63.

[142] Petrovskii S. V. and Malchow H., *Wave of chaos: new mechanism of pattern formation in spatiotemporal population dynamics*, Theoretical Population Biology, 59(2)(2001), 157–174.

[143] Petrovskii S. V., Malchow H., Hilker F. M., Venturino E., *Patterns of patchy spread in deterministic and stochastic models of biological invasion and biological control*, Biological Invasions, 7(5)(2005), 771–793.

[144] Petrovskii S. V., Morozov A. Y., Venturino E., *Allee effect makes possible patchy invasion in a predator–prey system*, Ecology Letters, 5(3)(2002), 345–352.

[145] Pettet G. J., Please C. P., Tindall M. J., McElwain D. L. S., *The migration of cells in multicell tumor spheroids*, Bulletin of Mathematical Biology, 63(2)(2001), 231–257.

[146] Pham K., Chauviere A., Hatzikirou H., Li X., Byrne H. M., Cristini V., Lowengrub J., *Density-dependent quiescence in glioma invasion: instability in a simple reaction-diffusion model for the migration/proliferation dichotomy*, Journal of Biological Dynamics, 6(1)(2012), 54–71.

[147] Plaza R. G., Sanchez-Garduno F., Padilla P., Barrio R. A., Maini P. K., *The effect of growth and curvature on pattern formation*, Journal of Dynamics and Differential Equations, 16(4)(2004), 1093–1121.

[148] Preziosi L., *From population dynamics to modelling the competition between tumors and immune system*, Mathematical and Computer Modelling, 23(6)(1996), 135–152.

[149] Prigogine I. and Lefever R., *Stability problems in cancer growth and nucleation*, Comparative Biochemistry and Physiology Part B: Comparative Biochemistry, 67(3)(1980), 389–393.

[150] Rao F. and Kang Y., *The complex dynamics of a diffusive prey–predator model with an Allee effect in prey*, Ecological Complexity, 28(1)(2016), 123–144.

[151] Rescigno A. and DeLisi C., *Immune surveillance and neoplasia. II. A two–stage mathematical model*, Bulletin of Mathematical Biology, 39(4)(1977), 487–497.

[152] Riaz S. S., Sharma R., Bhattacharya S. P., Ray D. S., *Instability and pattern formation in reaction–diffusion systems: a higher order analysis*, The Journal of Chemical Physics, 127(6)(2007), 064503–064512.

[153] Rosenberg S. A., Sherry R. M., Morton K. E., Scharfman W. J., Yang J. C., Topalian S. L., Royal R. E., Kammula U., Restifo N. P., Hughes M. S., Schwartzentruber D., Berman D. M., Schwarz S. L., Ngo L. T., Mavroukakis S. A., White D. E., Steinberg S. M., *Tumor progression can occur despite the induction of very high levels of self/tumor antigen-specific CD8+ T cells in patients with melanoma*, The Journal of Immunology, 175(9)(2005), 6169–6176.

[154] Sarkar R. R. and Banerjee S., *Cancer self remission and tumor stability–a stochastic approach*, Mathematical Biosciences, 196(1)(2005), 65–81.

[155] Schall T. J., Bacon K., Toy K. J., Goeddel D. V., *Selective attraction of monocytes and T lymphocytes of the memory phenotype by cytokine RANTES*, Nature, 347(6294)(1990), 669–669.

[156] Schulz W., *Molecular Biology of Human Cancers*, Springer, 2005.

[157] Segel L. A. and Jackson J. L., *Dissipative structure: an explanation and an ecological example*, Journal of Theoretical Biology, 37(3)(1972), 545–559.

[158] Shaver G. R., *Spatial Heterogeneity: Past, Present, and Future*, Ecosystem Function in Heterogeneous Landscapes, Springer, 443–449, 2005.

[159] Smoller J., *Shock Waves and Reaction-Diffusion Equations*, Springer–Verlag, 1983.

[160] Smyth M. J., Godfrey D. I., Trapani J. A., *A fresh look at tumor immunosurveillance and immunotherapy*, Nature Immunology, 2(4)(2001), 293–299.

[161] Stein A. M., Demuth T., Mobley D., Berens M., Sander L. M., *A mathematical model of glioblastoma tumor spheroid invasion in a three–dimensional in vitro experiment*, Biophysical Journal, 92(1)(2007), 356–365.

[162] Stephens P. A. and Sutherland W. J., *Consequences of the Allee effect for behaviour, ecology and conservation*, Trends in Ecology and Evolution, 14(10)(1999), 401–405.

[163] Sud D., Bigbee C., Flynn J. L., Kirschner D. E., *Contribution of CD8+ T cells to control of Mycobacterium tuberculosis infection*, The Journal of Immunology, 176(7)(2006), 4296–4314.

[164] Swanson K. R., *Mathematical Modeling of the Growth and Control of Tumors*, University of Washington Seattle, 1999.

[165] Swanson K. R., Alvord E. C., Murray J. D., *A quantitative model for differential motility of gliomas in grey and white matter*, Cell Proliferation, 33(5)(2000), 317–329.

[166] Swanson K. R., Alvord E. C., Murray J. D., *Quantifying efficacy of chemotherapy of brain tumors with homogeneous and heterogeneous drug delivery*, Acta Biotheoretica, 50(4)(2002), 223–237.

[167] Swanson K. R., Bridge C., Murray J. D., Alvord E. C., *Virtual and real brain tumors: using mathematical modeling to quantify glioma growth and invasion*, Journal of the Neurological Sciences, 216(1)(2003), 1–10.

[168] Szeto M. D., Chakraborty G., Hadley J., Rockne R., Muzi M., Alvord E. C., Krohn K. A., Spence A. M., Swanson K. R., *Quantitative metrics of net proliferation and invasion link biological aggressiveness assessed by MRI with hypoxia assessed by FMISO–PET in newly diagnosed glioblastomas*, Cancer Research, 69(10)(2009), 4502–4509.

[169] Szymańska Z., *Analysis of immunotherapy models in the context of cancer dynamics*, International Journal of Applied Mathematics and Computer Science, 13(3)(2003), 407–418.

[170] Tang X. and Song Y., *Stability, Hopf bifurcations and spatial patterns in a delayed diffusive predator–prey model with herd behavior*, Applied Mathematics and Computation, 254(2)(2015), 375–391.

[171] Tanner J. T., *The stability and the intrinsic growth rates of prey and predator populations*, Ecology, 56(6)(1975), 855–867.

[172] Thoma J. A., Thoma G. J., Clark W., *The efficiency and linearity of the radiochromium release assay for cell–mediated cytotoxicity*, Cellular Immunology, 40(2)(1978), 404–418.

[173] Thorn R. M. and Henney C. S., *Kinetic analysis of target cell destruction by effector T cell*, The Journal of Immunology, 117(6)(1976), 2213–2219.

[174] Thorn R. M. and Henney C. S., *Kinetic analysis of target cell destruction by effector cells. II. Changes in killer cell avidity as a function of time and dose*, The Journal of Immunology, 119(6)(1977), 1973–1978.

[175] Tracqui P., Cruywagen G. C., Woodward D. E., Bartoo G. T., Murray J. D., Alvord E. C., *A mathematical model of glioma growth: the effect of chemotherapy on spatiotemporal growth*, Cell Proliferation, 28(1)(1995), 17–31.

[176] Tran H., Michelson S., Ito K., Leith J. T., *Stochastic models for subpopulation emergence in heterogeneous tumors*, Bulletin of Mathematical Biology, 51(6)(1989), 731–747.

[177] Tsygvintsev A., *Evolutionary paradigm in cancer immunology*, ESAIM: Proceedings and Surveys, 45(2)(2014), 285–289.

[178] Tsygvintsev A., Marino S., Kirschner D. E., *A Mathematical Model of Gene Therapy for the Treatment of Cancer*, Mathematical Methods and Models in Biomedicine, Springer, 367–385, 2013.

[179] Turing A. M., *The chemical basis of morphogenesis*, Philosophical Transactions of the Royal Society of London B: Biological Sciences, 237(641)(1952), 37–72.

[180] Upadhyay R. K., Patra A., Dubey B., Thakur N. K., *A predator–prey interaction model with self-and cross-diffusion in aquatic systems*, Journal of Biological Systems, 22(4)(2014), 691–712.

[181] Upadhyay R. K., Thakur N. K., Dubey B., *Nonlinear non-equilibrium pattern formation in a spatial aquatic system: Effect of fish predation*, Journal of Biological Systems, 18(1)(2010), 129–159.

[182] Vanag V. K., Yang L., Dolnik M., Zhabotinsky A. M., Epstein I. R., *Oscillatory cluster patterns in a homogeneous chemical system with global feedback*, Nature, 406(6794)(2000), 389–391.

[183] Verdy A., *Modulation of predator–prey interactions by the Allee effect*, Ecological Modelling, 221(8)(2010), 1098–1107.

[184] Vinatier F., Tixier P., Duyck P. F., Lescourret F., *Factors and mechanisms explaining spatial heterogeneity: a review of methods for insect populations*, Methods in Ecology and Evolution, 2(1)(2011), 11–22.

[185] Wang J., Shi J., Wei J., *Dynamics and pattern formation in a diffusive predator–prey system with strong Allee effect in prey*, Journal of Differential Equations, 251(5)(2011), 1276–1304.

[186] Wang S. E., Hinow P., Bryce N., Weaver A. M., Estrada L., Artega C. L.,

Webb G. F., *A mathematical model quantifies proliferation and motility effects of TGF–β on cancer cells*, Computational and Mathematical Methods in Medicine, 10(1)(2009), 71–83.

[187] Wang W., Liu Q. X., Jin Z., *Spatiotemporal complexity of a ratio–dependent predator–prey system*, Physical Review E, 75(5)(2007), 051913–051922.

[188] Webb S. D., Owen M. R., Byrne H. M., Murdoch C., Lewis C. E., *Macrophage–based anti–cancer therapy: modeling different modes of tumour targeting*, Bulletin of Mathematical Biology, 69(5)(2007), 1747–1776.

[189] Xu C., Yuan S., Zhang T., *Global dynamics of a predator–prey model with defense mechanism for prey*, Applied Mathematics Letters, 62(1)(2016), 42–48.

[190] Yang L., Dolnik M., Zhabotinsky A. M., Epstein I. R., *Pattern formation arising from interactions between Turing and wave instabilities*, The Journal of Chemical Physics, 117(15)(2002), 7259–7265.

[191] Yi F., Wei J., Shi J., *Bifurcation and spatiotemporal patterns in a homogeneous diffusive predator–prey system*, Journal of Differential Equations, 246(5)(2009), 1944–1977.

[192] Yochelis A., Hagberg A., Meron E., Lin A. L., Swinney H. L., *Development of standing–wave labyrinthine patterns*, SIAM Journal on Applied Dynamical Systems, 1(2)(2002), 236–247.

[193] Yuan S., Xu C., Zhang T., *Spatial dynamics in a predator–prey model with herd behavior*, Chaos: An Interdisciplinary Journal of Nonlinear Science, 23(3)(2013), 033102–033113.

[194] Zheng Q. Q., Shen J. W., *Dynamics and pattern formation in a cancer network with diffusion*, Communications in Nonlinear Science and Numerical Simulation, 27(1)(2015), 93–109.

[195] Zhou S. R., Liu Y. F., Wang G., *The stability of predator–prey systems subject to the Allee effects*, Theoretical Population Biology, 67(1)(2005), 23–31.

[196] Zhang X. A., Lansun C., Avidan U. N., *The stage-structured predator–prey model and optimal harvesting policy*, Mathematical Biosciences, 168(2)(2000), 201–210.

[197] Zhang X. C., Sun G. Q., Jin Z., *Spatial dynamics in a predator–prey model with Beddington-DeAngelis functional response*, Physical Review E, 85(2)(2012), 021924–021938.

List of Publications

1. Singh T. and Banerjee S., *Spatial aspects of hunting cooperation in predators with Holling type II functional response*, Journal of Biological Systems, World Scientific, 26(4)(2018), 1–21.

2. Singh T. and Banerjee S., *Spatiotemporal model of a predator–prey system with herd behavior and quadratic mortality*, International Journal of Bifurcation and Chaos, World Scientific (Accepted).

3. Singh T. and Banerjee S., *Spatiotemporal dynamics of malignant gliomas and immune system considering the role of immunotherapeutic agent T11 target structure*, Computers and Mathematics with Applications, Elsevier (Under review).

4. Singh T. and Banerjee S., *Spatiotemporal dynamics of immunogenic tumors*, Indian Journal of Pure and Applied Mathematics, Springer (Under review).